



**UCLouvain**

Institute of Mechanics,  
Materials and Civil Engineering

## Robust optimisation of the pathway towards a sustainable whole-energy system

A hierarchical multi-objective  
reinforcement-learning based approach

Doctoral dissertation presented by

**Xavier RIXHON**

in partial fulfillment of the requirements for  
the degree of Doctor in Engineering Sciences

December 2023

### Thesis committee

Pr. Francesco CONTINO (supervisor, UCLouvain)

Pr. Hervé JEANMART (supervisor, UCLouvain)

Dr. Stefano MORET (ETH Zurich)

Pr. Sylvain QUOILIN (ULiège)

---

---

© 2023  
Xavier Rixhon  
All Rights Reserved

---

---

---

# Contents

<b>Symbols</b>	<b>iii</b>
<b>1 Methodology: Through a variety of complementary tools</b>	<b>1</b>
1.1 Whole-energy system transition model optimisation: EnergyScope Pathway . . . . .	3
1.1.1 Perfect foresight: One global optimisation of the transition . . . . .	3
1.1.2 Myopic: Sequential optimisation of the transition with limited foresight . . . . .	6
1.2 Uncertainty quantification . . . . .	10
1.2.1 Uncertainty characterisation . . . . .	11
1.2.2 Polynomial Chaos Expansion . . . . .	12
1.2.3 Preliminary screening and selection . . . . .	16
1.3 Agent-based reinforcement learning for energy transition support . . . . .	16
1.3.1 Reinforcement learning fundamentals and application to energy systems . . . . .	17
1.3.2 Problem formulation and algorithm . . . . .	17
1.4 Robustness assessment via PCA . . . . .	19
1.4.1 Principal Component Analysis: General concept . . . . .	19
1.4.2 Principal components of the transition . . . . .	21
<b>2 Case study: the Belgian energy system</b>	<b>27</b>
2.1 End-use demands . . . . .	29
2.1.1 Non-energy demand . . . . .	29
2.1.2 Forecast of the demands over the transition . . . . .	31
2.2 Resources . . . . .	32
2.3 Conversion technologies . . . . .	34
2.3.1 Small modular reactor . . . . .	36

2.3.2	Technologies supplying the non-energy demand . . . . .	37
2.4	Uncertainty ranges . . . . .	39
2.5	CO <sub>2</sub> -budget for the transition . . . . .	40
<b>3</b>	<b>The atom-molecules dilemma: deterministic and uncertain analyses</b>	<b>43</b>
3.1	Deterministic impact of integrating small modular reactor (SMR) in 2040 . . . . .	43
3.1.1	Power sector . . . . .	44
3.1.2	System-level impacts . . . . .	44
3.1.3	Non-power sectors . . . . .	46
3.2	Uncertainty quantification on the cost, the atom and the molecules . . . . .	49
3.2.1	Total transition cost . . . . .	50
3.2.2	Atom and molecules . . . . .	52
3.2.3	Local renewables . . . . .	57
<b>Bibliography</b>		<b>59</b>
<b>A EnergyScope Pathway: Its choice and its formulation</b>		<b>75</b>
A.1	EnergyScope Pathway: The right model to choose . . . . .	75
A.2	EnergyScope Pathway and its linear formulation . . . . .	80
A.2.1	The starting point: a scenario analysis model . . . . .	81
A.2.2	Extending the model for pathway optimisation . . . . .	85
<b>B Case study: the Belgian energy system</b>		<b>93</b>
B.1	Belgian energy system in 2020 . . . . .	93
B.2	Belgian energy transition pathway towards carbon-neutrality in 2050 . . . . .	93
B.2.1	Greenhouse gases and primary energy . . . . .	95
B.2.2	Electricity sector: Capacities and yearly balance . . . . .	97
B.2.3	Costs: Investments and operation . . . . .	99
B.3	Myopic versus perfect foresight pathway optimisation . . . . .	102
B.4	Assessment of different emissions-trajectories . . . . .	106
B.4.1	CO <sub>2</sub> -budget versus linear decrease of emissions . . . . .	106
B.4.2	Comparison without restriction on greenhouse gases (GHG) . . . . .	107
B.5	Uncertainty characterisation for the 5-year steps transition . . . . .	109
<b>C Pathway optimisation under uncertainties</b>		<b>111</b>
C.1	Total transition cost . . . . .	111
C.2	Imported renewable electrofuels . . . . .	114

---

---

# Symbols

## Acronyms

<b>API</b>	application programming interface
<b>BEV</b>	battery electric vehicle
<b>BTX</b>	benzene, toluene and xylene
<b>CAPEX</b>	capital expenditure
<b>CCGT</b>	combined cycle gas turbine
<b>CHP</b>	combined heat and power
<b>CNG</b>	compressed natural gas
<b>DHN</b>	district heating network
<b>ESOMs</b>	energy system optimisation models
<b>EnergyScope TD</b>	EnergyScope Typical Days
<b>EUD</b>	end-use demand
<b>FC</b>	fuel cell
<b>GHG</b>	greenhouse gases
<b>GSA</b>	global sensitivity analysis
<b>GWP</b>	global warming potential
<b>HP</b>	heat pump
<b>HT</b>	high-temperature
<b>HVC</b>	high value chemicals
<b>ICE</b>	internal combustion engine
<b>IEA</b>	International Energy Agency
<b>IPCC</b>	intergovernmental panel for climate change
<b>IQR</b>	interquatile range
<b>LCA</b>	life cycle assessment
<b>LCOE</b>	levelised cost of energy
<b>LFO</b>	light fuel oil

<b>LOO</b>	leave-one-out
<b>LPG</b>	liquefied petroleum gas
<b>LT</b>	low-temperature
<b>MMSA</b>	Methanol Market Services Asia
<b>MTBE</b>	methyl tert-butyl ether
<b>MTO</b>	methanol-to-olefins
<b>NED</b>	non-energy demand
<b>NG</b>	fossil gas
<b>NN</b>	neural network
<b>NRE</b>	non-renewable energy
<b>NSC</b>	naphtha steam cracker
<b>OPEX</b>	operational expenditure
<b>PC</b>	principal component
<b>PCA</b>	Principal Component Analysis
<b>PCE</b>	Polynomial Chaos Expansion
<b>PDF</b>	probability density function
<b>PV</b>	photovoltaic
<b>RE</b>	renewable energy
<b>RL</b>	reinforcement learning
<b>SAC</b>	Soft Actor Critic
<b>SDGs</b>	Sustainable Development Goals
<b>SMR</b>	small modular reactor
<b>SVD</b>	singular value decomposition
<b>UQ</b>	Uncertainty Quantification
<b>VRES</b>	variable renewable energy sources

---

---

## List of publications

Limpens, G., **Rixhon, X.**, Contino, F., & Jeanmart, H. (2024). “*EnergyScope Pathway: An open-source model to optimise the energy transition pathways of a regional whole-energy system.*” In Applied Energy, (Vol. 358). URL: <https://doi.org/10.1016/j.apenergy.2023.122501>

**Rixhon, X.**, Limpens, G., Coppitters, D., Jeanmart, H.,& Contino, F.(2022). “*The role of electrofuels under uncertainties for the Belgian energy transition.*” In Energies (Vol. 14). URL: <https://doi.org/10.3390/en14134027>

**Rixhon, X.**, Tonelli, D., Colla, M., Verleysen, K., Limpens, G., Jeanmart, H. ,& Contino, F.(2022). “*Integration of non-energy among the end-use demands of bottom-up whole-energy system models.*” In Frontiers in Energy Research, Sec. Process and Energy Systems Engineering, (Vol. 10). URL: <https://doi.org/10.3389/fenrg.2022.904777>

**Rixhon, X.**, Colla, M., Tonelli, D., Verleysen, K., Limpens, G., Jeanmart, H., & Contino, F.(2021). “*Comprehensive integration of the non-energy demand within a whole-energy system: Towards a defossilisation of the chemical industry in Belgium.*” In proceedings of ECOS 2021 conference (Vol. 34, p. 154).

**Rixhon, X.**, Limpens, G., Contino, F., & Jeanmart, H. (2021). “*Taxonomy of the fuels in a whole-energy system.*” In Frontiers in Energy Research, Sec. Sustainable Energy Systems, (Vol. 9). URL: <https://doi.org/10.3389/fenrg.2021.660073>

Limpens, G., Coppitters, D., **Rixhon, X.**, Contino, F., & Jeanmart, H. (2020). “*The impact of uncertainties on the Belgian energy system: application of the Polynomial Chaos Expansion to the EnergyScope model.*” In proceedings of ECOS 2020 conference (Vol. 33, p. 711).

---

---

## **Chapter 1**

### **Methodology: Through a variety of complementary tools**

Assessing the robustness of a whole-energy system transition pathway calls a variety of methodological tools. First and foremost, such an extensive system needs to be represented, i.e. modelled, to further be optimized. This model requires some characteristics to capture the peculiarities of this system (e.g. intermittency of variable renewable energy sources (VRES), sector coupling) while keeping an affordable computational time and an open-documentation. Then, as looking into the future (i.e. up to 2050 in this work) comes with its lot of uncertainties, these have to be assessed carefully in terms of characterisation and quantification. The former aims at defining the range over which parameters of the model vary. The latter allows assessing the impact that such uncertainties can have on the output of the model. Finally, meeting the environmental objectives while minimizing the cost of the system, accounting for this decision-making process, the uncertainties, and potential shocks/crisis, require therefore a framework to assess the relevance and the timing of the decisions throughout the transition. Finally, given the limited foresight in the uncertain future that has to deal with long-term objective, i.e. limiting the cumulative GHG emissions to a certain budget by 2050, this work encompasses the optimisation of the policy, i.e. set of actions to take along the transition with a specific methodology to assess its robustness.

Detailing the different tools needed to answer the research questions, this chapter starts with the presentation of the whole-energy system optimization model, EnergyScope Pathway and its myopic formulation. Then, the focus is put on the uncertainties, their characterisation as well as quantification. Finally, an agent-based reinforcement learning (RL) approach is detailed to address the sequential decision-making

process in the uncertain transition with limited vision in the future. The robustness of these policies is assessed via the use of the Principal Component Analysis (PCA).

## **Contributions**

The main methodological contribution of this work is the implementation of the reinforcement learning (RL) approach to simulate and optimize the behaviour of an artificial agent interacting with its environment, i.e. the transition of the energy system. Given the uncertainties and potential shocks of the future, this approach allows the agent to play the transition in a sequential, i.e. myopic, way and optimize the choice and the timing of its actions. This optimization is done through multiple tries-and-errors where the agent repeats the transition with a new set of uncertainties.

Then, to support this step-by-step transition with limited foresight in the future, we have extended the EnergyScope Pathway model [1]. Originally developed to optimize the transition in one global optimisation up to 2050, i.e. perfect foresight, part of this thesis consisted in making this model able to optimize the same transition but with sequential more limited time windows, i.e. myopic approach.

The third principal methodological added-value is the use of Principal Component Analysis (PCA) to assess the robustness of a policy. Given the uncertainties and the timespan of the transition, this approach allows highlighting the main “directions” of variation of the system design (i.e. the installed capacities). After this step of identification, strategies and policies can be projected on these directions to see how robust they are to the overall transition uncertainties.

Finally, more minor methodological developments are part of this thesis. Following an approach similar to Guevara et al. [2], we have extended the ranges of uncertainty developed by Moret et al. [3] to the pathway optimisation. After assessing the relevance of using Polynomial Chaos Expansion (PCE) on the optimisation of a whole-energy system [4], we have applied this uncertainty quantification method on the snapshot model subject to different emission-constraints Rixhon et al. [5] as well as the pathway model. Eventually, starting from the initial investigation of Goffaux [6], this work has converged to the most relevant formulation of the salvage value, i.e.  $C_{\text{inv},\text{return}}$  in Eq. 1.5, for the model EnergyScope.

## **Other authors’ main contribution statement**

Novelty does not stand in the reinvention of the wheel. This thesis, instead, finds its fundamentals in great tools previously developed by other authors. As developers of

the building blocks of the main contributions of this thesis, three main authors are to be mentioned for having brought a significant part of the methodological work. Based on Stefano Moret's monthly whole-energy system model (i.e. EnergyScope) [7], Gauthier Limpens has developed the hourly version of the snapshot model (i.e. EnergyScope TD) [8], as well as the perfect foresight pathway model [9], to which I personally contributed too. Diederik Coppitters has developed the RHEIA framework allowing to quantify the impact of uncertainties and carry out robust optimisation of energy systems [10]. The current work used this framework for the first of these functionalities. Finally, Stefano Moret extensively assessed the uncertainty characterisation on the Swiss energy system [3]. This thesis follows the same methodology, updating the uncertainty ranges for the pathway model.

## **1.1 Whole-energy system transition model optimisation: EnergyScope Pathway**

This work optimises the entire transition pathway from a known system in 2020 up to 2050 thanks to EnergyScope Pathway [9]. According to pathway models review (see Appendix A.1), EnergyScope Pathway can be categorised as an investment and operation optimisation model that assesses the whole-energy system, has a hourly time-resolution and is an open-source documented model. Moreover, it maintains a low computational cost (i.e. around 15 minutes for a 30-year pathway with a hourly discretisation). From the perfect to the myopic foresight of the transition optimisation, this section presents only the main constraints of the former approach to further dig into more details about the latter. The reader is invited to refer to Appendix A.2 for more details about the formulation of the model and its extension from a snapshot approach, EnergyScope TD. More extensive information about the formulation choices, for instance, can be found in [9] and the documentation [11].

### **1.1.1 Perfect foresight: One global optimisation of the transition**

The whole-energy system model developed in this work originates from the perfect foresight (PF) formulation (Figure 1.1) of EnergyScope—the entire transition is computed in one optimisation, assuming a complete but uncertain knowledge of the different parameters until 2050 [9]. All the variables and constraints of the snapshot model, EnergyScope TD [8], and summarized in Appendix A.2.1, are kept as is with an extra-dimension to relate them to a specific representative year,  $y$ , of the pathway. For instance, the energy balance is guaranteed at every hour of each of these years.

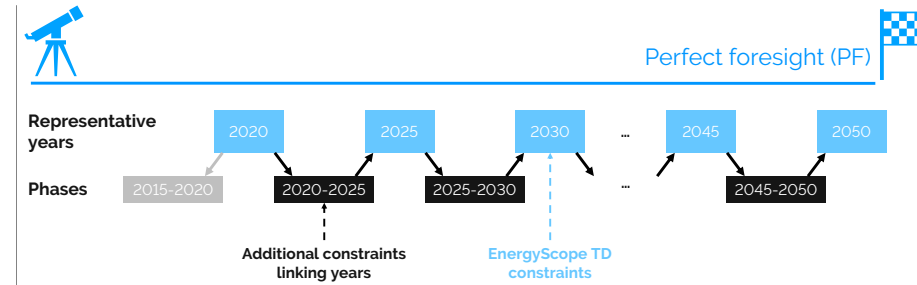


**Figure 1.1.** Illustration of the pathway methodology based on an existing energy system model. The methodology spans from 2020 to 2050, with one representative year every five years. The model EnergyScope Typical Days (EnergyScope TD) is applied in 7 representative years (light blue boxes). The formulation includes additional constraints (black boxes) that link the years together. The pathway's initialisation assumes that all capacities installed in 2020 were built during the pseudo-phase of 2015-2020 (grey box). The overall problem is defined as the pathway model.

The optimised objective of the pathway model, i.e. the total transition cost  $C_{\text{tot,trans}}$ , is computed as follows:

$$\min C_{\text{tot,trans}} = C_{\text{tot,capex}} + C_{\text{tot,opex}} \quad (1.1)$$

$$C_{\text{tot,capex}} = \sum_{p \in \text{PHASE} \cup \{2015\_2020\}} C_{\text{inv,phase}}(p) - \sum_{j \in \text{TECH}} C_{\text{inv,return}}(j) \quad (1.2)$$

$$C_{\text{tot,opex}} = C_{\text{opex}}(2020) + t_{\text{phase}} \cdot \tau_{\text{phase}}(p) \cdot \sum_{p \in \text{PHASE} | y_{\text{start}} \in P_{\text{START}}(p), y_{\text{stop}} \in P_{\text{STOP}}(p)} \left( C_{\text{opex}}(y_{\text{start}}) + C_{\text{opex}}(y_{\text{stop}}) \right) / 2 \quad (1.3)$$

$$\tau_{\text{phase}}(p) = 1 / (1 + i_{\text{rate}})^{\text{diff\_2015\_year}(p)} \quad (1.4)$$

$$C_{\text{inv,return}}(i) = \sum_{p \in \text{PHASE} \cup \{2015\_2020\} | y_{\text{start}} \in Y_{\text{START}}(p), y_{\text{stop}} \in Y_{\text{STOP}}(p)} \tau_{\text{phase}}(p) \cdot (c_{\text{inv}}(y_{\text{start}}, i) + c_{\text{inv}}(y_{\text{stop}}, i)) / 2 \cdot \frac{\text{remaining\_years}(i, p)}{\text{lifetime}(y_{\text{start}}, i)} \left( \mathbf{F}_{\text{new}}(p, i) - \sum_{p2 \in \text{PHASE}} \mathbf{F}_{\text{decom}}(p2, p, i) \right) \quad \forall i \in \text{TECH} \quad (1.5)$$

where  $t_{\text{phase}} = 5$  years and  $\text{diff\_2015\_year}(p)$  are respectively the duration of a phase between two representative years and the number of years between the middle of a phase and 2015 for a correct annualisation.  $C_{\text{inv,return}}$  accounts for the residual value, also called *salvage value*, of the technologies installed during the transition and having

not reached the end of their lifetime by 2050. This last variable is crucial to avoid penalising heavy (and potentially long-lifetime) investments at the end of the transition as these assets would still be operational beyond 2050. The interested reader will find more information about the formulation choices related to it in the work of Limpens et al. [9]. The other variables in Eq. (1.2-1.3) are detailed here below:

$$C_{\text{opex}}(y) = \sum_{j \in TECH} C_{\text{maint}}(y, j) + \sum_{i \in RES} C_{\text{op}}(y, i) \quad \forall y \in YEARS \quad (1.6)$$

$$C_{\text{inv,phase}}(p) = \sum_{j \in TECH} F_{\text{new}}(p, j) \cdot \tau_{\text{phase}}(p) \cdot (c_{\text{inv}}(y_{\text{start}}, j) + c_{\text{inv}}(y_{\text{stop}}, j)) / 2$$

$$\forall p \in PHASE | y_{\text{start}} \in P\_START(p), y_{\text{stop}} \in P\_STOP(p) \quad (1.7)$$

where  $F_{\text{new}}$  are the capacities newly installed. In Eq. (1.6-1.7), the costs related to each representative year are:

$$C_{\text{inv}}(y, j) = c_{\text{inv}}(y, j)F(y, j) \quad \forall y \in YEARS, \forall j \in TECH \quad (1.8)$$

$$C_{\text{maint}}(y, j) = c_{\text{maint}}(y, j)F(y, j) \quad \forall y \in YEARS, \forall j \in TECH \quad (1.9)$$

$$C_{\text{op}}(y, i) = \sum_{t \in T} c_{\text{op}}(y, i)F_t(y, i, t)t_{\text{op}}(t) \quad \forall y \in YEARS, \forall i \in RES \quad (1.10)$$

where the variable  $F$  represents the size of the installed capacities (for all technologies  $j$ ) and the variable  $F_t$  is the hourly consumption of the resources; the parameters  $c_{\text{inv}}$  and  $c_{\text{maint}}$  are the CAPEX and the OPEX of the technologies, and the parameter  $c_{\text{op}}$  is the cost of purchasing resources. For the sake of simplicity, as done by Limpens et al. [9], the sum over the 8760 hours of the year is written as the sum over  $t \in T$ .

Then, as detailed in section 2.5, the CO<sub>2</sub>-budget for the transition,  $\mathbf{GWP}_{\text{tot,trans}}$ , is computed and constrained as follows:

$$\mathbf{GWP}_{\text{tot,trans}} = \mathbf{GWP}_{\text{tot}}(2020) + t_{\text{phase}} \sum_{p \in PHASE | y_{\text{start}} \in P\_START(p), y_{\text{stop}} \in P\_STOP(p)} (\mathbf{GWP}_{\text{tot}}(y_{\text{start}}) + \mathbf{GWP}_{\text{tot}}(y_{\text{stop}})) / 2 \quad (1.11)$$

$$\mathbf{GWP}_{\text{tot,trans}} \leq gwp_{\text{lim,trans}} \quad (1.12)$$

where the computation of the yearly emissions are based on the global warming potential (GWP) of the resources:

$$\mathbf{GWP}_{\text{tot}}(y) = \sum_{i \in RES} \mathbf{GWP}_{\text{op}}(y, i) \quad \forall y \in YEARS \quad (1.13)$$

$$\mathbf{GWP}_{\text{op}}(y, i) = \sum_{t \in T} gwp_{op}(y, i, t) \mathbf{F}_t(y, i, t) t_{op}(t) \quad \forall y \in \text{YEARS}, \forall i \in \text{RES} \quad (1.14)$$

where  $gwp_{op}$  is the specific emissions (i.e. in  $\text{kt}_{\text{CO}_2,\text{eq}}/\text{GWh}$ ) of each resource. Based on an approach developed by the Intergovernmental Panel on Climate Change (IPCC) [12], this work considers the indicator “GWP100a - IPCC2013” to compute the emissions related to the use of resources. This includes the emissions due to the extraction, the transportation and the combustion of the energy carrier. EnergyScope proposes to account for the embodied emissions of the technologies based on a life cycle assessment (LCA). These stand for extraction of materials, refining, construction and end of life [13]. However, this work is still in progress and the database is not yet complete. Consequently, it is not included in this work and not accounted for.

Besides this constraint on the emissions, the main constraint to link years with each other is the one dictating the installed capacities at the end of each year:

$$\mathbf{F}(y_{\text{stop}}, j) = \mathbf{F}(y_{\text{start}}, j) + \mathbf{F}_{\text{new}}(p, j) - \mathbf{F}_{\text{old}}(p, j) - \sum_{p2 \in \text{PHASE} \cup \{2015\_2020\}} \mathbf{F}_{\text{decom}}(p, p2, j)$$

$$\forall p \in \text{PHASE}, y_{\text{stop}} \in Y\_STOP(p), y_{\text{start}} \in Y\_START(p), j \in \text{TECH} \quad (1.15)$$

where the variables  $\mathbf{F}_{\text{old}}$  and  $\mathbf{F}_{\text{decom}}$  are the capacities respectively having reached the end of their lifetime and prematurely decommissioned. Moreover, to account for the society inertia and to prevent unrealistically fast modal share change, constraints limit this change for the sectors of the low-temperature, the passenger mobility and freight mobility demands. The parameters  $\Delta_{\text{change,LT\_heat}}$ ,  $\Delta_{\text{change,pass}}$  and  $\Delta_{\text{change,freight}}$  respectively limit their respective modal share change up to 33%, 50% and 50% per phase of 5 years.

### **1.1.2 Myopic: Sequential optimisation of the transition with limited foresight**

One of the main methodological contributions of this work regarding the development of the whole-energy system model consists in giving it the possibility to optimise the transition pathway in a myopic approach. After introducing the general concept of it, this section details more the additions brought to the model in terms of implementation.

#### **General concept of the myopic optimisation**

Compared to the perfect foresight, the myopic approach (Figure 1.2) has two main advantages: shorter computational time and more realistic representation of the short-sightedness of decision-makers. For this reason, several studies are based on this ap-

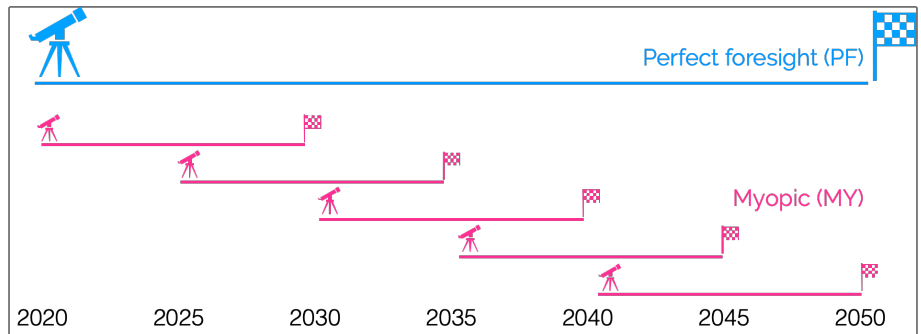


**Figure 1.2.** The myopic approach (in pink) uses several instances of the pathway model (illustrated in Figure A.4). In this example, the pathway instance has a time horizon of 10 years ( $N_{\text{year, opti}} = 10$ ) with a 5 year-overlap ( $N_{\text{year, overlap}} = 5$ ). As a comparison the Perfect foresight (in blue) has a time horizon of 30 years.

proach [14–17]. Babrowski et al. [14] analysed the benefit of the myopic approach to reduce the computational time. Poncelet et al. [15] uses this approach to analyse the expansion planning of the power sector beyond 2050. Nerini et al. [16] analysed the impact of the horizon windows and overlapping time. Overall these studies decided to choose the myopic approach to analyse the speed of change compared to a perfect foresight approach. Moreover, the myopic approach allows a sequential optimisation process that opens the doors to decision-making/policy-learning methodologies, like assessing shock events. This approach is used by Heuberger et al. [17] who assessed the speed of integration of technologies due to these events. In their analysis of the overcapacity in European power systems, Moret et al. [18] emphasised that such a “possibility of *recourse*” is very appropriate to address uncertainty gradually unfolding over time. Consequently, the development of the myopic approach represents the foundations of the further implementation of the agent-based reinforcement learning framework (see Section 1.3).

As illustrated in Figure 1.3, after optimising, in design and operation, one time window (e.g. from 2020 to 2030), the intermediate system design (i.e. the installed capacities) is set as initial conditions for the start of the next time window (e.g. from 2025 to 2035) as well as the historical investment decisions (i.e.  $\mathbf{F}_{\text{new}}$ ,  $\mathbf{F}_{\text{old}}$  and  $\mathbf{F}_{\text{decom}}$ ). Consequently, the solution obtained at the end of the first time window (e.g. 2030) as well as potential investment decisions between the start of the second time window and this end-year are discarded. In other words, they are not taken into account for the optimisation of the second time window. This process goes on until the stated end of the transition (i.e. 2050, in this case).



**Figure 1.3.** Sequential optimisation of the transition pathway in the myopic approach: (i) first time-window optimisation, (ii) set-up of the initial conditions of the second time-window, (iii) second time-window optimisation discarding intermediate results

#### Additional sets, parameters and variables

The major add-on from the original EnergyScope Pathway model [1] to the myopic version developed in this thesis, is the possibility to carry out the optimisation on a limited time window, of which the duration is defined by  $N_{\text{year,opti}}$ . Moreover, to ensure the “possibility of *recourse*”, there is also the possibility of having an overlap between two consecutive time windows. The timespan of this overlap is defined by the parameter  $N_{\text{year,overlap}}$ . The philosophy followed behind the development of the myopic approach was to add another layer on top of the perfect foresight model in order to make it more modular. For this reason, the already existing constraints are marginally adapted. This way, the newly developed model can easily be used to perform a perfect foresight optimisation by setting the time window to  $N_{\text{year,opti}} = 30$  years (i.e. between 2020 and 2050) and the overlap between the time windows to  $N_{\text{year,overlap}} = 0$ . Consequently, as defining the actual time window on which the system is optimised as well as the history, i.e. what has already been optimised earlier in the transition, are fundamental, four new sets are implemented:  $\text{YEARS}_{\text{WND}}$ ,  $\text{YEARS}_{\text{UP TO}}$ ,  $\text{PHASE}_{\text{WND}}$  and  $\text{PHASE}_{\text{UP TO}}$  (see Table 1.1).

$\text{YEARS}_{\text{WND}}$  and  $\text{PHASE}_{\text{WND}}$  substitute  $\text{YEARS}$  and  $\text{PHASE}$  in the constraints defined in the pathway model in Section 1.1.1. These two sets aim at setting the optimization to a more limited time window. Progressing through the transition,  $\text{YEARS}_{\text{UP TO}}$  and  $\text{PHASE}_{\text{UP TO}}$  allow keeping track of the history of the investments (e.g. technologies installation, decommissioning or retirement), the consumption of resources, the cumulative amount of emissions, etc.

On top of these four specific sets, some artefacts were also necessary to avoid computational rounding errors. Indeed, optimizing the first year of a time window that has already been optimized in the previous time window could lead to rounding errors

**Table 1.1.** New SETs for myopic pathway formulation.

<b>Set</b>	<b>Index</b>	<b>Description</b>
YEARS <sub>WND</sub>	$y \in Y$	Representative years of the time window to optimize
YEARS <sub>UP TO</sub>	$y \in Y$	Representative years including the years already optimised, i.e. the history
PHASE <sub>WND</sub>	$p \in P$	Phases of the time window to optimize
PHASE <sub>UP TO</sub>	$p \in P$	Phases including the phases already optimised, i.e. the history

preventing from the optimization to converge. For this reason, the set YEAR<sub>ONE</sub> accounts for the first representative year of the time window to optimize that is excluded from YEARS<sub>WND</sub> to avoid these errors. This remark stays valid for any time window except the first one of the transition where the year 2020 is optimized even though its technological strategy is set according to the actual system presented in Appendix B.1. Finally, as the end of time windows changes for each of them, the parameter *remaining\_years* has to be updated accordingly to keep a meaningful definition of C<sub>inv,return</sub> in Eq. 1.5.

### Myopic pathway implementation

Starting this work in 2017, AMPL Optimization Inc. has developed a Python application programming interface (API) called amplpy [19]. In a nutshell, this API allows the pre/post-processing of an ampl optimisation problem by accessing its features (e.g. constraints,parameters, variables, objective function) from within Python. Using this API, this updated version of the model interacts with the AMPL problem representing the optimization of the whole-energy system transition pathway as represented in Figure 1.4.

### Impact of myopic formulation on the system

As expected, the computational time is reduced drastically (i.e. by 55%) while the design remains similar. Given the continuous change of the input parameters over the considered time frame, the perfect foresight and myopic approaches results are very similar, like in [20]: less than 1% cost difference over the transition, similar system designs by 2050 and slight shifts in time in terms of adoption of technologies.

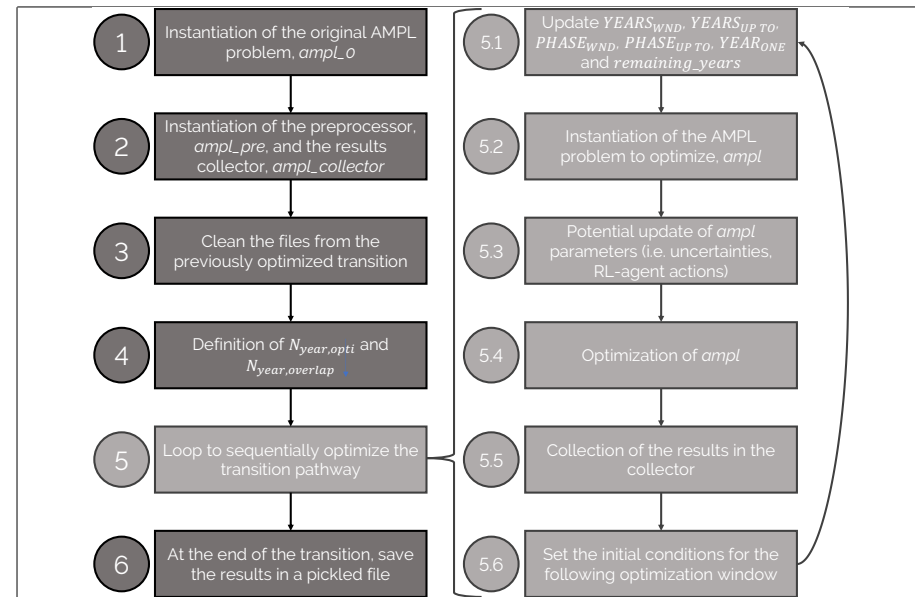


**Figure 1.4.** Schematic of the iterative optimization of the whole-energy system transition pathway.

The main difference lies in the transition itself and especially in the earlier deployment of PVs and offshore wind turbines. These induce the reinforcement of the grid that is a capital-intensive and long-lifetime asset. This is mostly due to the chosen formulation of the salvage value, Eq. 1.5. Since the objective function is now the transition cost over a more limited time window (i.e. 10 years rather than 30 years), a bigger salvage value, deduced from the total investments, leads to a temporary better optimum at early stages of the transition. A more detailed comparison between the myopic and perfect foresight approaches is available in Appendix B.3.

## 1.2 Uncertainty quantification

In their systematic review, Yue et al. [21] highlighted that a wide majority of studies addressing the optimisation of energy systems (i.e. 75% out of the 134 reviewed studies) were not investigating the impact of uncertainties. However, disregarding these impacts can have drastic consequences on the system design. For instance, historical low fossil gas (NG) prices have led to overcapacity of combined cycle gas turbine (CCGT) in Europe [18]. This is why accounting for uncertainty in energy system optimisation

models (ESOMs) is crucial [22], especially when it comes to optimise several decades in an inherently uncertain future [23].

This section aims at briefly presenting the methods followed to first characterise these uncertainties, then to quantify their impact on different outputs of interest of the model (e.g. amount of molecules imported from abroad, the installed capacity of SMR or the total transition cost) and finally, the screening and selection of the parameters to analyse.

### 1.2.1 Uncertainty characterisation

Characterising precisely the uncertainty—ideally with their respective probability density functions (PDFs)—of the thousands of parameters in the model is daunting if not impossible because of lack of data [24]. Therefore, we used a workaround developed by Moret et al. [3] that defines relative ranges of variation for different groups of parameters. These ranges have been adapted for the Belgian energy system and the pathway formulation. Moreover, some ranges have been added to account for new parameters coming from the pathway formulation described in Section 1.1 like the society inertia. Like other works [25, 26], the uncertain parameters are assumed to be independent and uniformly distributed between their respective lower and upper bounds.

Following the methodology defined by Moret et al. [3], uncertainties of types I (investment-type) and II (operation-type, constant uncertainty over time) keep the same range for the whole transition. However, parameters with an uncertainty increasing over time, type III, (i.e. end-use demands, in this case) will have a wider and wider range over the transition. In this work, a +50% linear increase has been arbitrarily set between the width of the range of such parameters in 2025 and the same ranges in 2050. In Figure 1.5, this means that for type III uncertainties only,  $R_{2050}^+$  is 50% bigger than  $R_{2025}^+$  and  $R_{2050}^-$  is 50% smaller than  $R_{2025}^-$ . For uncertainties of types I and II, the relative variation versus the nominal value remain the same over the transition. Inspired by Guevara et al. [2], the values of the uncertain parameters are set at a fixed relative position from the nominal values for each sampled transition—the values do not zigzag from 2025 to 2050 within the bounds (Figure 1.5).

Finally, the model accounts for thousands of parameters. The computational burden to consider all of them separately would be completely overwhelming ( $\sim 10^7$  model runs). Therefore, similarly to other works [3, 4], the model parameters that would follow the same uncertainty have been grouped to one single uncertain parameter. For instance, the uncertainty on the cost of purchasing renewable electrofuels,  $c_{\text{op,electrofuels}}$ , identically affects the cost of e-hydrogen, e-methane, e-ammonia and

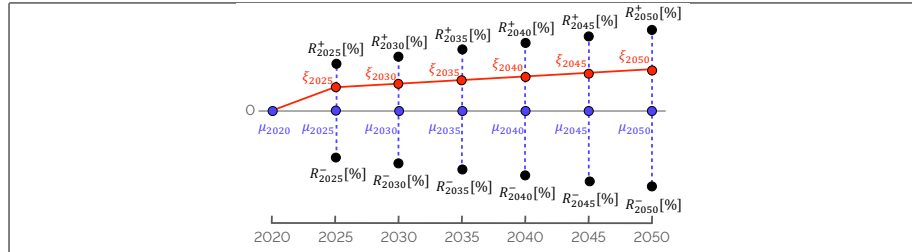


**Figure 1.5.**  $\mu_{2020}, \mu_{2025}, \dots, \mu_{2050}$  are the nominal values equal to 0 as the uncertain parameters represent a relative increase/decrease of actual parameters of the model.  $R^+$  and  $R^-$  are respectively the upper and lower bounds of the range and  $\xi_{2025}, \xi_{2030}, \dots, \xi_{2050}$  are the values taken by one parameter for a specific sample of the global sensitivity analysis (GSA) for each of the representative years of the transition, always starting from the nominal value in 2020,  $\mu_{2020}$ . The graph has been adapted from [2].

e-methanol. Indeed, besides their respective specificities, each of these fuels will be similarly affected by the variation of cost of electricity or the electrolyser, that drive the majority of their cost of purchasing [27]. Similarly, the uncertainties impacting the industrial demand, *industry\_EUD*, alters equally the industrial high- and low-temperature and electricity demands as well as the non-energy demand.

### 1.2.2 Polynomial Chaos Expansion

We used Polynomial Chaos Expansion (PCE), an approach for surrogate-assisted Uncertainty Quantification (UQ), to propagate uncertainties in input parameters through the system model. This allowed us to assess statistical moments on the quantity of interest and determine Sobol' indices [28]. To construct a PCE of the EnergyScope Pathway model, we employed the open-source Python framework RHEIA [29, 30]. Where the first part of this section is dedicated to the mathematical definition of this approach, the second details its choice and summarises the comparison made with another approach (i.e. Morris method) in a previous work [4].

#### Definition

The PCE model ( $\hat{M}$ ) is a representation of the relationship between the input parameters and the output variable of interest (i.e. results) in the EnergyScope Pathway model ( $M$ ). This representation is constructed as a truncated series of multivariate orthonormal polynomials  $\Psi$ , weighted by coefficients  $u$ :

$$\hat{M}(\xi) = \sum_{\alpha \in \mathcal{A}^{d,p}} u_\alpha \Psi_\alpha(\xi) \approx M(\xi), \quad (1.16)$$

where the vector  $\xi = (\xi_1, \xi_2, \dots, \xi_d)$  comprises the independent random input parameters (section B.5),  $d$  corresponds to the number of input distributions and  $\alpha$  is a multi-index, i.e. a vector of non-negative indices of length  $d$ , where each index corresponds to the degree of each univariate polynomial that forms the basis of the multivariate polynomial  $\Psi_\alpha$ . As uniform distributions are considered, the Legendre polynomials are adopted, as they are the associated family of polynomials that are orthogonal with respect to standard uniform distributions [31].

A truncation scheme is implemented to restrict the number of multivariate polynomials in the series. This is done based on two factors: a specified limiting polynomial order ( $p$ ) and the number of uncertain parameters ( $d$ ) involved. The multivariate polynomial order  $|\alpha|$  is the summation of the orders for each univariate polynomial in the multivariate polynomials space. Thus, only the multi-indices corresponding to an order that is less than or equal to the specified limiting order are retained and stored in the truncated series denoted as  $\mathcal{A}^{d,p}$ :

$$\mathcal{A}^{d,p} = \{\alpha \in \mathbb{N}^d : |\alpha| \leq p\}. \quad (1.17)$$

The number of multi-indices satisfying this condition is as the cardinality of  $\mathcal{A}$ , i.e. the number of its elements:

$$\text{card}(\mathcal{A}^{d,p}) = \binom{p+d}{p} = \frac{(d+p)!}{d!p!} = P+1. \quad (1.18)$$

The coefficients  $(u_0, u_1, \dots, u_{P+1})$  are quantified using a regression method applied to orthonormal polynomials [31]. To ensure a well-posed least-square minimisation, it is recommended to have a number of training samples at least twice the number of coefficients [31]. Therefore,  $2(P+1)$  samples are evaluated in the system model, and the model response for each quantity of interest is recorded. To generate the training samples, the quasi-random Sobol' sampling technique is employed [32]. As a low-discrepancy sequence, this technique exhibits the main advantage to investigate efficiently and (almost) uniformly the hypercube of uncertainties, unlike uniformly distributed random numbers.

The process of defining the polynomial degree includes incrementally increasing it until a desired level of accuracy is achieved [29]. Starting with  $p = 1$ , a PCE is constructed and the leave-one-out (LOO) error is evaluated. If the LOO error is below a specified threshold, the corresponding polynomial order is considered sufficient for

generating an accurate PCE. However, if the error exceeds the threshold, the order is increased, and additional samples are generated following the rule of Eq.(1.18).

For the specific study of this work, a polynomial order of 2 is necessary (with 1260 training samples as per Eq. (1.18)) to achieve a LOO error below 1 % for the total transition cost.

Lastly, the statistical moments can be analytically derived from the PCE coefficients, eliminating the need for further model evaluations. The mean  $\mu$  and standard deviation  $\sigma$  are obtained as follows:

$$\mu = u_0, \quad (1.19)$$

$$\sigma^2 = \sum_{i \neq 0} u_i^2. \quad (1.20)$$

Furthermore, the Sobol' indices can also be determined analytically. The total-order Sobol' indices ( $S_i^T$ ) assess the overall influence of a stochastic input parameter on the performance indicator, encompassing all possible interactions:

$$S_i^T = \sum_{\alpha \in A_i^T} u_\alpha^2 / \sum_{i=1}^P u_i^2 \quad A_i^T = \{\alpha \in A | \alpha_i > 0\}. \quad (1.21)$$

Here,  $A$  denotes the collection of all PCE coefficients, and  $\alpha_i$  corresponds to the coefficient associated with the uncertain parameter  $i$ .

### Comparison with a proven method

Besides being an in-house used method, an early step of this thesis consisted in assessing PCE with similar approach used in the literature [4].

After characterising the uncertainty ranges, Moret et al. [3] quantified the impact of these uncertainties on the snapshot model of EnergyScope, i.e. ranking them, using the Morris method [33]. This method, as a statistical analysis, relies on individually randomized one-factor-at-a-time designs. Given the  $d$  model parameters  $\vec{\xi} = (\xi_1, \xi_2, \dots, \xi_d)$ , the first step of the method consists in generating independent random samples of  $\vec{\xi}$  in a standardised and discretised  $p$ -level *region of experimentation*,  $\omega$ . In this *region of experimentation*, each  $\xi_i$ , varying in the interval  $[\xi_{i,\min}, \xi_{i,\max}]$ , can take a random discrete value as follows :

$$\xi_i = \xi_{i,\min} + j \cdot \frac{1}{p-1} (\xi_{i,\max} - \xi_{i,\min}) \quad \text{with } j \in \{0, 1, \dots, p-1\} \quad (1.22)$$

Then, given these random one-factor-at-a-time samples, Morris method defines, for a given set of  $\vec{\xi}$ , the elementary effect of the  $i$ th parameter ( $EE_i$ ) as :

$$EE_i = \frac{M(\xi_1, \xi_2, \dots, \xi_i + \Delta, \dots, \xi_d) - M(\vec{\xi})}{\Delta} \quad (1.23)$$

where  $M$  is the objective function,  $\vec{\xi} \in \omega$ , except  $\xi_i \leq 1 - \Delta$  and  $\Delta$  is a set multiple of  $1/(p-1)(\xi_{i,max} - \xi_{i,min})$ . As in other studies [3, 34, 35], we consider  $p$  as even and  $\Delta = p/[2(p-1)](\xi_{i,max} - \xi_{i,min})$ .

Finally, in order to evaluate the importance of the  $i$ th parameter over an output, Morris method relies on  $F_i$ , the distribution of  $r$  elementary effects. Computing the mean,  $\mu_i = \mu(F_i)$ , and the standard deviation,  $\sigma_i = \sigma(F_i)$ , of the  $F_i$  distribution, allows ranking the parameters based on their influence on the concerned output. Usually, in Morris method,  $p$  and  $r$  respectively get values as follows :  $p \in \{4, 6, 8\}$  and  $r \in [15; 100]$  depending on,  $d$ , the number of uncertain parameters. The higher this number is, the higher shall be, simultaneously,  $p$  and  $r$ . In the following comparative analysis, we set  $p$  and  $r$  to their maximum values, respectively 8 and 100 in order to get the most reliable parameters ranking.

Beyond the original Morris method, we used the standardized elementary effects,  $SEE_i$ , formulation [34], given by

$$SEE_i = EE_i \cdot \frac{\sigma(\xi_i)}{\sigma(M)}. \quad (1.24)$$

Among other things, the  $SEE$  allows comparing the influence of different inputs on the same output or compare the influence of a same parameter on different outputs, even if these parameters or outputs are significantly different in terms of variation range or average amplitude. Moreover, this standardized analysis does not require any additional model evaluations.

Therefore, in the following results, we rather use

$$\mu_i^* = \mu(|SF_i|) \quad (1.25)$$

to rank parameters among each other. In (1.25),  $SF_i$  is the distribution formed by the  $r$  standardized elementary effects, as done in Moret [35].

In [4], we have assessed the PCE approach, comparing the Top-14 most impacting parameters obtained from this approach with the one provided by the improved Morris method based on  $\mu_i^*$ . Even if the output of each method does not have the same physical

meaning, both methods can rank the parameters by their impact on the total annual cost of the energy system. Both rankings were very similar which validates the use of PCE in the rest of this work.

### **1.2.3 Preliminary screening and selection**

After the initial phase of grouping (Section 1.2.1), a preliminary screening was necessary to identify the key parameters to account for in this GSA. Rixhon et al. [5] performed a similar sensitivity analysis on the 2050 Belgian whole-energy system under different CO<sub>2</sub>-limits using the snapshot model, i.e. EnergyScope TD [8]. Screening the results of this work, we have discarded some parameters with negligible impact (e.g. CAPEX of electrolyzers or variation of the freight demand), selected a subset of parameters and added others that were intrinsic to the pathway formulation, e.g. modal share changes, or related to the integration of SMR,  $f_{\max,SMR}$ . The exhaustive list of these 34 parameters is presented in Appendix B.5.

## **1.3 Agent-based reinforcement learning for energy transition support**

The transition towards carbon-neutrality of a whole-energy system (i.e. including all streams of energy carriers and demands) is uncertain. Therefore, instead of establishing single-shot definitive plans towards 2050 (and beyond), i.e. perfect foresight, policy makers rather go through multiple rolling-horizon short-term decisions, i.e. myopic approach. Yet, these decisions can have long-term impacts, 20 to 50 years. Meeting the environmental objectives while minimizing the cost of the system, accounting for this decision-making process, the uncertainties, and potential shocks/crisis, require therefore a framework to assess the relevance and the timing of the decisions throughout the transition. To navigate through the transition and investigate the efficiency of different policies, this work implements the reinforcement learning approach. This section aims first at presenting the general concepts of this approach as well as the policy optimisation algorithm. Then, the environment, actions, state and reward are detailed.

### 1.3.1 Reinforcement learning fundamentals and application to energy systems

### 1.3.2 Problem formulation and algorithm

At the initial state, i.e. the energy system in 2020, the agent gets an initial observation,  $o_0$ . An observation represents a set of the characteristics of the environment accessible to the agent for it to take the next action. The state, though, is the exhaustive list of these characteristics. Even though an observation is a subset of the state, this work uses these two words interchangeably. Then, it takes an action,  $a_0$ , impacting its environment, i.e. the energy system limited transition over the first decision window (2020-2030). Through this interaction with its environment, the agent is given a reward,  $r_1 = r(a_0|o_0)$ , and ends up in a new state, i.e. the energy system in 2025, characterised by a new observation,  $o_1$ , and so on (see Figure 1.6).

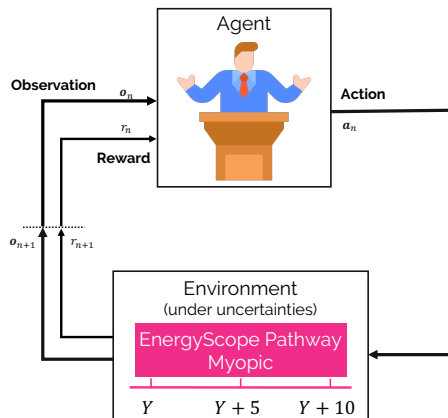


**Figure 1.6.** Reinforcement learning (RL) framework made of the agent interacting with its environment, i.e. the energy-system model on a limited decision window of 10 years.

A learning episode is a succession of such learning steps. In the context of the transition pathway between 2020 and 2050, an episode can come to an end for different reasons. First, if the actions taken by the agent make the optimisation unfeasible, the episode is prematurely stopped before reaching 2050. Similarly, cumulative emissions of the system over the predefined CO<sub>2</sub>-budget (see Section 2.5) lead to an anticipated end of the episode. Finally, the “natural” end is the prescribed end of the transition, i.e. 2050. Consequently, the maximum value of steps for an episode is equal to  $N_{ep,max} = 5$ .

The goal of a RL approach is to optimise the mapping between inputs (i.e. the observations) and output (i.e. the actions), called the policy  $\pi(\mathbf{a}_n|\mathbf{o}_n)$ . To do so, an objective function,  $J(\pi)$ , built on the cumulative rewards collected during each episode. Finally, a back-propagation process updates the weights and biases of the neural network (NN) during the learning of the agent. Among the wide variety of RL algorithms applied in energy systems [36], this work opted for Soft Actor Critic (SAC) [37] to train and update the NN. This algorithm is model-free and off-policy. The former characteristic is necessary as the agent is assumed to have no knowledge about the dynamics of the environment, i.e. its transition or reward functions. The transition function is, given the current state of the environment and the action taken by the agent, a function that outputs a probability to end up to any of the next states. The reward function, on its turn, gives a reward given the current state and the taken action. In practice, in this model-free approach, the agent estimates the optimal policy directly from experience and without estimating the dynamics of the environment. However, model-free methods suffer from two major drawbacks: their sample inefficiency and their brittleness with respect to their hyper-parameters (e.g. learning rates, exploration constants) [37]. The former leads to a too expensive computational burden while the second requires meticulous settings to get good results. SAC overcomes these two challenges as an off-policy (i.e. efficiently re-using past episodes to update the target policy-network) actor-critic deep RL algorithm based on the entropy-augmented objective function:

$$J(\pi) = \mathbb{E}_{\pi} \left[ \sum_{n=0}^{N_{ep}} \gamma^n r_n(\mathbf{o}_n, \mathbf{a}_n) - \zeta \log(\pi(\mathbf{a}_n|\mathbf{o}_n)) \right] \quad (1.26)$$

where  $\gamma$  is the discount factor and  $\zeta$  the temperature parameter. The former determines how much importance we want to give to future rewards within an episode. The latter balances the trade-off between exploitation of proven actions via the return maximisation, i.e.  $\sum_{n=0}^{N_{ep}} \gamma^n r_n(\mathbf{o}_n, \mathbf{a}_n)$ , and exploration through the entropy<sup>1</sup> term, i.e.  $\log(\pi(\mathbf{a}_n|\mathbf{o}_n))$ . This way, SAC ensures sample efficiency and low sensitivity to hyper-parameters while improving exploration [38] and robustness [39]. These make SAC a state-of-the-art algorithm and one of the most efficient model-free deep RL method nowadays. In this work, the authors used the open-source SAC package developed by STABLE-BASELINES3 [40] where the policy NN is a fully connected multilayer perceptron (MLP) built with TENSORFLOW [41]. For further information on RL and

---

<sup>1</sup>Where entropy represents the amount of energy in a system not available to produce work in thermodynamics, this term stands for the randomness or stochasticity of the policy in the current context.

the SAC algorithm, the interested reader is invited to refer to the works of Sutton and Barto [42] and Haarnoja et al. [37], respectively.

## 1.4 Robustness assessment via PCA

When optimizing a transition pathway of a whole-energy system, including its uncertainties, capturing the most variable changes of design (i.e. installed capacities of each technology) can become overwhelming due to the curse of dimensionality. For the case study detailed in Chapter 2, this consists of i.e. 7 representative years of the transition (i.e. from 2020 to 2050), 113 possible technologies subject to uncertain parameters. To tackle this challenge, we have developed a methodology based on the Principal Component Analysis (PCA). This methodology provides two main outputs. First and foremost, using the model runs necessary to quantify the impact of the uncertain parameters on the total cost of the transition (see Section 1.2), it gives a metric on which to assess the robustness of energy transition policies resulting from different approaches. This metric gives more insight that, for instance, the variation of the total transition cost that encompasses too many aspects (i.e. design and operation strategies, variation along the transition) in one single value. Second, these “directions of variation” can highlight key modal shifts or highly varying design strategies over the transition. After introducing the general concept of PCA, this section aims at detailing the methodology proposed to give these “directions of variation” and to assess the robustness of policies.

### 1.4.1 Principal Component Analysis: General concept

Born in the early 20th century [43, 44], the Principal Component Analysis (PCA) finds its fundamentals from the singular value decomposition (SVD). The latter is a generalization, to an arbitrary (i.e. not especially square) matrix, of the spectral theorem stating that a normal matrix can be diagonalized by an orthonormal basis of eigenvectors. The core concept of principal component analysis (PCA) involves simplifying a dataset with numerous interconnected variables by reducing its dimensionality. The aim is to preserve as much variability within the data as feasible. This is accomplished by transforming the data,  $\mathbf{x}$ , into a new set of variables called principal components (PCs),  $\mathbf{z}$ . These components are uncorrelated and arranged in such a way that the first ones retain the majority of the variability found in all of the original variables. On the other hand, the final principal components (PCs) pinpoint directions where there is

minimal variation, indicating nearly constant linear relationships among the original variables [45].

Easier to represent in two dimensions, let us consider a vector  $\mathbf{x}$  composed of the variables  $x_1$  and  $x_2$ ,  $p = 2$ , and 25 realisations of them (See Figure 1.7 (left)). The first principal component (PC),  $z_1$ , is a linear function,  $\alpha_1^T \mathbf{x}$ , of the different variables of  $\mathbf{x}$  with maximum variance:

$$z_1 = \alpha_1^T \mathbf{x} = \alpha_{11}x_1 + \alpha_{12}x_2 + \dots + \alpha_{1p}x_p = \sum_{j=1}^p \alpha_{1j}x_j \quad (1.27)$$

where  $T$  means the transpose vector. Then,  $z_2 = \alpha_2^T \mathbf{x}$ , is another linear function of  $\mathbf{x}$ , uncorrelated with  $z_1$  and maximizing the variance. These transformations lead to the construction of the PCs (see Figure 1.7 (right)). In more general cases, one can write  $z_k = \alpha_k^T \mathbf{x}$  as the  $k^{\text{th}}$  PC. There can be up to  $p$  PCs even though, usually, most of the variance of the original data can be captured by  $m$  PCs where  $m \ll p$ .

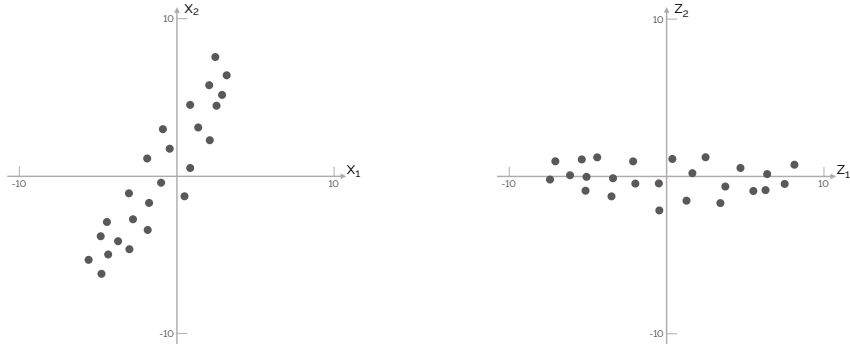


**Figure 1.7.** Original observations of the dataset (left) and their projection with respect to their PCs (right). The variation of the realisations is more significant in the direction of  $x_2$  than  $x_1$ . Once projected with respect to their PCs, the variation is even more significant in the direction of  $z_1$  than in either of the original variables, as it captures most of their variance. Graph adapted from [45].

The PCs are computed based on the covariance matrix of  $\mathbf{x}$ ,  $\Sigma$ . The diagonal of this matrix gives the variance of the  $i^{\text{th}}$  variable whereas the other elements give the covariance between the  $i^{\text{th}}$  and the  $j^{\text{th}}$  variables where  $i \neq j$ . Out of this matrix,  $\alpha_k$  is the eigenvector of  $\Sigma$  corresponding to its  $k^{\text{th}}$  highest eigenvalue  $\lambda_k$ . Finally, as the  $\alpha_k$  for all  $k = 1, 2, \dots, p$  are normalized, i.e.  $\alpha_k^T \alpha_k = 1$ ,  $\text{var}(z_k) = \lambda_k$ , where  $\text{var}(z_k)$  is the variance of  $z_k$ . In other words,  $\alpha_{ki}$ , i.e. the components of  $\alpha_k$ , give the weight of the  $i^{\text{th}}$  original variable,  $x_i$ , in the  $k^{\text{th}}$  PC, i.e.  $z_k$ , where  $\lambda_k$  gives the variance of the

original data captured by  $z_k$ . In other words, a high absolute value of  $\alpha_{ki}$  means that  $x_i$  has a significant impact in the direction given by the  $k^{\text{th}}$  PC [46]. The interested reader is invited to refer to the work of Jolliffe [45] for further mathematical demonstrations, information and examples.

#### 1.4.2 Principal components of the transition

As introduced, the objective is to define the main technological drivers of the variation through the transition to 2050 subject to uncertainties. To do so, before calculating the PCs of the transition, three preliminary steps are necessary: (i) data selection, (ii) data scaling and, (iii)outliers management. After this preprocessing, PCs can be computed for each of the year of the transition then aggregated to give a bigger picture over the whole transition.

##### Data selection

Prior to any data processing, the choice of the original dataset is fundamental. In the will to characterize the variations of design within the transition under uncertainties, we have focused on the installed capacities,  $F(y, j)$  for all  $y \in \text{YEARS}$  and  $j \in \text{TECH}$  (see Eq. 1.15). Even though these represent only a part of the result of the optimization, along with the operation, focusing on the installed capacities give a direct information regarding the required capital investment (see Eq. 1.8) and, more indirectly, the resources to use. In other words, it captures the technological landscape of the transition. Having defined the type of variable to consider, we need to assemble a relevant dataset. This is given by the runs to quantify the impact of the uncertain parameters on the total cost of transition required by the method described in Section 1.2. Overall, the original dataset is  $\mathbf{x}(y, j, s)$  where, on top of  $y$  and  $j$  previously defined,  $s \in [1, 2, \dots, S]$  states for the sample number of the uncertainty quantification method. For the investigated case detailed in Chapter 3, this represents  $S = 240$  samples resulting from the perfect foresight optimization of the transition pathway under uncertainties. Finally, among the seven representative years of the transition, we do not consider 2020 as it is the initialisation year for which the design of the system is fixed, to be representative of the actual design that was in place (see Appendix B.1). In other words, we focus here only on the years 2025, 2030, 2035, 2040, 2045 and 2050. This gives the whole dataset considered in this PCA (see Figure 1.8).

##### Data scaling

Sample <sub>s</sub>	TECH <sub>1</sub>	TECH <sub>2</sub>	TECH <sub>3</sub>	...	TECH <sub>n</sub>
2025					
2030					
Sample <sub>2</sub>	TECH <sub>1</sub>	TECH <sub>2</sub>	TECH <sub>3</sub>	...	TECH <sub>n</sub>
2025	F <sub>1,2025</sub>	F <sub>2,2025</sub>	F <sub>3,2025</sub>	...	F <sub>n,2025</sub>
2030	F <sub>1,2030</sub>	F <sub>2,2030</sub>	F <sub>3,2030</sub>	...	F <sub>n,2030</sub>
2035	F <sub>1,2035</sub>	F <sub>2,2035</sub>	F <sub>3,2035</sub>	...	F <sub>n,2035</sub>
2040	F <sub>1,2040</sub>	F <sub>2,2040</sub>	F <sub>3,2040</sub>	...	F <sub>n,2040</sub>
2045	F <sub>1,2045</sub>	F <sub>2,2045</sub>	F <sub>3,2045</sub>	...	F <sub>n,2045</sub>
2050	F <sub>1,2050</sub>	F <sub>2,2050</sub>	F <sub>3,2050</sub>	...	F <sub>n,2050</sub>

**Figure 1.8.** Original raw data considered in the Principal Component Analysis (PCA) of the variation of the design strategy through the transition,  $\mathbf{x}(y, j, s)$ .

Preprocessing the dataset before employing a method to reduce dimensionality, like PCA, can greatly affect the structure of the simplified representation and the characteristics of the features extracted from the dataset [47, 48]. Scaling the original raw data via normalization, i.e. reducing data to  $[0, 1]$  interval has a double purposes: to assess variables (i) representing different sorts of features, with different units (e.g. installed capacity of electricity and mobility technologies) and, (ii) ranging over the different orders of magnitude (e.g. installed capacity of private and public mobility) (see Appendix B.1). Consequently, the first part of this data preprocessing consists in scaling the installed capacities versus their respective sector and representative year (see Eq. 1.28). The sectors, as defined in EnergyScope, are the electricity, high-temperature (HT) heat, low-temperature (LT) heat, passenger mobility, freight mobility, non-energy demand (NED), storage and infrastructures. For instance, the installed capacity of photovoltaic (PV) panels in the year  $y$  of the sample  $s$  is scaled by the maximum installed capacity in the electricity sector in the year  $y$  among all the samples.

$$\mathbf{x}^*(y, j, s) = \frac{\mathbf{x}(y, j, s)}{\max_{sec,y}(\mathbf{x}(y, j, s))} \quad \forall y \in YEARS, sec \in SECTORS \quad (1.28)$$

Then, to give “directions/metrics” representative to the size of each sector within the energy system, we added another weight based on the relative share of commodity produced by each sector (see Figure 1.9).

To do so, we have arbitrarily considered these shares from the REF case, where the pathway is optimized according to the perfect foresight approach and considering all the uncertain parameters to their nominal value (see Chapter 3). The end-use-demands

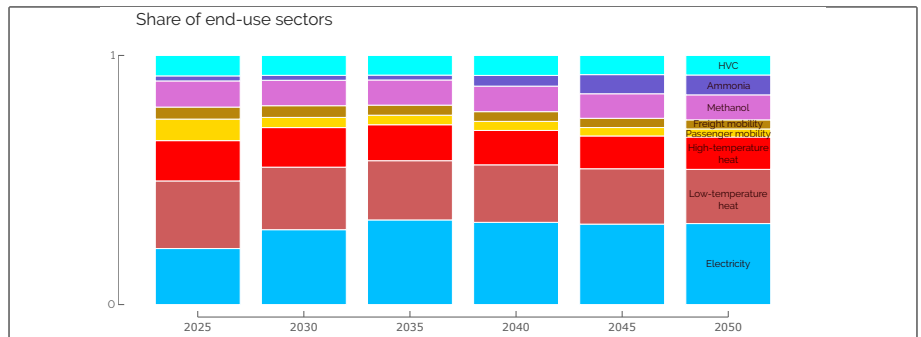


**Figure 1.9.** Multiplying factor for each of the end-use sectors. Over the transition, sectors like electricity or methanol become more important due to sector coupling, e.g. e-mobility or methanol-to-olefins (MTO).

as well as the commodity produced for the sector coupling are based on the results of this deterministic REF case. For instance, the share of the electricity sector accounts for its end-use demand (EUD) and the electricity produced to supply other sectors (e.g. heat, mobility). Finally, to compare apples with apples, we converted the EUD in the mobility sectors, i.e. passenger and freight, into the ?? they require in the REF case. This gives the second weighing factor to scale data, on top of the one of Eq. 1.28 (see Eq. 1.29).

$$\mathbf{x}^{**}(y, j, s) = \mathbf{x}^*(y, j, s) \cdot \text{share}_{\text{EUD}}(y, sec) \quad \forall y \in \text{YEARS}, sec \in \text{SECTORS} \quad (1.29)$$

One would notice that this second scaling factor omits the infrastructure and storage technologies. In the process to define “metrics” to assess the robustness of a policy for the case of Belgium, this has a negligible impact. Indeed, the variation of the installed capacity of these technologies are either limited compared to end-use-type (EUT) technologies, i.e. limiting their influence in the definition of PCs, or directly linked to these EUT technologies (e.g. district heating network (DHN) installed capacity is directly proportional to technologies producing LT heat in DHN or the additional capacity of grid is caused by additional capacities of VRES).

### Outliers management

Handling outliers is one of the biggest challenges in data science [49]. These are defined as data points differing significantly from the rest of the data set. Being extreme

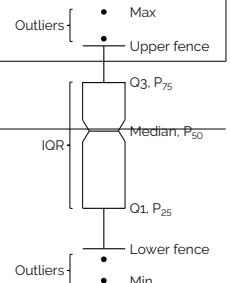


**Figure 1.10**

values, outliers influence the overall dataset variance and, consequently, rotate the PCs directions towards them [50]. In the context of PCA, outliers could be defined as “model fit outliers” as their presence influences the fit of the model. There are several techniques to detect/define and handle the outliers [49]. In this work, detection is performed via the box plot technique, as outliers are identified as those points lying beyond the plot’s whiskers, or fences. These whiskers are themselves constructed as being 1.5 times the interquartile range (IQR) ( $Q_3 - Q_1$ ) higher or lower than the third ( $Q_3$ ) or first quartile ( $Q_1$ ), respectively (see Figure 1.10). Therefore, the installed capacity of a technology in the year  $y$  of the sample  $s$  is defined as an outlier if it falls out of this range compared to the rest of the dataset for this specific technology and year across all the samples. Then, one option to handle these outliers would be to remove the whole data point for which one technology presents an outlying installed capacity. However, it would lead to reducing the entire dataset (i.e. several thousands of points) to too few data points (i.e. several tens) limiting the applicability of the PCA approach. Consequently, we have decided to keep these points but carry out a modification of them [49]. In practice, the value of “high outliers” or “low outliers” is set to the upper or lower fence, respectively.

### **Principal components of each representative year**

Now that data are selected and preprocessed, principal components are first computed for each representative year separately, using the Python package PCA from `SKLEARN.DECOMPOSITION`. As explained in Section 1.4.1, the number of PCs per year to retain can go up to the number of considered variables (i.e.  $73^2$  in our case study) which is intractable. Moreover, the first PCs keep track of most of the variance of the system whereas the last ones present a smaller interest. Choosing the appropriate threshold involves a trade-off. Retaining too few principal components may result in loss of important information, while retaining too many may lead to over-fitting or computational inefficiency. The good practice followed in this work is to compute, for each of the representative years of the transition (except 2020), the PCs that capture 90% of the total variance of this year [45]. At the end of this step, we have a list of  $m$  PCs, i.e.  $\text{PC}_{y,i}$  where  $y$  stands for the year between 2025 and 2050 and

---

<sup>2</sup>73 technologies out of the 113 in total as we do not consider the 15 infrastructure technologies nor the 25 storage technologies.

$$\sum_{i=0}^m \text{var}(\text{PC}_{y,i}) \geq 90\% \sum_{i=0}^p \text{var}(\text{PC}_{y,i}) \quad \forall y \in \text{YEARS} \quad (1.30)$$

where  $m$  is presumably different for each representative year and  $p$  is the total number of variables, hence the maximum number of PCs. For the entire transition, it gives a total of  $M$   $\text{PC}_{y,i}$ .

### Principal components of the transition

The final step consists in defining metrics on the whole transition based on the  $\text{PC}_{y,i}$  computed for each representative year, separately. To do so, all the  $\text{PC}_{y,i}$  from every year are sorted together in a descending order based on their respective variance. Then, starting with the one with the highest absolute variance, all the other  $\text{PC}_{y,i}$  similar to it are clustered together. The similarity between two PCs is defined according to the cosine similarity approach. Indeed, as detailed in Section 1.4.1, a PC represents a vector for which the components are related to each variable of interest. Therefore, in this work, PCs are considered similar if their cosine similarity,  $S_C(A, B)$ , is greater or equal to 90%:

$$S_C(A, B) := \cos(\theta) = \frac{\mathbf{A} \cdot \mathbf{B}}{\|\mathbf{A}\| \|\mathbf{B}\|} = \frac{\sum_{i=1}^n A_i B_i}{\sqrt{\sum_{i=1}^n A_i^2} \cdot \sqrt{\sum_{i=1}^n B_i^2}} \geq 90\% \quad (1.31)$$

where  $A$  and  $B$  represent two different PCs. The components of these similar PCs are then averaged to form the first PC of the transition,  $\text{PC}_{\text{transition},1}$ . Then, the process repeats with the  $\text{PC}_{y,i}$  with the highest absolute variance but that has not been integrated in the construction of  $\text{PC}_{\text{transition},1}$ , to form  $\text{PC}_{\text{transition},2}$ . This goes on until the sum of the absolute variance of the  $N$   $\text{PC}_{y,i}$  used to construct these  $\text{PC}_{\text{transition}}$  is greater or equal to 90% of the sum of the absolute variance of all the  $M$   $\text{PC}_{y,i}$  generated at the previous step:

$$\sum_{i=0}^N \text{var}(\text{PC}_{y,i}) \geq 90\% \sum_{i=0}^M \text{var}(\text{PC}_{y,i}) \quad (1.32)$$

### Robustness assessment of roadmaps

Similarly to the work of Moret et al. [18], roadmaps are defined by setting minimal installed capacities based on the results of different transition pathway optimizations

(see Chapter ??). The  $PC_{transition}$  are the “direction/metrics” on which are projected the results from the myopic pathway optimization subject to minimal installed capacities set by these roadmaps. In conclusion, a roadmap would be defined as more robust than another one if the projection of its myopic runs on the different  $PC_{transition}$  span on a more narrow range.

---

---

## Chapter 2

# Case study: the Belgian energy system

As detailed by Limpens et al. [9], the analysis carried out in this work can be applied to any regional whole-energy system. As a densely-populated and highly-industrialised country with limited local renewable potentials (i.e. mainly solar and wind representing up to 50% of the primary mix by 2050), the transition of Belgium from a fossil-dominated system in 2020 (Appendix B.1) to carbon-neutrality in 2050 makes it an intricate case study. Moreover, this case study and the subsequent analyses can be transferred - to some extent - to other industrialised countries highly dependent on fossil fuels with limited local renewable potentials (e.g. the Netherlands or Germany) [51]. This chapter presents the different demands to satisfy, with a particular focus on the non-energy demand, as well as the resources available and the conversion technologies to supply those. For a comprehensive understanding and detailed descriptions of the technologies, please refer to the documentation [11]. Then, the uncertainty ranges considered for some of the parameters are detailed. Finally, the CO<sub>2</sub>-budget over the 2020-2050 transition is presented.

### Contributions

First, as pointed out by Rixhon et al. [52], where most of the studies assessing whole-energy system integrate energy demands (i.e. electricity, heat and mobility), the non-energy demand (NED) is often not considered. The latter is defined as '*energy products used as raw materials in the different sectors; that is not consumed as a fuel or transformed into another fuel*' [53]. The previous analyses carried out with EnergyScope Typical Days (EnergyScope TD) considered the non-energy demand as the related primary energy needs, i.e. either natural gas or light fuel oil (LFO). To minimise the

total cost of the system, the model simply selected the cheapest between the two resources (i.e. natural gas). This work goes one step further and accounts for the NED as a demand of three commodities (i.e. high value chemicals (HVC), ammonia and methanol) as well as with associated production technologies. This allows bringing the non-energy sector to a similar level of details as the other sectors. Keeping the same methodology to define EUD in EnergyScope as Limpens et al. [54], this work considers updated values given the latest release of the “EU reference scenario 2020 : energy, transport and GHG emissions: Trends to 2050 ”by the European Commission [55].

Second, given the focus of this work on the electrofuels, the case study includes a more explicit representation of them: where the previous definition of the case study considered only renewable hydrogen and methane [1], now, e-ammonia and e-methanol (as well as their fossil-based equivalents), are implemented in the case study. As detailed later on, these electrofuels are considered as renewable in the sense that their global warming potential (GWP) is zero. This more explicit representation of the molecules themselves also comes with a more exhaustive integration of the ways to produce and use them in the system. For instance, considering the case of ammonia, on the top of the import routes, the Haber-Bosch process ,on one hand, is accounted for to supply this molecule. On the other hand, ammonia-driven CCGT or ammonia-cracking-to-hydrogen are included as ways to consume it.

Third, as nuclear energy could be a real game-changer in the energy transition worldwide [56], and especially in Belgium, this thesis has integrated the uncertain potential to install SMR from 2040 onward.

Fourth, where previous works considered a prescribed CO<sub>2</sub> trajectory to reach carbon-neutrality by 2050 [1, 9], the case study analysed in this thesis is subject to a CO<sub>2</sub>-budget for the transition, i.e. limiting the total amount of emissions over the transition. Based on the estimated world budget provided by the intergovernmental panel for climate change (IPCC) to limit the global warming to +1.5°C by the end of the century, the grandfathering approach has been used to allocate part of this budget to the Belgian energy transition.

Finally, to a smaller extent, this work includes updated values for some parameters compared to the work of Limpens [1]. The main change concerns the cost and performance of private mobility vehicles, which is specifically a key components in the European [57] and Belgian [58] energy transitions. Based on the work of National Research Council [59], Limpens [1] excessively favoured fuel cell (FC) car versus battery electric vehicle (BEV). Besides their lower efficiencies (i.e. about 50% less efficient), FC car had the lion share of the private mobility, compared to BEV given the higher

CAPEX (i.e. up to 10% more expensive) and limited range (i.e. 24kWh battery) of the latter, in previous works ???. In these, the more limited potential to import electricity from abroad and produce it locally via VRES forced the model to rather electrify the low-temperature heat sector rather than the private mobility running on supposedly infinitely available renewable hydrogen. To align with other similar works on the modelling of whole-energy system [55, 60], the CAPEX and efficiency of fuel cell cars have been increased. Regarding BEV, while the CAPEX has been kept unchanged, the efficiency and the battery capacity, i.e. the range, have been increased. As seen in the results, this change of data made BEV often more competitive than its hydrogen-based equivalent.

## 2.1 End-use demands

End-use demands, exogenously imposed as inputs to the model, are characterised by yearly quantities to satisfy and are also distributed over the different hours of each representative years of the transition, in order to account for their daily or seasonal variability [1, 54]. In this work, the yearly end-use demands (EUD) for all sectors are calculated from the forecast proposed by the European Commission for Belgium (Appendix 2 in report [55]).

### 2.1.1 Non-energy demand

The NED currently represents around 20% of the final energy consumption in Belgium [61]. This section summarises the rationale of adding a higher level of details to the NED compared to what was done in the previous version of the case study [1]. Then, it explains the methodology used to quantify this demand.

#### Definition and historical trend

The NED can be split into four main categories of final molecules [62]: (i) HVC (worldwide production of  $\sim 365\text{Mt/year}$ , equivalent to  $\sim 4770\text{TWh/year}$ ); (ii) ammonia ( $\sim 185\text{Mt/year}$ , equivalent to  $\sim 964\text{TWh/year}$ ); (iii) methanol ( $\sim 100\text{Mt/year}$ , equivalent to  $\sim 540\text{TWh/year}$ ) and (iv) the other products. HVC gather the light olefins (e.g. ethylene, propylene) and aromatics (benzene, toluene, xylene – BTX), mainly for the production of plastics, synthetic fibers or rubber. Their production today relies mainly on petroleum products such as naphtha, ethane or liquified petroleum gas. Ammonia is mainly used for the production of fertilizers ( $\sim 80\%$  of global ammonia consumption). Its production is dominated by fossil gas via steam methane reforming to produce hy-

drogen, used as feedstock in the Haber-Bosch process. Methanol is mainly converted to formaldehyde (resin) but also used for the production of other chemicals (e.g. solvents and gasoline-blends). Currently, its synthesis, like ammonia, is mainly relying on natural gas via steam methane reforming. Finally, the other products gather all chemicals not mentioned in the other categories such as bitumen, lubricants and other heavy products from oil refineries [63].

Over the recent history, there has been a relatively constant evolution of three main categories of the final consumption for non-energy use in Belgium, [64]: (i) naphtha and liquefied petroleum gas (LPG) (between 59% and 67% of the total final consumption, around 59.4 TWh in 2019), (ii) fossil gas (between 9% and 14%, 11.8 TWh in 2019), and (iii) others (i.e. bitumen, coal tar and other oil products) (between 21% and 28%). Naphtha and LPG are consumed in a naphtha cracker, which results in ethylene and propylene, what will be considered as HVC in the rest of this work. Similarly, fossil gas, as non-energy carrier, is used in steam methane reformer to produce the required hydrogen to the synthesis process of ammonia. The small shares of bitumen and coal tar are respectively used for roadworks and to produce synthetic gas through gasification. Finally “other oil products” take into account, indistinguishably, tar and sulphur as well as by-products of the refineries (e.g. benzene, toluene and xylene (BTX)). About methanol, there is currently no production plant in Belgium even if the country plays a role in trading this commodity between its neighbouring countries and consumes part of what it imports.

### **Methodology of quantification**

The non-energy demand studied in this analysis focuses on the chemical industry (more than 90% of the non-energy use in Belgium) and, similarly to other studies [62, 63], is split between the three aforementioned main groups of products (i.e. HVC, ammonia and methanol). Before describing these three demands, this study excludes bitumen, coal tar and “other oil products”. The first two represent marginal shares of the current non-energy use (i.e. 4% and 5% respectively) in such a way that they should not affect the conclusions provided by this study. As described previously, the latest are mostly by-products from refineries that the system uses because they are available. However, in a perspective of defossilisation, since the future of fossil-based refineries is unclear, they have not been implemented in this study nor their by-products.

Regarding HVC, the future of their production is highly uncertain. Because of the new regulations and strategies promoting recycling and limitation of single-use plastics [65]. Besides this uncertainty, Belgium stays a major exporter as approximately 2/3 of plastic raw materials produced locally are exported abroad [66]. Even if a significant

part of HVC produced in Belgium is not locally consumed, this demand has been set based on the assumption that Belgium will keep its industrial activity in this sector. In other words, this assumption does not deduce the part of local production of HVC being then exported (and not consumed locally), unlike ammonia and methanol, which will be more traded commodities in the future (as energy carriers and non-energy products). Therefore, the actual demand of HVC is inferred from the consumption of naphtha and LPG as non-energy use as well as energy-carrier in the chemical and petrochemical industries [64]. This assumption is based on the fact that, in the conversion processes to produce HVC from naphtha or LPG, these fuels also serve as energy-carrier to supply the process itself. Then, given the respective efficiencies ( $1.83t_{naphtha}/t_{HVC}$  and  $1.67t_{LPG}/t_{HVC}$ ) [62], the current demand of HVC is estimated equal to 3069 kt, without making distinctions between the different chemicals (i.e. ethylene, propylene and BTX).

The ammonia sector in Belgium is quite different: the country locally produces and imports ammonia much more than it exports it. Thanks to a database from the United Nations [67] and the National Bank of Belgium, it has been identified that, over the last ten years, Belgium has imported 1010 kt of ammonia, exported 105 kt and locally produced 990 kt on average. Therefore, on top of the local production, the net import (i.e. import minus export) is also included in this non-energy demand. This gives a current demand of 1895 kt of ammonia.

Concerning the demand of methanol, similarly to ammonia, this work solely considers the net imports as there is no local production in Belgium. To define the actual non-energy demand of methanol, only a 51%-share of this net import is kept since, according to the Methanol Institute and Methanol Market Services Asia (MMSA), this share is used for formaldehyde production in Belgium [68]. Currently, the rest of the methanol is used for energy purposes, mostly as methyl tert-butyl ether (MTBE) in gasoline blending. This methodology gives a current non-energy demand of methanol of 269 kt.

Eventually, after converting these masses of products into energy content (i.e. LHV: HVC - 47 MJ/kg, ammonia - 18.8 MJ/kg and methanol - 19.9 MJ/kg), two final assumptions are made: (i) the current shares of each of the three commodities (i.e. 77.9%, 19.2% and 2.9% for HVC, ammonia and methanol, respectively) are supposed to remain unchanged over the transition; (ii) the overall NED, in absolute terms, follows the growing rate presented by Capros et al. [69], i.e. around 7% between 2020 and 2050.

### **2.1.2 Forecast of the demands over the transition**

In their latest report [55], the European Commission forecasts a significant and abrupt increase of the NED compared to their previous report [69], i.e. +80% over the 2020-2030 time window. Given this discrepancy that is unsubstantiated and specific to the case of Belgium, the evolution trend of the NED of the current work has been inferred from the previous edition, published in 2016, [69]. Between 2020 and 2050, one observes a noteworthy increase of the electricity (+40%), passenger (+45%) and freight mobility (+35%) demands (see Figure 2.1). The rise of the non-energy demand is more limited, i.e. +6%, whereas the heating demands is forecast to decrease: -11% for the low-temperature heat demand and -3% for the high-temperature heat demand. This is explained by a better insulation of buildings and an improved efficiency of industrial processes. Regarding the center graph of Figure 2.1, it is the aggregation of the same data as in the left graph but per category, rather than per sector, with the non-energy demand being associated with the industry. This illustrates how industrialised is Belgium, compared to households and services, and, consequently, highly energy-intensive. The right graph of Figure 2.1 gives the passenger and the freight mobility. The sharp increase from 2020 to 2025 is due the COVID-crisis that has significantly reduced these demands in 2020. As far as the hourly discretisation of these demands is concerned, time series are based on historical values of 2015 for the fluctuating parts of electricity and low-temperature heating demands [54]. A daily time series is used for the passenger mobility and applied similarly to every days of the year. Finally, for the other demands (i.e. high-temperature heat, freight mobility, NED and constant share of electricity and low-temperature heat demands), the yearly demand is distributed uniformly over the different hours of the year.

## **2.2 Resources**

To supply the aforementioned demands, EnergyScope Pathway implements a variety of resources defined by their cost of purchasing,  $c_{op}$ , their global warming potential,  $gwp_{op}$ , as well as their availability, as detailed by Limpens et al. [9]. First, the evolution of the respective costs of purchasing is presented (see Figure 2.2). Regarding “renewable electrofuels”, these are in line with the recent study of Genge et al. [70] who carried out an extensive review and “meta-analysis[71, 72] of 30 studies on the supply costs of chemical energy carriers”. Then, besides their cost, the resources are either limited or unlimited in terms of availability and either renewable or not. The limitation in terms of availability can be direct or indirect. On the one hand, woody (23.4 TWh) and wet biomass (38.9 TWh) are arbitrarily limited by their local poten-

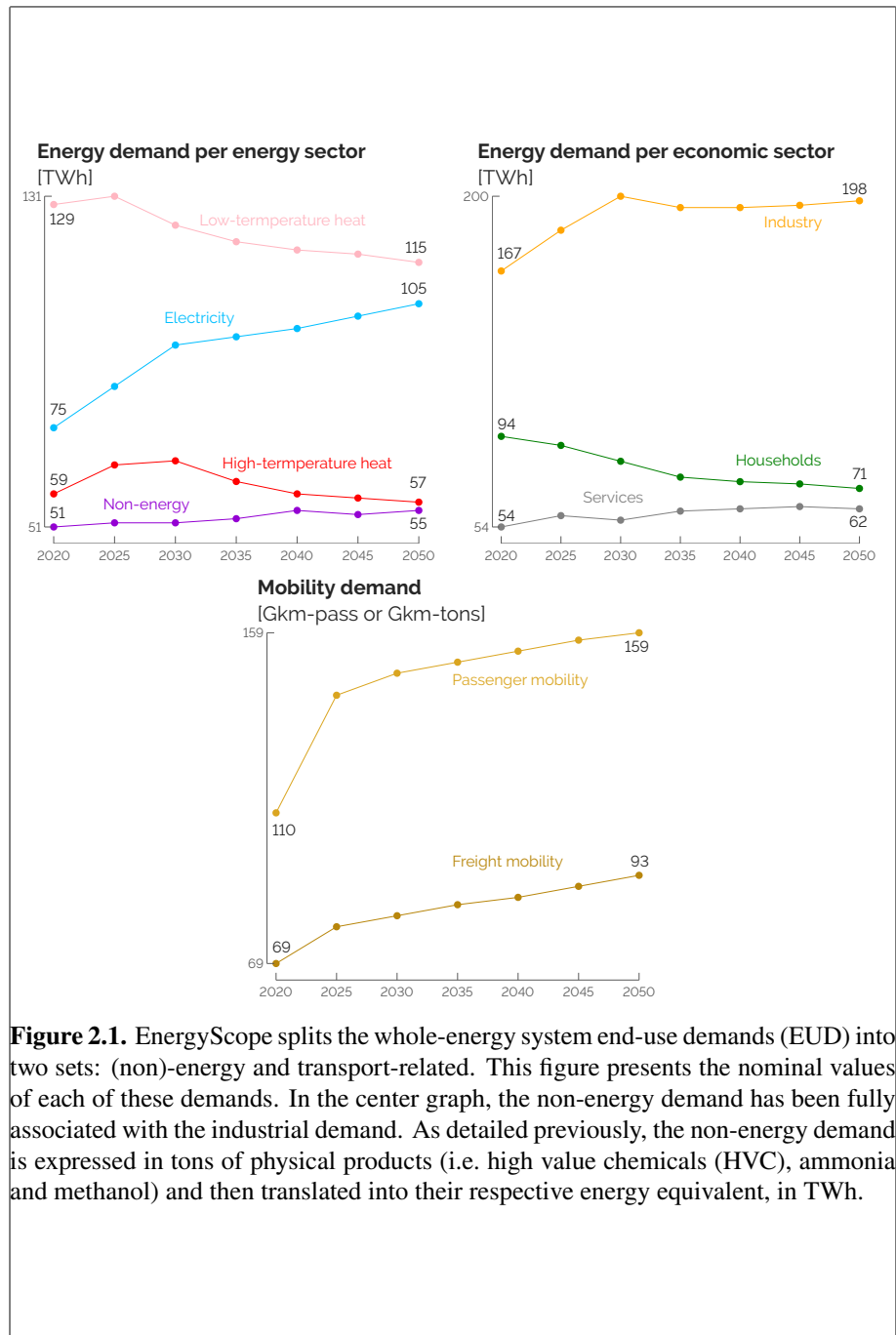


**Figure 2.1.** EnergyScope splits the whole-energy system end-use demands (EUD) into two sets: (non)-energy and transport-related. This figure presents the nominal values of each of these demands. In the center graph, the non-energy demand has been fully associated with the industrial demand. As detailed previously, the non-energy demand is expressed in tons of physical products (i.e. high value chemicals (HVC), ammonia and methanol) and then translated into their respective energy equivalent, in TWh.

tials and the consumption of waste (17.8 TWh) and coal (33.4 TWh) is assumed not to exceed the current use. On the other hand, wind, solar, hydro and uranium are limited by the technical potentials of PV panels (59.2 GW), onshore (10 GW) and offshore (6 GW) wind turbines, run-of-the-river power plants (0.1 GW) and nuclear power plants (6 GW), respectively. In line with the work of EnergyVille [73] and the maximum capacity of conventional nuclear reactors that have been installed in Belgium, the same 6 GW are assumed to be the maximum capacity for SMR. Imported electricity is limited in two ways: the potential of instantaneous capacity of interconnection with neighbouring countries (i.e. 11.9 GW by 2050 [74]) and a limitation to 30% of the yearly electricity end-use demand (i.e. 32.4 TWh by 2050) [1]. In the current work, the electrofuels (i.e. e-methane, e-hydrogen, e-methanol and e-ammonia) are assumed to be “sustainable” in the sense that they do not increase the concentration of CO<sub>2</sub> in the atmosphere [75]. In practice, it means that their GWP is assumed to be zero in the model. Regarding specifically these electrofuels, the Hydrogen Import Coalition [27] has carried out an extensive techno-economic analysis to estimate their respective cost of purchasing, after having identified some key locations from which importing these energy carriers (e.g. Chile, Australia or Morocco). As the amount to import from each of these locations is hard to forecast, the current work considers the average cost between the different locations. Besides these, every other resource has its specific GWP like coal ( $gwp_{op,coal} = 0.40 \text{ ktCO}_2,\text{eq}/\text{GWh}$ ), natural gas ( $gwp_{op,NG} = 0.27 \text{ ktCO}_2,\text{eq}/\text{GWh}$ ) or the fossil-based molecules equivalent to the electrofuels (e.g.  $gwp_{op,ammonia} = 0.46 \text{ ktCO}_2,\text{eq}/\text{GWh}$  or  $gwp_{op,methanol} = 0.41 \text{ ktCO}_2,\text{eq}/\text{GWh}$ ).

### **2.3 Conversion technologies**

As the end-use demands are defined as energy (and non-energy with the NED) services rather than a certain quantity of oil or solar irradiance, for instance, technologies are implemented to convert these resources into the end-use demands. Besides their CAPEX, OPEX and lifetime defined in Section 1.1, production and conversion technologies (i.e. CCGT, car or boiler) have a conversion efficiency whereas storage technologies (i.e. thermal storage, battery or molecule storage) exhibit their own charge/discharge losses. There are also infrastructure technologies. They encompass, for instance, the power grid, the DHN or technologies to produce intermediate energy carriers (e.g. wood pyrolysis, biomethanolation or steam methane reforming to produce hydrogen). Not digging into too much details about the exhaustive list of these technologies presented in previous works [1], this section rather focuses on the

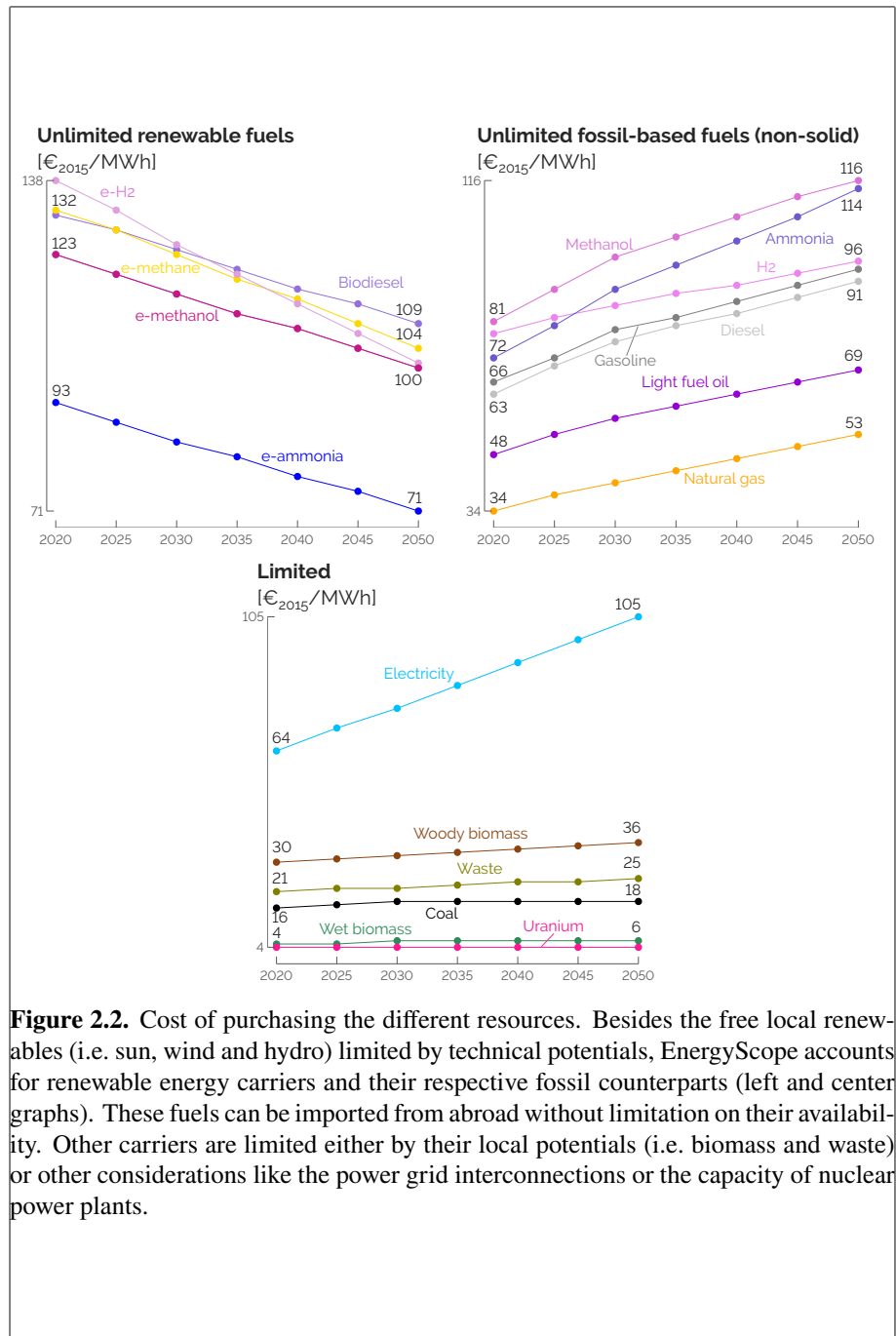


**Figure 2.2.** Cost of purchasing the different resources. Besides the free local renewables (i.e. sun, wind and hydro) limited by technical potentials, EnergyScope accounts for renewable energy carriers and their respective fossil counterparts (left and center graphs). These fuels can be imported from abroad without limitation on their availability. Other carriers are limited either by their local potentials (i.e. biomass and waste) or other considerations like the power grid interconnections or the capacity of nuclear power plants.

implementation of small modular reactor (SMR) then the technologies to supply the non-energy demand (NED).

### **2.3.1 Small modular reactor**

A specific attention is to put on the implementation of SMR whereas the 6 GW of conventional nuclear are assumed to drop to 2 GW in 2025 and total phase-out by 2035. Similarly to the analysis of EnergyVille [73], a Belgian consortium for energy research, and in line with the Belgian Nuclear Research Centre (SCK-CEN) [76], SMR are implemented with the features listed in Table 2.1. Where most of the features are similar to conventional nuclear power plants, it differs from these on two main points: their potential year start, 2040, and their flexibility. Indeed, unlike the current nuclear power plants, constrained in the model to produce a constant power output at every hour of the year (i.e. baseload production as it is actually the case in Belgium), SMRs, are flexible in the sense that their production can vary between 0 and their full capacity independently at any hour of each representative year. Here, we simplify SMRs as only producing electricity and disregard the heat produced by the nuclear reaction. This is considered as lost to the atmosphere.

**Table 2.1.** Nominal features of the SMRs in EnergyScope. SMR exhibits the advantage to have a fully flexible production (i.e. between 0 to the full capacity) unlike conventional nuclear that is constrained to produce a constant baseload at every hour of the year.

Feature	Value	Unit
CAPEX	4850	€/kW
Annual OPEX	103	€/kW/year
Lifetime	60	year
Efficiency	40%	-
Maximum capacity	6	GW
Annual availability	85% <sup>a</sup>	-
Operational year	2040 <sup>b</sup>	-
Flexibility	Full	-

<sup>a</sup>This annual availability accounts for yearly maintenance where the reactors might not operate or, at least, not at their maximum capacity.

<sup>b</sup>2040 is the soonest year at which SMR could be available, optimistically assuming industrial prototypes being completed by 2035 and 5 additional years for their commercial installation.

For the sake of comparison, the levelised cost of energy (LCOE) of the principal technologies to produce electricity, based on the computation used by Limpens [1],

are detailed (see Figure 2.3). Not including here the cost of integrating a technology in the system (e.g. reinforcement of the grid and storage capacities for VRES), the LCOE aims at aggregating and normalizing the CAPEX and OPEX of technologies providing a common commodity, i.e. electricity. Compared to the other flexible generation units (i.e. CCGT), SMR is significantly more cost-effective. Besides being about six times more capital-intensive in €/kW, the investment is amortized over a longer expected lifetime (i.e. 60 years versus 25 for CCGT). Moreover, the cost of purchasing uranium driving SMR is expected to remain stable and low whereas the expected increase of the cost of purchasing fossil fuels dominates the LCOE of CCGT. In addition, one sees that CCGT supplied by e-ammonia outcompetes its e-methane equivalent, unlike their respective fossil-based equivalent. This due to the fact that e-ammonia, not requiring carbon capture, is expected to be more cost-effective to produce versus e-methane [27]. On the contrary, fossil-based ammonia, mostly relying on steam methane reforming, requires additional steps in the production process compared to fossil gas, as introduced in Section 2.1.1.

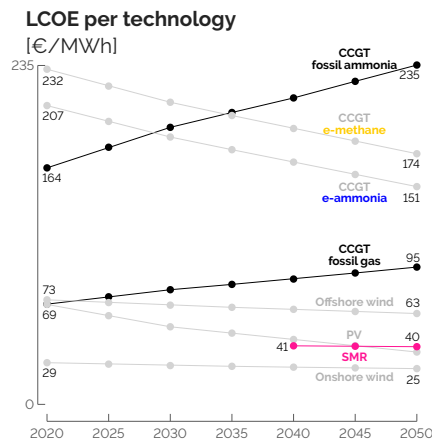


**Figure 2.3.** Levelised cost of energy (LCOE) for the main technologies in the power sector. Gray and black curves are related to technologies running on renewable and fossil resources, respectively. Where SMR is cheaper than the other flexible options, CCGT running on e-ammonia is, a priori, cheaper than its e-methane alternative.

### 2.3.2 Technologies supplying the non-energy demand

Different paths are implemented to produce the final molecules of the NED (see Figure 2.4). Similarly to Tsiropoulos et al. [77], naphtha, here considered as LFO, result-

ing from refinery operation is modeled as an imported commodity. Presented here for the specific year of 2035, all data and related references can be found in [78]. To keep the same level of details with other sectors of the model, the implementation of the conversion technologies consists of a single kind of technology per type of resource to produce a certain product. For instance, in the model, there is only one technology to produce HVC either from naphtha or from LPG, two liquid fossil hydrocarbons, i.e. naphtha steam cracker (NSC). For ammonia and methanol, the molecules can either be produced locally from other resources or directly imported (with distinction between non-renewable and renewable molecules).

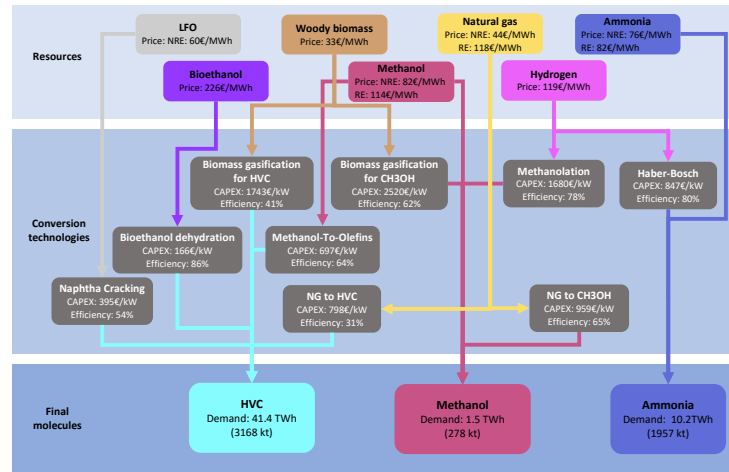


**Figure 2.4.** Schematic view of the different resources able to produce HVC, ammonia and methanol with their related conversion technologies (including energy efficiency and their CAPEX - in €/kW of final molecules). Values stand for 2035. Graph from [79]

### The impact of integrating the NED in the Belgian whole-energy system

Works of Rixhon et al. [52, 79] assessed the impact of the integration of the NED in the case of Belgium, using EnergyScope TD (see Appendix A.2.1). This snapshot model, i.e. optimising the system in a target future year (i.e. 2050 in this case) considering a green field approach, investigated the defossilisation of the system. To analyse the whole-energy system at different “climate targets”, the model forced the total emissions to decrease by reducing their upper limit while optimising the total cost. In practice, 10% steps of GWP reduction were made from the “reference scenario - 100%”. This

strategy gave the following points of analysis: 100% (i.e. cost-optimum with no limitation on the total GWP), 90%, 80%, ..., down to 0% (i.e. carbon-neutrality).

First and foremost, when the NED is implemented with this higher level of details, we highlighted that woody biomass was “cannibalised” to produce methanol, instead of high-temperature heat, in the cost-optimum situation. At more ambitious “climate targets”, e-methanol rises as the keystone to defossilise the NED sector as MTO becomes the favoured option to produce HVC, representing the major share of the NED. Then, including the NED affects the selection of the technologies for the satisfaction of the heat and the electricity demands. The additional high-temperature demand required by the NED forces the system to invest in more efficient technologies like combined heat and power (CHP) instead of CCGT. This additional heat demand mostly supplies naphtha-cracking substituted by MTO at more ambitious “climate targets” to produce HVC. To a lesser extent, to respect the emissions-caps, integrating the NED leads to a higher integration of solar-PV to support the electrification of the low-temperature heat sector.

For further details on these analyses, the interested reader is invited to refer to aforementioned for further published works.

## 2.4 Uncertainty ranges

As detailed in Section 1.2, accounting for uncertainty in ESOMs is crucial [22], especially when it comes to optimise several decades in an inherently uncertain future. The fundamental step in this ambition is to characterise these uncertainties. In this work, following the approach of Moret [35], we have defined range of uncertainties for the model parameters. Table 2.2 gives the uncertainty ranges of some key parameters. Like other works [25, 26], the uncertain parameters are assumed to be independent and uniformly distributed between their respective lower and upper bounds. A particular attention is to pay to the potential installation of SMR, at the bottom of Table 2.2. As detailed before, the commercial availability of such a technology is uncertain but would not be before 2040. Consequently, for SMR, the parameter  $f_{\max,SMR}$  influences the maximum capacity to install to translate somehow the readiness of this technology. Arbitrarily, we have then assumed the following probability of availability of such a technology: 10% of chance to be installable from 2040, 20% from 2045 and 40% from 2050<sup>1</sup>. Based on the local sensitivity analysis carried out by EnergyVille [73], the

<sup>1</sup>In other words, if this parameter, ranging between 0 and 1, is (i) smaller than 0.6, there is no possibility to install SMR during the transition; (ii) between 0.6 and 0.8, these 6 GW can be installed only in 2050; (iii) between 0.8 and 0.9, these can be installed from 2045 onward and; (iv) higher than 0.9, the prescribed maximum capacity can be installed from 2040 onward.

current work also considers a [-40%; +44%] range on the CAPEX of SMR, on top of the uncertainty about the availability. Finally, the cost of purchasing renewable electrofuels presents a wide range, [-64.3%; +179.8%], like the other imported commodities.

The exhaustive list of the parameters accounted in this work is presented in Appendix B.5.

**Table 2.2.** Illustration of the uncertainty characterisation for different parameters for the year 2025.

Category	Parameter	Meaning	Type <sup>a</sup>	Relative variation <sup>b</sup>	
				min	max
<b>Cost of purchasing</b>	$c_{\text{op},\text{fossil}}$	Purchase fossil fuels	II	-64.3%	179.8%
	$c_{\text{op},\text{electrofuels}}$	Purchase electrofuels	II	-64.3%	179.8%
<b>Investment cost</b>	$c_{\text{inv},\text{car}}$	CAPEX car	I	-21.6%	25.0%
	$c_{\text{inv},\text{e\_prop}}$	CAPEX electric motor	I	-39.6%	39.6%
	$c_{\text{inv},\text{fc\_prop}}$	CAPEX fuel cell engine	I	-39.6%	39.6%
	$c_{\text{inv},\text{PV}}$	CAPEX PV	I	-39.6%	39.6%
	$c_{\text{inv},\text{nuclear\_SMR}}^c$	CAPEX SMR <sup>c</sup>	I	-40.0%	44.0%
<b>Consumption</b>	$\eta_{\text{e\_prop}}$	Consumption electric vehicles	I	-28.7%	28.7%
<b>Potential installed capacity</b>	$f_{\text{max,PV}}$	Max capacity PV	I	-24.1%	24.1%
	$f_{\text{max,wind}}$	Max capacity onshore wind	I	-24.1%	24.1%
<b>Hourly load factor</b>	$c_{\text{p,t,PV}}$	Hourly load factor PV	II	-22.1%	22.1%
	$c_{\text{p,t,winds}}$	Hourly load factor wind turbines	II	-22.1%	22.1%
<b>Resource availability</b>	$avail_{\text{elec}}$	Available electricity import	I	-32.1%	32.1%
	$avail_{\text{biomass}}$	Available local biomass	I	-32.1%	32.1%
<b>End-use demand</b>	$pass\_EUD$	Passenger mobility EUD	III	-7.5%	7.5%
	$industry\_EUD$	Industry EUD	III	-20.5%	16.0%
<b>Miscellaneous</b>	$i_{\text{rate}}$	Interest rate	I	-46.2%	46.2%
	$\Delta_{\text{change,freight}}$	Modal share change freight mobility	-	-30%	30%
	$\Delta_{\text{change,pass}}$	Modal share change passenger mobility	-	-30%	30%
	$f_{\text{max,SMR}}$	Potential capacity SMR	-	0	1

<sup>a</sup>Per Moret [35], “I: investment-type, II: operation-type (constant uncertainty over time), III: operation-type (uncertainty increasing over time)”.

<sup>b</sup>The nominal values of each of the parameters is 0, meaning no variation compared to the nominal values of the impacted parameter in the model.

<sup>c</sup>This range has been inferred from the local sensitivity analysis performed by EnergyVille [73].

## 2.5 CO<sub>2</sub>-budget for the transition

In most of the studies carried out on the pathway optimisation of a whole-energy system, a CO<sub>2</sub>-trajectory is *a priori* set to reach carbon-neutrality by 2050. Nerini et al. [16] used the emission trajectory indicated by the UK’s Committee on Climate Change in their analysis of the impact of limited foresight to achieve the target of 80% reduction of GHG by 2050 in the United Kingdom. In their assessment of the impacts of

economy-wide emissions policies in the water-energy-land nexus, Licandeo et al. [80] analysed different CO<sub>2</sub>-trajectories considering more or less severe water scarcity for the US. Poncelet et al. [15] with LUSYM (Leuven University SYstem Model) and EnergyVille [73] with TIMES-BE also set decreasing emission trajectories in their analysis of respectively the Belgian power sector and whole-energy system. Others only set the objective as the carbon-neutrality by 2050. For instance, Heuberger et al. [17] investigated the impact of different factors (e.g. limit of the foresight in the future, availability of “unicorn technologies” or committed versus market-driven decarbonisation strategies) to reach this ultimate objective in the UK system.

In this work, the effect of greenhouse gases is cumulative over time and a constraint is set on the overall emissions of the transition—a CO<sub>2</sub>-budget for the transition. This approach is in line with the works defining safe operating spaces within the nine different global planetary boundaries (i.e. (i) novel entities, (ii) stratospheric ozone depletion, (iii) atmospheric aerosol loading, (iv) ocean acidification, (v) biogeochemical flows, (vi) fresh water change, (vii) land system change, (viii) biosphere integrity, and, (ix) climate change) [81–83]. This “systemic framework for addressing global anthropogenic impacts on Earth system” gives quantitative recommendations about the CO<sub>2</sub> concentration, among others, to maintain “the stability and resilience of Earth system as a whole” [81]. In their review, Ryberg et al. [84] identified three main sharing principle categories when considering these safe spaces: i.e. *utilitarian*, *egalitarian* and *acquired rights* principles. In a nutshell, the former, mostly applied to the scale of industry sector [85, 86], aims at maximising the sum of welfare. The second shares the so-called “budget” equally among the total population, allocating the same share to each individual [87, 88]. Finally, in *acquired rights* principles, also called “grandfathering”, the sharing is based on “maintaining that prior emissions increase future emission entitlements”[89]. In this thesis, we have chosen the latter principle to allocate the CO<sub>2</sub>-budget to the Belgian transition. This budget (1.2 Gt<sub>CO<sub>2</sub>,eq</sub>) corresponds to the proportion of Belgium’s emissions in the world emissions in 2020 (34.8 Gt<sub>CO<sub>2</sub>,eq</sub> [90]) applied to the global budget to have a 66% chance of limiting warming to 1.5°C of 420 Gt<sub>CO<sub>2</sub>,eq</sub> [91]. Therefore, in this work, a limit has been put on  $gwp_{lim,trans} = 1.2 \text{ Gt}_{\text{CO}_2,\text{eq}}$  in Eq. (1.12). This is another sign of the urgency to act to mitigate climate change as this 30-year budget represents only 10 years of the current emissions.

Compared to a linear decrease from the current emissions, as done by Limpens et al. [9], this budget represents a 60% reduction of the cumulative emissions over the transition. Appendix B.4.1 compares the emissions trajectory between the REF case

and a case (without SMR) where the linear decrease is imposed between 2020 and carbon-neutrality in 2050.

---

---

## Chapter 3

# The atom-molecules dilemma: deterministic and uncertain analyses

Add here references and analyses of nuclear and/or molecules as THE solution [92]

### Contributions

- Pathway UQ
- Contrast analysis between atom and molecules and local renewables
- Influence of the parameters on the import of molecules and the installation of SMR

After the model and the frameworks have been introduced in Chapter 1 and the case study presented in Chapter 2, this one focuses on the atom-molecules dilemma in two ways. First, Section 3.1 targets the impact of integrating SMR from 2040 onward on the whole-energy system, in a deterministic way (i.e. considering only nominal values of the parameters). Second, accounting for uncertainties as presented in section ??, section 3.2 will identify the key factors driving higher or lower imports of electrofuels as well as the installation of SMR.

### 3.1 Deterministic impact of integrating SMR in 2040

In this section, like in the rest of the thesis, the **REF** case is without any deployment of SMR anytime during the transition and whereas in the **SMR** case this technology

is available, up to 6 GW, from 2040 onward. After investigating the deployment of SMR through the power sector, the first part of this section focuses on this impact on macro/system-level considerations (i.e. overall transition costs, primary energy mix and yearly emissions per sector). The second part will address the impact of SMR on each of the other sectors of the system.

### **3.1.1 Power sector**

Figure 3.1 shows that SMR is deployed as soon as available, i.e. 2040, to their maximum capacity, i.e. 6 GW, substituting other flexible power generation units: no ammonia-CCGT at the end of the transition and the anticipatory reduction of methane CCGT (i.e. 2.1 GW in 2040 versus 3.7 GW for the REF case). To a lesser extent, the last 2% deployment of solar-PV is slightly delayed as the capacity in 2025 is 1.3 GW smaller than in the REF case. Overall, given the smaller efficiency of SMR, i.e. 40% versus 51% for ammonia-CCGT, the restriction on yearly availability and the slightly higher electrification (Figure 3.2), the total power capacity installed by 2050 is 3.5% higher for the SMR case.

**Compare here with EnergyVille - PATHS2050 and other works from Seb's report.**

When assessing the electricity production-versus-consumption-balance (Figure 3.2), SMR, as a cheaper, flexible and low-emitting power generation system, produces to its full capacity, given the 15% maintenance off-time assumed in this work: 44.6 TWh. By 2050, it represents 24.6% of the total electricity production which is less than the current share of conventional nuclear in Belgium, 38.5%. This resurgence of nuclear electricity occurs at the expense of other, although more efficient technologies: CCGT and industrial CHP. Besides the unchanged end-use-demand, we observe a slight increase of the electrification of the rest of the system: +9.4% which corresponds to +5.8 TWh, mostly consumed by electric heaters in industry (+48%) to produce industrial high-temperature heat.

### **3.1.2 System-level impacts**

First of all, as far as the objective function (i.e. the total transition cost) is concerned, Figure 3.3 shows that the 6 GW SMR installed from 2040 allow reaching a 3.3% (-36.9 b€, ~6% of the Belgian GDP) cheaper overall transition. Interestingly, as the model can freely spend the constrained CO<sub>2</sub>-budget over the transition, knowing ahead

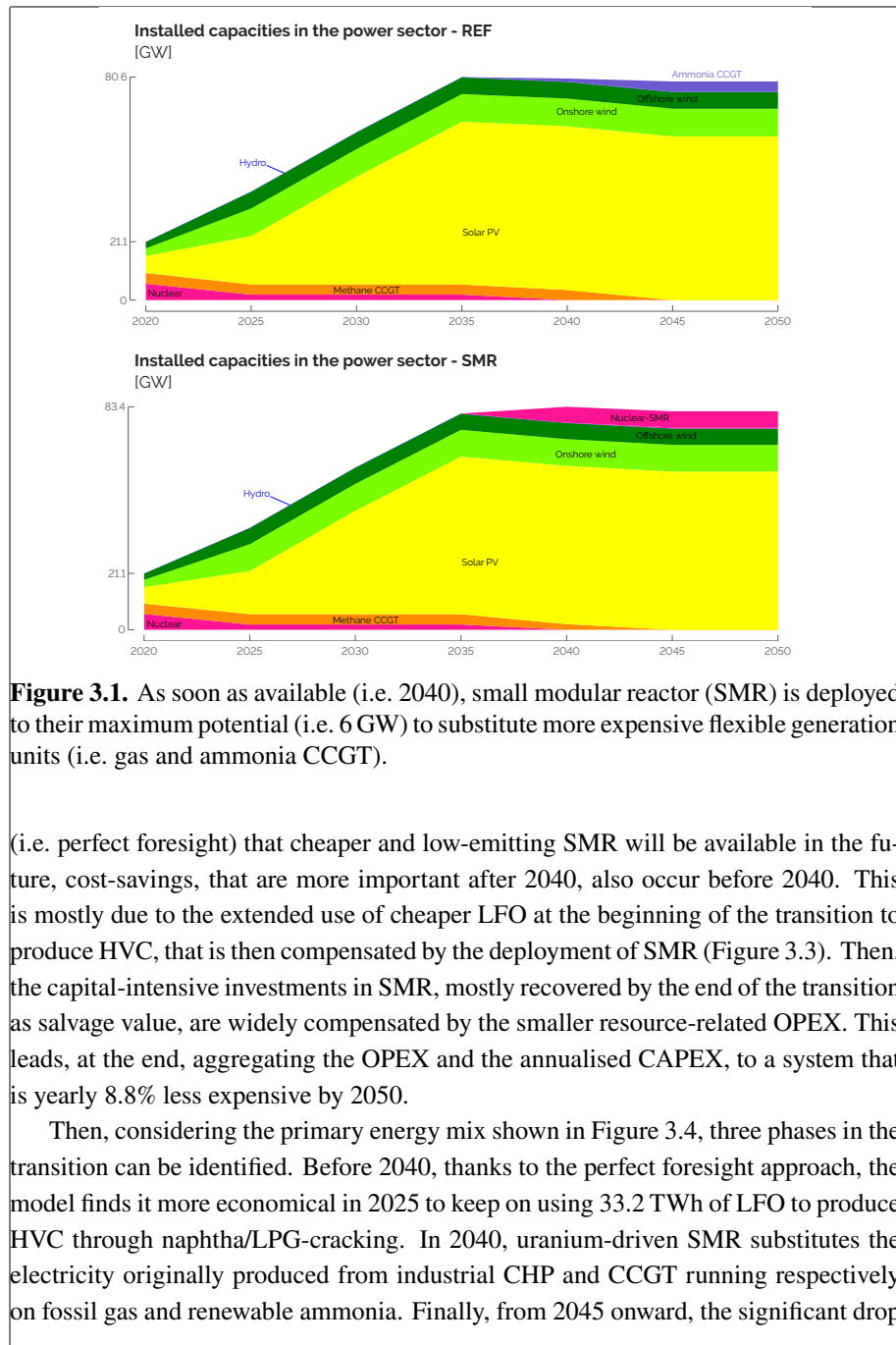


**Figure 3.1.** As soon as available (i.e. 2040), small modular reactor (SMR) is deployed to their maximum potential (i.e. 6 GW) to substitute more expensive flexible generation units (i.e. gas and ammonia CCGT).

(i.e. perfect foresight) that cheaper and low-emitting SMR will be available in the future, cost-savings, that are more important after 2040, also occur before 2040. This is mostly due to the extended use of cheaper LFO at the beginning of the transition to produce HVC, that is then compensated by the deployment of SMR (Figure 3.3). Then, the capital-intensive investments in SMR, mostly recovered by the end of the transition as salvage value, are widely compensated by the smaller resource-related OPEX. This leads, at the end, aggregating the OPEX and the annualised CAPEX, to a system that is yearly 8.8% less expensive by 2050.

Then, considering the primary energy mix shown in Figure 3.4, three phases in the transition can be identified. Before 2040, thanks to the perfect foresight approach, the model finds it more economical in 2025 to keep on using 33.2 TWh of LFO to produce HVC through naphtha/LPG-cracking. In 2040, uranium-driven SMR substitutes the electricity originally produced from industrial CHP and CCGT running respectively on fossil gas and renewable ammonia. Finally, from 2045 onward, the significant drop

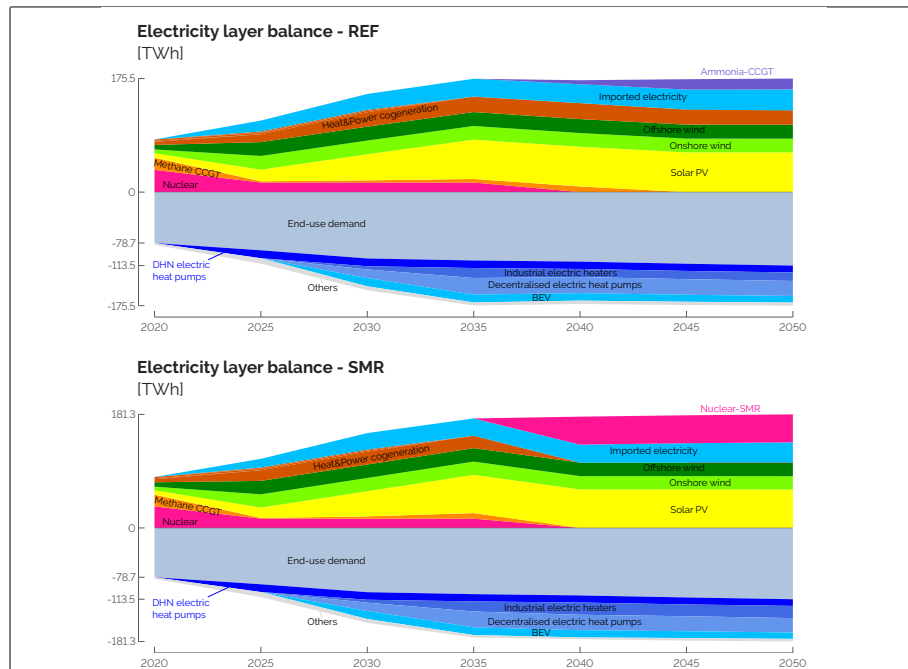


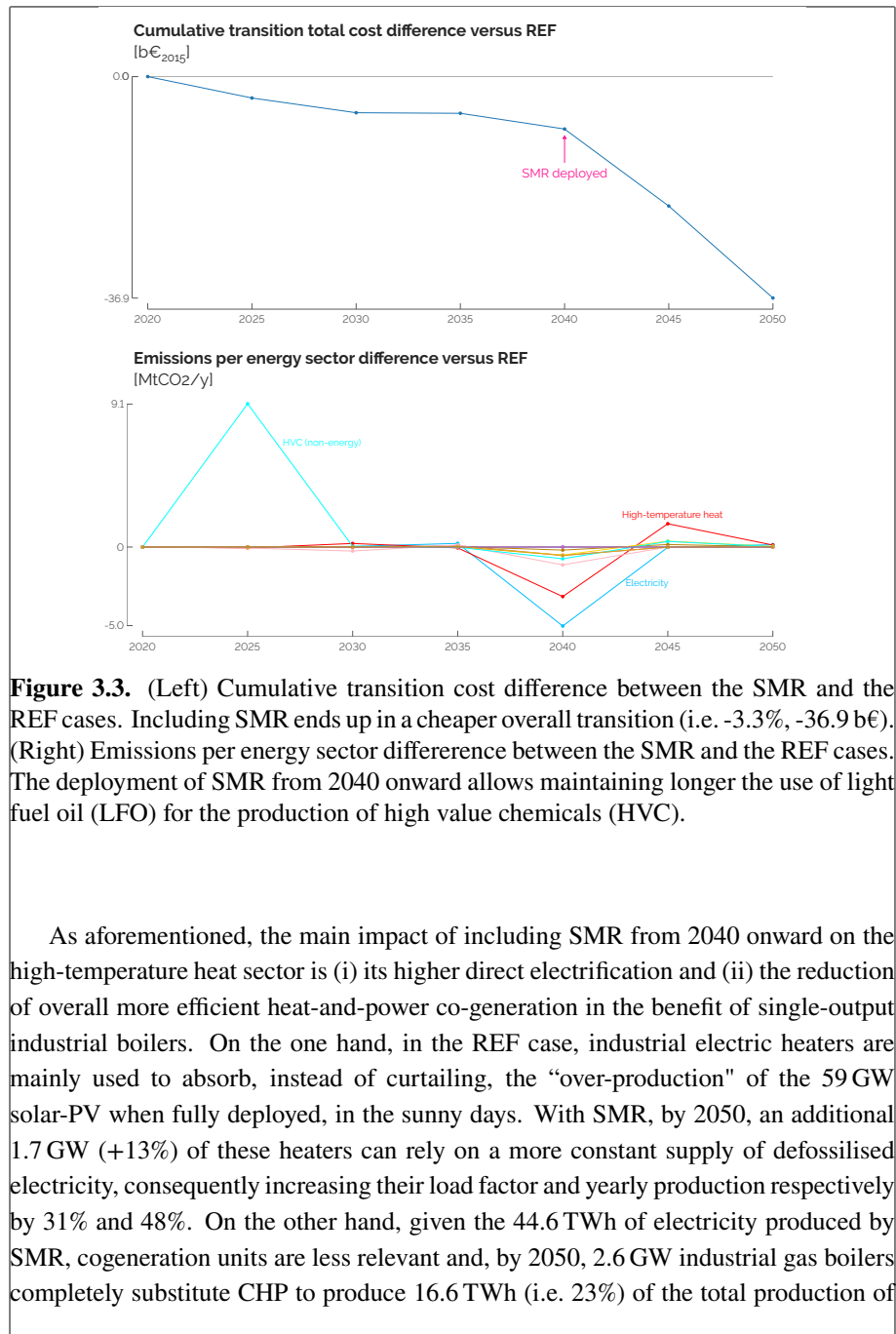
**Figure 3.2.** The production of electricity from SMR substitutes more efficient technologies (i.e. CCGT and CHP) and boosts the electrification of the rest of the system, mostly the industrial high-temperature heat sector.

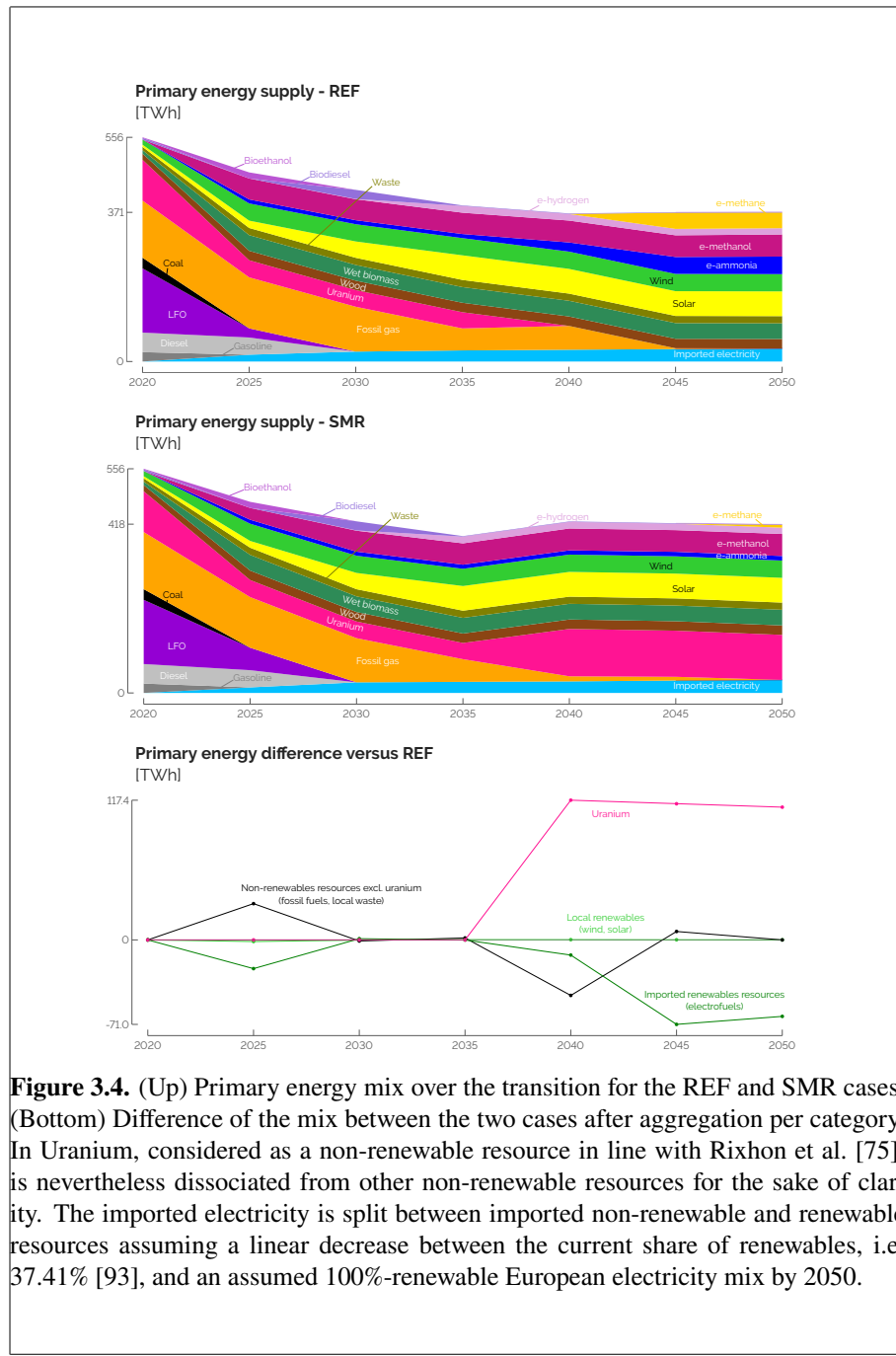
in the consumption of electrofuels comes from the same industrial CHP. This is the illustration of the atom-molecules dilemma where the consumption of local renewables is, on its side, not much affected. In other words, SMR competes with importing electrofuels while both support the integration of local solar and wind energies. Then, like the power sector, the SMR case ends up in a less efficient whole-energy system by 2050 at it consumes 47 TWh (+12.7%) primary energy more to supply an unchanged EUD. Interestingly, in both cases, given the assumptions made on the GWP of the resources (i.e.  $gwp_{op,electrofuels} = 0 \text{ kt}_{\text{CO}_2,\text{eq}}/\text{GWh}$  and  $gwp_{op,uranium} = 0.004 \text{ kt}_{\text{CO}_2,\text{eq}}/\text{GWh}$ ), the constraint on the CO<sub>2</sub>-budget leads to “carbon-neutrality” by 2050<sup>1</sup>.

### 3.1.3 Non-power sectors

#### High-temperature heat

<sup>1</sup>The model being constrained to keep on using all the waste that would keep on being locally produced, the system in 2050 reaches a  $\sim 3.5 \text{ Mt}_{\text{CO}_2,\text{eq}}/\text{year}$ .





high-temperature heat.

### **Low-temperature heat**

This sector is marginally impacted. In both cases, the major shift of supply from decentralised to centralised productions operates early in the transition, to hit the constraint that DHN cannot supply more than 37% of the LT-heat production. Then, from a mix between oil (53%), gas (43%) and wood (4%) boilers for the decentralised production of LT-heat in 2020, the system progressively shifts towards electric heat pump (HP) only. Similarly for the centralised production of LT-heat, electric HP remains the most efficient and economic option.

### **Mobility**

The passenger mobility is not affected either as the electrification of the system is preferentially done in this sector with BEV progressively substituting internal combustion engine (ICE) cars for the private sector. About the public mobility, trains and tramways supply their *a priori* set maximum share, respectively, 50% and 30% complemented by compressed natural gas (CNG) buses substituting diesel-driven buses. Similarly, considering the freight transport, technology shifts (i.e. from diesel to FC trucks) or modal shares (i.e. 53%-47% split between NG and (bio)-diesel boats) are identical between the two cases.

### **Non-energy demand**

The supply of ammonia (i.e. from Haber-Bosch to direct import of renewable ammonia) and methanol (i.e. import of renewable methanol) are unchanged between the two cases. However, as introduced previously, to produce HVC, the full substitution of naphtha/LPG-cracking by MTO is delayed as the emissions of the former are compensated by the later integration of SMR.

## **3.2 Uncertainty quantification on the cost, the atom and the molecules**

*“It is difficult to make predictions, especially about the future.”* (Niels Bohr, foundational contributor to the understanding of atomic structure and quantum theory). Besides the deep understanding of the deterministic results, it is important to challenge these conclusions out-of-sample, accounting for the uncertainty of the parameters. To mitigate the computational burden, we have used the PCE approach (Section 1.2.2) on

the monthly version of EnergyScope Pathway. As detailed by Limpens et al. [9], this simplified model does not implement daily storage technologies and integrates much more easily intermittent renewables (PVs and wind turbines) in the system as the daily supply-demand intermittency and mismatch are not at stake. Consequently, it requires less flexibility options (i.e. electrification of the heating sector or import of electricity from the neighbouring countries) and ends up with a cheaper transition (-3%). Although, it allows to quantify the full set of 34 uncertain parameters (i.e. 1260 samples for an order-2 PCE), and avoid the computational burden of the hourly pathway. Nevertheless, comparing the UQ on the hourly pathway with a limited set of uncertain parameters and on the monthly model, Appendix C.1 shows that the most impacting parameters are correctly captured by the latter.

After briefly assessing the GSA on the objective function of the model, the total transition cost, this section investigates more deeply the atom-molecules dilemma. This time, the Sobol' indices are computed for import of renewable molecules and installed capacities of SMR.

### 3.2.1 Total transition cost

Exhaustively listed in Appendix C.1, Table 3.1 gathers the most impacting parameters<sup>2</sup> on the total transition cost, highlighting the cost of purchasing electrofuels as well as the potentiality to install SMR and its CAPEX. The former is the most impacting parameter whereas the two others have much lower influence on the variation of the total transition cost. Given the uncertainty characterisation presented in Section 2.4, there are 60% chance that no SMR could be installed. In other words, the variation of the parameter  $f_{\max,SMR}$  has zero impact on the variation of the total transition cost in 60% of the samples. Then, in perspective with the local sensitivity analysis of Section 3.1, the 3.3% reduction has been observed when SMR is installed from 2040 onward. This represents only 10% of the samples. Moreover, given its characteristics detailed in Table 2.1, mostly its cheap and low-emitting fuel (i.e. uranium) and the long lifetime leading to lower annualised CAPEX and higher salvage value, this explains why SMR has this lower impact. On the contrary, more expensive renewable electrofuels are always imported, to a smaller or larger extent depending on the sample. For instance, in the REF case (Section 3.1.2), the imported electrofuels represent, by 2050, 152.9 TWh (i.e. 41% of the primary energy mix) with an average 93€/MWh cost of purchasing and,

<sup>2</sup>Per Turati et al. [94], parameters are considered as “impacting” if their Sobol’ index is above the threshold =  $1/d$ ,  $d$  being the total number of uncertain parameters after the pre-selection phase. In this case,  $d = 34$ , and, consequently, the threshold is equal to 2.9%.

over the entire transition, a 273 b€ cumulative OPEX (i.e. 25% of the total transition cost).

**Table 3.1.** Total Sobol' indices of the uncertain parameters over the total transition cost. Where the cost of purchasing electrofuels is the top-1 parameter, SMR-related parameters have a negligible impact on this cost.

Parameter	Ranking	Sobol' index
<b>Purchase electrofuels</b>	1	47.4%
Industry EUD	2	23.5%
Interest rate	3	11.0%
Purchase fossil fuels	4	6.9%
:	:	:
<b>Potential capacity SMR</b>	11	0.9%
:	:	:
<b>CAPEX SMR</b>	32	<0.1%

Given the relatively wide uncertainty range (i.e. up to [-30.8%; +24.0%] by 2050) and, above all, the major share among the total demand, between 53% and 60%, the industrial EUD is the second most impacting parameter. Then, as the driving factor for the annualisation and the salvage value of the assets, the interest rate has a 11% Sobol' index<sup>3</sup>. Finally, similarly to electrofuels, the cost of purchasing fossil fuels is also to consider in the perspective to reduce the uncertainty over the total transition cost. However, due to the ambitious CO<sub>2</sub>-budget, phasing out of fossil fuels is urgent and makes their uncertain impact smaller than their renewable alternatives.

Figure 3.5 shows the probability density function (PDF) of the total transition cost given the 1260 samples. Stretching between 680 b€ and 1940 b€, the mean, the median and the nominal value (i.e. REF case) are close to each other, respectively 1160 b€, 1150 b€ and 1080 b€. Similarly to the analysis carried out by Coppitters and Contino [96], one observes here that the distribution is right-skewed. It could then be qualified as "fragile" as the top 50% of the samples cover a bigger range (i.e. between 1150 and 1940) than the bottom 50% of the samples (i.e. between 680 and 1150). In other words, the bad scenarios, resulting in a total transition cost higher than the median, have a bigger effect on this cost.

<sup>3</sup>It is important to note here that the model considers an overall interest rate for the entire system (i.e. 1.5% as a nominal value). In practice, the interest rate would vary depending on the technology investment risk. This variation would have, for instance, a major impact on the LCOE of technologies like nuclear power plants [95], given the important capital needs and long time horizons [92].

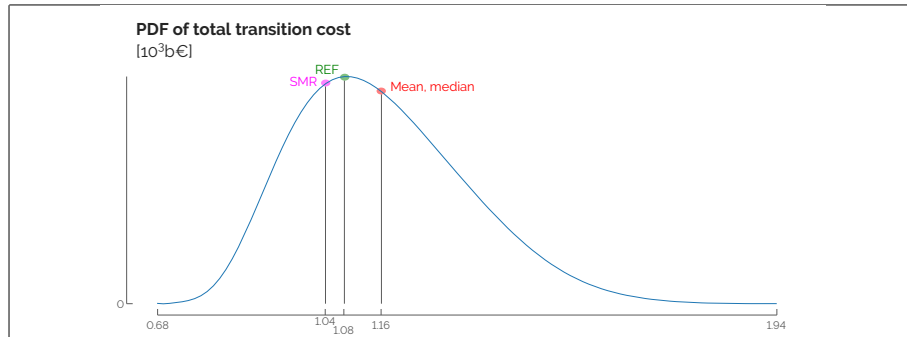


**Figure 3.5.** probability density function (PDF) of the total transition cost. The mean,  $\mu = 1.16 \cdot 10^3$  b€, is slightly higher than the median ( $P_{50} = 1.15 \cdot 10^3$  b€) and the nominal cases cost,  $1.08 \cdot 10^3$  b€ and  $1.04 \cdot 10^3$  b€ respectively for the REF and SMR cases. Also, with a standard deviation,  $\sigma = 185$  b€, a 95%-confidence interval would be about  $[0.8; 1.5] \cdot 10^3$  b€.

### 3.2.2 Atom and molecules

The samples used to carry out the GSA on the total transition cost, also provide the distribution of other outputs of the model. Among them, Figure 3.6 shows the evolution of the import of renewable electrofuels over the transition.

As the general trends are increasing, discrepancies exist between the different energy carriers. E-methane, as the renewable alternative to fossil natural gas, substitutes it, sometimes at a very early stage of the transition, 2025, and to a somehow unrealistically large extent, 173 TWh, which is more than 13% more than the total import of electrofuels in the REF case. The necessity to import this molecule is progressive through the transition to supply mostly industrial CHP and boilers.

E-hydrogen becomes rapidly the main stream of hydrogen in the system, on top of steam-methane-reforming or electrolysis, to reach a median and a maximum values of, respectively 13.6 TWh and 40.7 TWh in 2050. Hydrogen is more frequently used in the mobility sector. Like in the REF case, fuel cell trucks are often the first option but, in some outlying cases, fuel cell cars and buses appear to completely substitute respectively BEV cars and CNG buses by 2050. Moreover, some samples lead to local production of methanol via the methanolation process, to produce up to 16.3 TWh of methanol (i.e. 30% of the total supply of methanol of the nominal REF and SMR cases).

Then, the imported e-ammonia, becoming rapidly cost-competitive against its fossil alternative (Figure 2.2), quickly substitutes it and the Haber-Bosch process. Where the initial purpose of ammonia is to satisfy a relatively limited non-energy demand

(NED) (i.e.  $10 \pm 3$  TWh by 2050), the variation of its import is mostly due to the higher or lower need for ammonia-CCGT as a flexible option to produce electricity. From 2035, out of the four considered electrofuels, the imported e-ammonia is the one exhibiting the largest uncertainty with, for instance, an interquartile range (IQR)<sup>4</sup> of about 50 TWh. In some extreme cases, e-ammonia is the most imported molecules, i.e. up to 233 TWh or 63% of the total primary mix in the REF case in 2050.

Likewise, e-methanol early becomes the selected option to supply methanol even though alternatives like biomass-to-methanol or synthetic methanolation exist in some outlying cases. Given its lower NED (i.e.  $1.5 \pm 0.5$  TWh<sub>NED, methanol</sub> by 2050), the variation of imported e-methanol is almost exclusively due to its role in the industrial production of HVC, i.e. 78% of the total NED, through the methanol-to-olefins (MTO) process. In some rare samples, methanol is also used to supply the freight transport sector via boats or trucks.

Appendix C.2 gives a more detailed information. On the one hand, it compares the statistics (i.e. quartiles and median) with the quantity of imported electrofuels in the REF and SMR cases. On the other hand, this appendix shows the distributions of the different sources of supply and consumption of gas, hydrogen, ammonia and methanol.

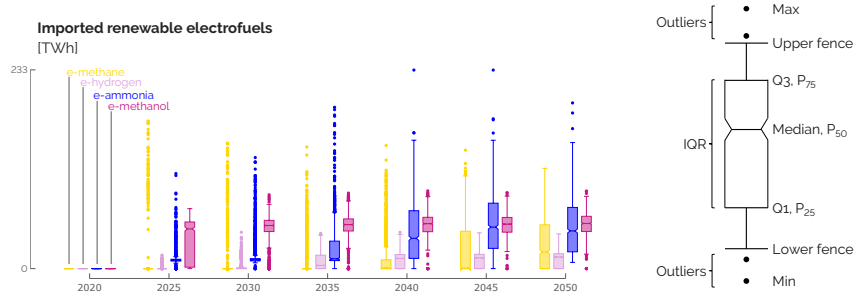


**Figure 3.6.** Distribution of the imported renewable electrofuels over the transition. Starting from no electrofuel in 2020, their respective import rises progressively along the transition (i.e. increasing median) at different growth rates and with different ranges of values. Observations being either 1.5 times the interquartile range (IQR) less than the first quartile (Q1) or 1.5 times the interquartile range greater than the third quartile (Q3) are defined as outliers.

After investigating the distribution of imports of electrofuels over the transition, this part assesses the space of uncertainties, like Pickering et al. [97] who investigated the space of feasibility to reach carbon neutrality in Europe. Figures 3.7 and 3.8 give

<sup>4</sup>The interquartile range is the difference between the third quartile ( $Q3$  or  $P_{75}$ ) and the first ( $Q1$  or  $P_{25}$ ). It is an indicator of statistical dispersion around the median,  $Q2$  or  $P_{50}$ .

the trend lines of the key parameters for these imports in 2050<sup>5</sup>, as well the installed capacities of SMR. Next to the name of a parameter, one can read its Sobol' index versus the output of interest<sup>6</sup>. Box plots also point out the distribution of this output for the extreme low or high values of some parameters.

As aforementioned, the industrial EUD impacts the most the import of e-methane. This parameter directly dictates the demand of industrial high-temperature heat for which industrial gas CHP, and industrial gas boilers to a lower extent, represent, on average over all the samples, respectively 25.6% and 6.1% of the total production. Then, considering the smaller-impact parameters, we notice that SMR plays a non-negligible role. Indeed, if deployed, SMR produces abundant low-emitting electricity for industrial electric heaters that substitute, even completely in some cases, gas alternatives. This confirms the observation made in Section 3.1.3. Highly available local biomass also leads to smaller import of e-methane to supply bio-hydrolysis and produce methane-equivalent gas. Finally, and surprisingly, costs of purchasing electrofuels and fossil fuels have a positive and negative correlation with the amount of e-methane, respectively. In other words, by 2050, more expensive electrofuels induce to more e-methane import and *vice versa* for the fossil fuels. Given the techno-economic optimum sought by EnergyScope, if electrofuels are more expensive, the system will, overall, import less of them, especially e-ammonia, mainly used by CCGT. Subject to the CO<sub>2</sub>-budget for the transition, the system goes towards more efficient technologies, like industrial methane-CHP to substitute e-ammonia-CCGT in the production of electricity. First running on fossil natural gas, these CHP consume more e-methane by 2050. In the contrary, if electrofuels are cheaper, there is more import of them, and especially of e-ammonia. This leaves room for more emitting and cheaper resources to be used while respecting the CO<sub>2</sub>-budget, i.e. coal in industrial boilers that produce, in these cases, on average 24% of the high-temperature (HT) heat in 2050. Consequently, there is smaller investment in methane CHP, and consequently import of e-methane as more abundant renewable electricity is produced via e-ammonia-CCGT and more HT-heat is supplied by industrial coal boilers. Even though we might expect that no more coal will be consumed in Belgium by 2050, the model still has the opportunity to use it if the CO<sub>2</sub>-budget allows it. About the cost of purchasing fossil fuels, the parameter has mainly an impact on the import of fossil NG as the most versatile energy carrier in the whole-energy system. If NG is more expensive, the system will import less of

<sup>5</sup>The authors picked this specific year as it is the one where electrofuels, if imported, are imported in the largest amount, in general, compared to the other years of the transition.

<sup>6</sup>For these outputs of interest, different from the total transition cost, the LOO error is generally higher than the threshold of 1 % defined in Section 1.2.2. Consequently, the Sobol' indices are less accurate but already allow a fair relative comparison between the different parameters.

it. Subsequently, the investments in methane-CHP and boilers are more limited. This ends up in smaller need for e-methane by 2050.

In relation to e-hydrogen, the sensitivity analysis highlights its dependence on various driving parameters, particularly those linked to the transport sector. As depicted in Figure C.1 in Appendix C.2, the utilisation of e-hydrogen is most prevalent in FC trucks, followed by FC cars and buses to a lesser extent. The adoption of fuel cell engines in trucks contributes, on average, to 63.5% of the total road freight transport, thereby affecting the level of e-hydrogen imports. Consequently, the smaller is the CAPEX of fuel cell engines, the more the system imports e-hydrogen. Similarly, the cost of purchasing electrofuels influences e-hydrogen imports. Subsequently, the cost of purchasing biofuels emerges as the third most influential parameter. Indeed, biodiesel trucks are the mostly picked alternative to FC trucks to provide, on average, 27.6% of the total. Additionally, CNG buses are preferred in public road transport (34.9%), followed by FC buses (11.2%) competing with biodiesel and hybrid biodiesel buses, accounting for 27.8% and 26.1%, respectively. Finally, the last noticeable parameter at stake is the CAPEX of electric vehicles. In competition with BEV that stand for 83.4% on average of the private mobility sector, the cheaper these cars are, the more cost-competitive are these vehicles, and vice versa, versus FC cars (i.e. 13.7% of the total passenger mobility, on average).

As already pointed out in Section 3.1.1, the installation of SMR drastically reduces the import of e-ammonia. As ammonia CCGT is the biggest consumer of ammonia by the end of the transition, low-emitting and cheap electricity flexibly produced by SMR substitutes the CCGT. With a higher cost of purchasing electrofuels, this import of e-ammonia drops down to 7.3 TWh, 83.4% less than in the REF case. Then, with a 9%-Sobol' index, industrial EUD also influences the need for this molecule, due to its NED.

The conclusions are more straightforward for the import of e-methanol and the installed capacity of SMR. For the former, industrial EUD is, by far (i.e. 81% Sobol' index), the key factor. Due to its own NED but, above all, since it is the low-emitting alternative picked by the model to supply the significant NED of HVC, the lower this demand, the lower the need to import e-methanol, and vice versa. For the latter, it is the availability of the technology that drives its installation. Not shown here but all the samples of the GSA highlight that SMR is installed to its maximum capacity, i.e. 6 GW, as soon as possible. In other words, the only parameter "Potential capacity

SMR” dictates the installation of this technology<sup>7</sup>. Surprisingly, the [-40%; +44%] variation of its CAPEX has a negligible impact, with a Sobol’ index of 0.9%.

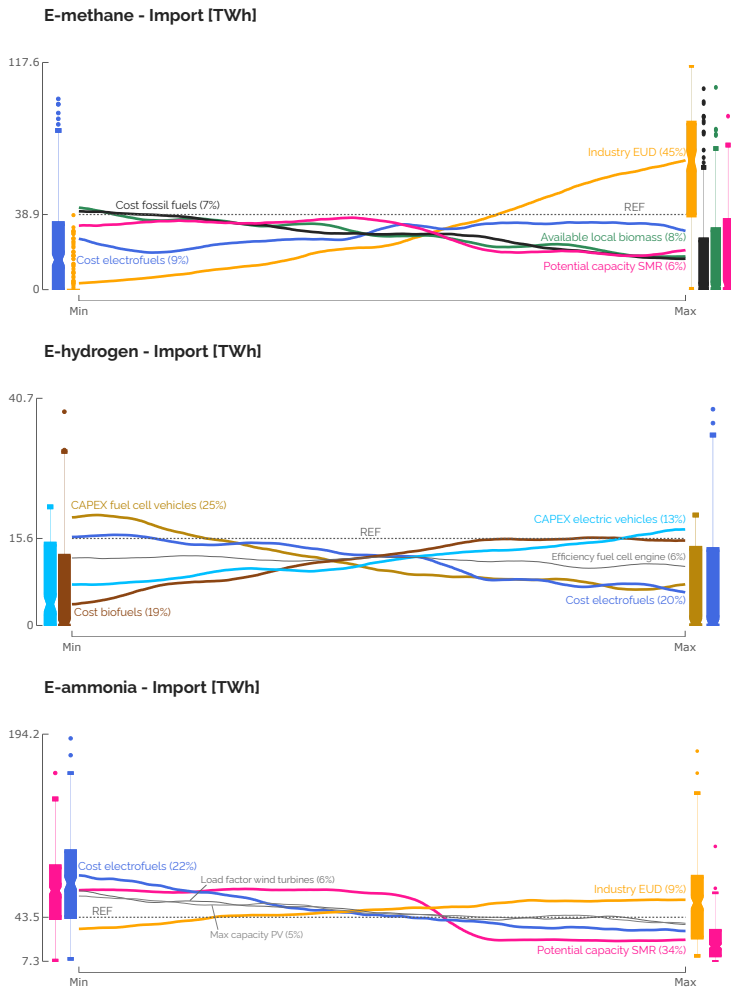


**Figure 3.7.** Trend lines of the key parameters on the import of e-methane, e-hydrogen and e-ammonia. Around these lines, box plots point out the distribution of the output of interest for the extreme values (either bottom-15% or top-15%) of some parameters. The grey dashed line gives the value of the output of interest in the REF case. Part A

<sup>7</sup>In practice, we observe that as soon as this parameter is equal or higher than 0.9, 0.8 and 0.6, 6 GW SMR is installed from, respectively, 2040, 2045 and 2050.

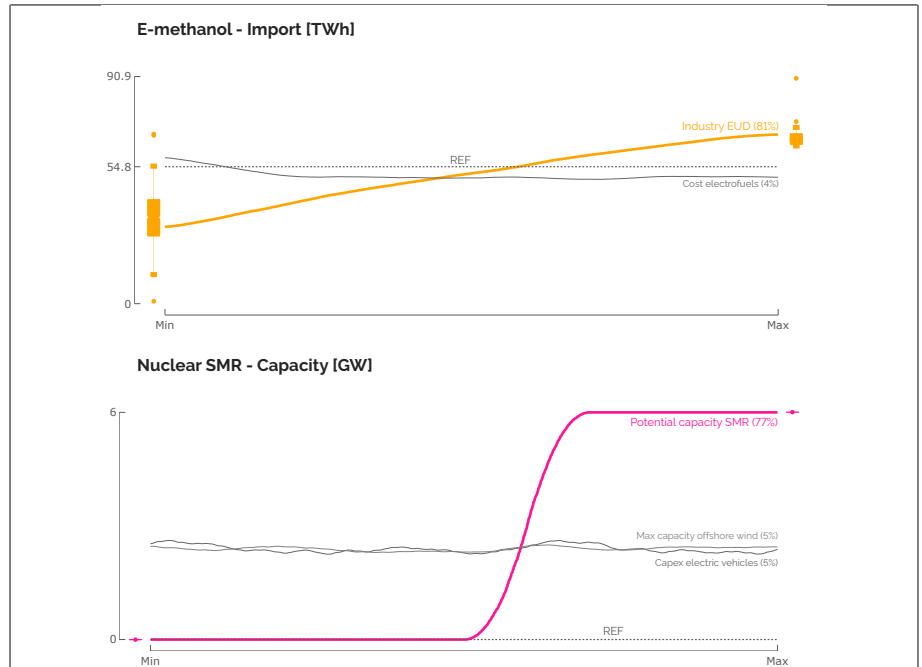


**Figure 3.8.** Trend lines of the key parameters on the import of e-methanol and the installed capacity of SMR, in 2050. Around these lines, box plots point out the distribution of the output of interest for the extreme values (either bottom-15% or top-15%) of some parameters. The grey dashed line gives the value of the output of interest in the REF case. Part B

### 3.2.3 Local renewables

In line with results given in Section 3.1, the GSA shows that SMR has negligible impact on the deployment of local VRES (i.e. PV, onshore and offshore wind turbines). Figure 3.9 gives the evolution of Sobol' indices for the most impacting parameters on the deployment of PV and offshore wind<sup>8</sup>. The key factor that drives the installed capacities of these two technologies is mostly their respective maximum potential, especially at the end of the transition, much more than their CAPEX. Given its higher LCOE (Figure 2.3), PV is more impacted in the short-term by the variation on the cost of purchasing electrofuels supplying e-methane (and e-ammonia to a lesser extent) CCGT. However, this impact gets negligible by 2050.

<sup>8</sup> As the installed capacities of onshore wind is totally driven by the uncertainty on its maximum potential,  $f_{\max,windon}$ , it is not represented in the figure.

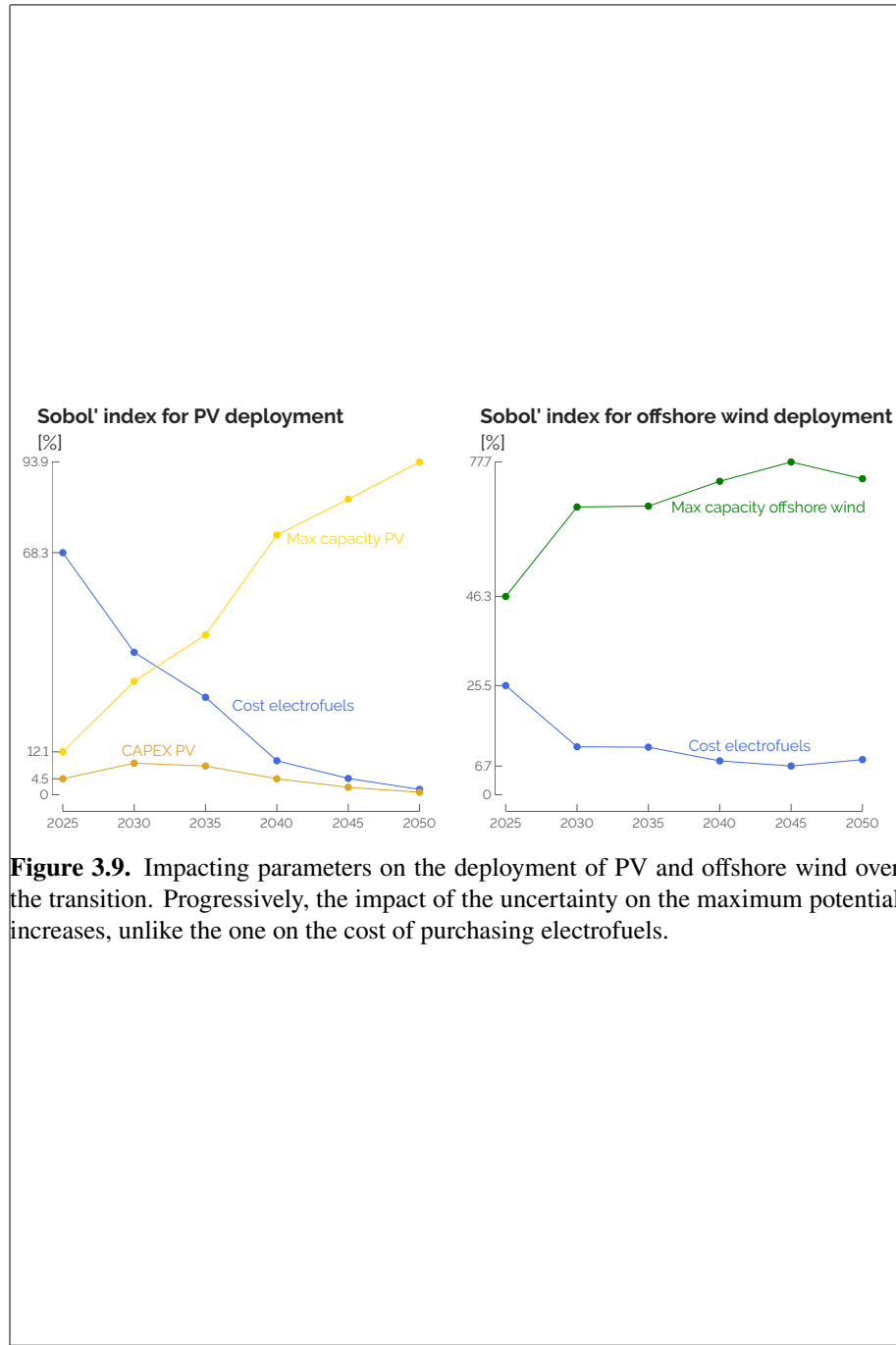


**Figure 3.9.** Impacting parameters on the deployment of PV and offshore wind over the transition. Progressively, the impact of the uncertainty on the maximum potential increases, unlike the one on the cost of purchasing electrofuels.

---

---

## Bibliography

- [1] G. Limpens, Generating energy transition pathways: application to Belgium, Ph.D. thesis, Université Catholique de Louvain, 2021.
- [2] E. Guevara, F. Babonneau, T. Homem-de Mello, Modeling uncertainty processes for multi-stage optimization of strategic energy planning: An autoregressive and markov chain formulation (2022).
- [3] S. Moret, V. Codina Gironès, M. Bierlaire, F. Maréchal, Characterization of input uncertainties in strategic energy planning models, Applied Energy 202 (2017) 597–617.
- [4] G. Limpens, D. Coppitters, X. Rixhon, F. Contino, H. Jeanmart, The impact of uncertainties on the belgian energy system: Application of the polynomial chaos expansion to the energyscope model, Proceedings of the ECOS (2020).
- [5] X. Rixhon, G. Limpens, D. Coppitters, H. Jeanmart, F. Contino, The role of electrofuels under uncertainties for the belgian energy transition, Energies 14 (2021) 4027.
- [6] B. Goffaux, Pathway towards energy sustainability in belgium under uncertainties, 2021. URL: <https://dial.uclouvain.be/memoire/ucl/object/thesis:30574>.
- [7] S. Moret, M. Bierlaire, F. Maréchal, Strategic energy planning under uncertainty: a mixed-integer linear programming modeling framework for large-scale energy systems, in: Computer Aided Chemical Engineering, volume 38, Elsevier, 2016, pp. 1899–1904.
- [8] G. Limpens, S. Moret, H. Jeanmart, F. Maréchal, Energyscope td: A novel open-source model for regional energy systems, Applied Energy 255 (2019) 113729.

- [9] G. Limpens, X. Rixhon, F. Contino, H. Jeanmart, Energyscope pathway: an open-source model to optimise the energy transition pathways of a regional whole-energy system, Elsevier in Applied Energy 358 (2024). doi:<https://doi.org/10.1016/j.apenergy.2023.122501>.
- [10] D. Coppitters, Robust design optimization of hybrid renewable energy systems, Vrije Universiteit Brussel (VUB), University of Mons (UMONS), Mons (2021).
- [11] G. Limpens, EnergyScope Pathway documentation, Accessed 2022. URL: <https://energyscope-pathway.readthedocs.io/en/v1.1/>.
- [12] T. Stocker, Climate change 2013: the physical science basis: Working Group I contribution to the Fifth assessment report of the Intergovernmental Panel on Climate Change, Cambridge university press, 2014.
- [13] J. Schnidrig, J. Brun, F. Maréchal, M. Margni, Integration of life cycle impact assessment in energy system modelling, Proceedings of ECOS 2023 (2023).
- [14] S. Babrowski, T. Heffels, P. Jochem, W. Fichtner, Reducing computing time of energy system models by a myopic approach: A case study based on the perseus-net model, Energy systems 5 (2014) 65–83.
- [15] K. Poncelet, E. Delarue, D. Six, W. D’haeseleer, Myopic optimization models for simulation of investment decisions in the electric power sector, in: 2016 13th International Conference on the European Energy Market (EEM), IEEE, 2016, pp. 1–9.
- [16] F. F. Nerini, I. Keppo, N. Strachan, Myopic decision making in energy system decarbonisation pathways. a uk case study, Energy strategy reviews 17 (2017) 19–26.
- [17] C. F. Heuberger, I. Staffell, N. Shah, N. Mac Dowell, Impact of myopic decision-making and disruptive events in power systems planning, Nature Energy 3 (2018) 634–640.
- [18] S. Moret, F. Babonneau, M. Bierlaire, F. Maréchal, Overcapacity in european power systems: Analysis and robust optimization approach, Applied Energy 259 (2020) 113970.
- [19] AMPL Optimization Inc., AMPL Python API, <https://amplpyAMPL.com/en/latest/>, 2024.

- [20] V. Krey, Vergleich kurz- und langfristig ausgerichteter optimierungsansätze mit einem multi-regionalen energiesystemmodell unter berücksichtigung stochastischer parameter (2006).
- [21] X. Yue, S. Pye, J. DeCarolis, F. G. Li, F. Rogan, B. Ó. Gallachóir, A review of approaches to uncertainty assessment in energy system optimization models, *Energy strategy reviews* 21 (2018) 204–217.
- [22] G. Mavromatidis, K. Orehounig, J. Carmeliet, Uncertainty and global sensitivity analysis for the optimal design of distributed energy systems, *Applied Energy* 214 (2018) 219–238.
- [23] J. Peace, J. Weyant, Insights not numbers: the appropriate use of economic models, White paper of Pew Center on Global Climate Change (2008).
- [24] C. Marnay, A. S. Siddiqui, Addressing an uncertain future using scenario analysis, Lawrence Berkeley National Laboratory, 2006.
- [25] X. Li, S. Moret, F. Baldi, F. Maréchal, Are renewables really that expensive? the impact of uncertainty on the cost of the energy transition, in: Computer Aided Chemical Engineering, volume 46, Elsevier, 2019, pp. 1753–1758.
- [26] D. Coppitters, W. De Paepe, F. Contino, Robust design optimization of a photovoltaic-battery-heat pump system with thermal storage under aleatory and epistemic uncertainty, *Energy* 229 (2021) 120692.
- [27] Hydrogen Import Coalition, Shipping sun and wind to belgium is key in climate neutral economy, <https://www.portofantwerp.com/sites/default/files/Hydrogen%20Import%20Coalition.pdf>, 2021.
- [28] D. Coppitters, W. De Paepe, F. Contino, Robust design optimization and stochastic performance analysis of a grid-connected photovoltaic system with battery storage and hydrogen storage, *Energy* 213 (2020) 118798.
- [29] D. Coppitters, P. Tsirikoglou, W. D. Paepe, K. Kyprianidis, A. Kalfas, F. Contino, RHEIA: Robust design optimization of renewable Hydrogen and dERived energy cArrier systems, *Journal of Open Source Software* 7 (2022) 4370. doi:10.21105/joss.04370.
- [30] D. Coppitters, RHEIA documentation, Accessed 2022. URL: <https://rheia.readthedocs.io/en/latest/index.html>.

- [31] B. Sudret, Polynomial chaos expansions and stochastic finite element methods, *Risk and reliability in geotechnical engineering* (2014) 265–300.
- [32] P. Bratley, B. Fox, Implementing sobols quasirandom sequence generator (algorithm 659), *ACM Transactions on Mathematical Software* 29 (2003) 49–57.
- [33] M. D. Morris, Factorial Sampling Plans for Preliminary Computational Experiments, *Technometrics* 33 (1991) 161–174.
- [34] G. Sin, K. V. Gernaey, Improving the morris method for sensitivity analysis by scaling the elementary effects, in: *Computer Aided Chemical Engineering*, volume 26, Elsevier, 2009, pp. 925–930.
- [35] S. Moret, Strategic energy planning under uncertainty, Ph.D. thesis, EPFL, 2017.
- [36] A. Perera, P. Kamalaruban, Applications of reinforcement learning in energy systems, *Renewable and Sustainable Energy Reviews* 137 (2021) 110618.
- [37] T. Haarnoja, A. Zhou, P. Abbeel, S. Levine, Soft actor-critic: Off-policy maximum entropy deep reinforcement learning with a stochastic actor, in: *International conference on machine learning*, PMLR, 2018, pp. 1861–1870.
- [38] T. Haarnoja, H. Tang, P. Abbeel, S. Levine, Reinforcement learning with deep energy-based policies, in: *International conference on machine learning*, PMLR, 2017, pp. 1352–1361.
- [39] B. D. Ziebart, Modeling purposeful adaptive behavior with the principle of maximum causal entropy, Carnegie Mellon University, 2010.
- [40] A. Raffin, A. Hill, A. Gleave, A. Kanervisto, M. Ernestus, N. Dormann, Stable-baselines3: Reliable reinforcement learning implementations, *The Journal of Machine Learning Research* 22 (2021) 12348–12355.
- [41] M. Abadi, A. Agarwal, P. Barham, E. Brevdo, Z. Chen, C. Citro, G. S. Corrado, A. Davis, J. Dean, M. Devin, et al., Tensorflow: Large-scale machine learning on heterogeneous distributed systems, *arXiv preprint arXiv:1603.04467* (2016).
- [42] R. S. Sutton, A. G. Barto, *Reinforcement learning: An introduction*, MIT press, 2018.

- [43] K. Pearson, On lines and planes of closest fit to systems of points in space., *The London, Edinburgh, and Dublin philosophical magazine and journal of science* 2 (1901) 559–572.
- [44] H. Hotelling, Analysis of a complex of statistical variables into principal components., *Journal of educational psychology* 24 (1933) 417.
- [45] I. T. Jolliffe, Principal component analysis for special types of data, Springer, 2002.
- [46] K. Zdybał, G. D'Alessio, G. Aversano, M. R. Malik, A. Coussement, J. C. Sutherland, A. Parente, Advancing reacting flow simulations with data-driven models, *arXiv preprint arXiv:2209.02051* (2022).
- [47] A. Parente, J. C. Sutherland, Principal component analysis of turbulent combustion data: Data pre-processing and manifold sensitivity, *Combustion and flame* 160 (2013) 340–350.
- [48] K. Peerenboom, A. Parente, T. Kozák, A. Bogaerts, G. Degrez, Dimension reduction of non-equilibrium plasma kinetic models using principal component analysis, *Plasma Sources Science and Technology* 24 (2015) 025004.
- [49] H. Aguinis, R. K. Gottfredson, H. Joo, Best-practice recommendations for defining, identifying, and handling outliers, *Organizational research methods* 16 (2013) 270–301.
- [50] I. Stanimirova, M. Daszykowski, B. Walczak, Dealing with missing values and outliers in principal component analysis, *Talanta* 72 (2007) 172–178.
- [51] J. Domisse, J.-L. Tychon, Modelling of Low Carbon Energy Systems for 26 European Countries with EnergyScopeTD : Can European Energy Systems Reach Carbon Neutrality Independently?, Master's thesis, UCLouvain, 2020. URL: <http://hdl.handle.net/2078.1/thesis:25202>.
- [52] X. Rixhon, D. Tonelli, M. Colla, K. Verleysen, G. Limpens, H. Jeanmart, F. Contino, Integration of non-energy among the end-use demands of bottom-up whole-energy system models, *Frontiers in Energy Research-Process and Energy Systems Engineering* 10 (2022).
- [53] Eurostat, Energy, Transport and environment statistics, 2019 edition, 2019.
- [54] G. Limpens, H. Jeanmart, F. Maréchal, Belgian energy transition: What are the options?, *Energies* 13 (2020) 261.

- [55] E. Commission, D.-G. for Climate Action, D.-G. for Energy, D.-G. for Mobility, Transport, A. De Vita, P. Capros, L. Paroussos, K. Fragkiadakis, P. Karkatsoulis, L. Höglund-Isaksson, W. Winiwarter, P. Purohit, A. Gómez-Sanabria, P. Rafaj, L. Warnecke, A. Deppermann, M. Gusti, S. Frank, P. Lauri, F. Fulvio, A. Florou, M. Kannavou, N. Forsell, T. Fotiou, P. Siskos, P. Havlík, I. Tsipopoulos, S. Evangelopoulou, P. Witzke, M. Kesting, N. Katoufa, I. Mitsios, G. Asimakopoulou, T. Kalokyris, EU reference scenario 2020 : energy, transport and GHG emissions : trends to 2050, Publications Office, 2021. doi:doi/10.2833/35750.
- [56] IEA, Nuclear Power and Secure Energy Transitions, Technical Report, IEA, Paris, 2022. <https://www.iea.org/reports/nuclear-power-and-secure-energy-transitions>, License: CC BY 4.0.
- [57] M. E. Biresselioglu, M. D. Kaplan, B. K. Yilmaz, Electric mobility in europe: A comprehensive review of motivators and barriers in decision making processes, Transportation Research Part A: Policy and Practice 109 (2018) 1–13.
- [58] Bureau Fédéral du Plan, Perspectives de l'évolution de la demande de transport en belgique à l'horizon 2030, 2015.
- [59] National Research Council, Transitions to alternative vehicles and fuels, National Academies Press (2013).
- [60] J. Schnidrig, T.-V. Nguyen, X. Li, F. Maréchal, A modelling framework for assessing the impact of green mobility technologies on energy systems, Technical Report, EPFL, 2021.
- [61] FPS Economy, ENERGY Key Data (2021).
- [62] IEA, The Future of Petrochemicals – Analysis, <https://www.iea.org/reports/the-future-of-petrochemicals>, 2018.
- [63] V. Daioglou, A. P. Faaij, D. Saygin, M. K. Patel, B. Wicke, D. P. van Vuuren, Energy demand and emissions of the non-energy sector, Energy & Environmental Science 7 (2014) 482–498.
- [64] Statbel, Energy statistics by economic sector and by energy source, <https://statbel.fgov.be/en/themes/energy/energy-statistics-economic-sector-and-energy-source>, (Accessed February 11, 2021).

- [65] European Commission, European strategy for plastics, [https://ec.europa.eu/environment/waste/plastic\\_waste.htm](https://ec.europa.eu/environment/waste/plastic_waste.htm), (Accessed February 16, 2021).
- [66] Agoria & essenscia, The belgian plastics industry and the circular economy, [https://www.essenscia.be/wp-content/uploads/2019/11/Plast\\_BROCH\\_A5\\_HR.pdf](https://www.essenscia.be/wp-content/uploads/2019/11/Plast_BROCH_A5_HR.pdf), (Accessed February 16, 2021).
- [67] United Nations - Climate change, National inventory submissions 2020, <https://unfccc.int/ghg-inventories-annex-i-parties/2020>, (Accessed February 16, 2021).
- [68] M. M. S. Asia), Mmsa supply and demand forecast, <https://www.methanolmsa.com/additional-mmsa-services/temp-price-forecasts/>, (Accessed February 16, 2021).
- [69] P. Capros, A. De Vita, N. Tasios, P. Siskos, M. Kannavou, A. Petropoulos, S. Evangelopoulou, M. Zampara, D. Papadopoulos, C. Nakos, et al., Eu reference scenario 2016-energy, transport and ghg emissions trends to 2050., European Commission Directorate-General for Energy (2016). doi:10.2833/9127.
- [70] L. Genge, F. Scheller, F. Müsgens, Supply costs of green chemical energy carriers at the european border: A meta-analysis, International Journal of Hydrogen Energy (2023).
- [71] M. J. Grant, A. Booth, A typology of reviews: an analysis of 14 review types and associated methodologies, Health information & libraries journal 26 (2009) 91–108.
- [72] M. J. Page, J. E. McKenzie, P. M. Bossuyt, I. Boutron, T. C. Hoffmann, C. D. Mulrow, L. Shamseer, J. M. Tetzlaff, E. A. Akl, S. E. Brennan, et al., The prisma 2020 statement: an updated guideline for reporting systematic reviews, International journal of surgery 88 (2021) 105906.
- [73] EnergyVille, Paths2050 - the power of perspective, <https://perspective2050.energyville.be/>, 2022 (accessed December 2022).
- [74] ELIA, Electricity scenarios for Belgium towards 2050, Technical Report, 2017.
- [75] X. Rixhon, G. Limpens, F. Contino, H. Jeanmart, Taxonomy of the fuels in a whole-energy system, Frontiers in Energy Research - Sustainable Energy Systems and Policies (2021). doi:10.3389/fenrg.2021.660073.

- [76] SCK-CEN, Small modular reactor (smr), <https://www.sckcen.be/en/expertises/nuclear-systems/small-modular-reactor-smr>, (Accessed July 2023).
- [77] I. Tsiropoulos, R. Hoefnagels, S. de Jong, M. van den Broek, M. Patel, A. Faaij, Emerging bioeconomy sectors in energy systems modeling—integrated systems analysis of electricity, heat, road transport, aviation, and chemicals: a case study for the netherlands, *Biofuels, Bioproducts and Biorefining* 12 (2018) 665–693.
- [78] [https://github.com/xrixhon/Non\\_energy\\_demand/tree/NED](https://github.com/xrixhon/Non_energy_demand/tree/NED), March 2021.
- [79] X. Rixhon, M. Colla, D. Tonelli, K. Verleysen, G. Limpens, H. Jeanmart, F. Contino, Comprehensive integration of the non-energy demand within a whole-energy system: towards a defossilisation of the chemical industry in belgium, in: 34th International Conference on Efficiency, Cost, Optimization, Simulation and Environmental Impact of Energy Systems (ECOS 2021). Taormina, Italy, 2021, pp. 152–163.
- [80] F. Licandeo, F. Flores, F. Feijoo, Assessing the impacts of economy-wide emissions policies in the water, energy, and land systems considering water scarcity scenarios, *Applied Energy* 342 (2023) 121115.
- [81] K. Richardson, W. Steffen, W. Lucht, J. Bendtsen, S. E. Cornell, J. F. Donges, M. Drüke, I. Fetzer, G. Bala, W. von Bloh, et al., Earth beyond six of nine planetary boundaries, *Science advances* 9 (2023) eadh2458.
- [82] W. Steffen, K. Richardson, J. Rockström, S. E. Cornell, I. Fetzer, E. M. Bennett, R. Biggs, S. R. Carpenter, W. De Vries, C. A. De Wit, et al., Planetary boundaries: Guiding human development on a changing planet, *Science* 347 (2015) 1259855.
- [83] J. Rockström, W. Steffen, K. Noone, Å. Persson, F. S. Chapin, E. F. Lambin, T. M. Lenton, M. Scheffer, C. Folke, H. J. Schellnhuber, et al., A safe operating space for humanity, *nature* 461 (2009) 472–475.
- [84] M. W. Ryberg, M. M. Andersen, M. Owsiania, M. Z. Hauschild, Downscaling the planetary boundaries in absolute environmental sustainability assessments—a review, *Journal of cleaner production* 276 (2020) 123287.

- [85] M. W. Ryberg, M. Owsiania, J. Clavreul, C. Mueller, S. Sim, H. King, M. Z. Hauschild, How to bring absolute sustainability into decision-making: an industry case study using a planetary boundary-based methodology, *Science of the Total Environment* 634 (2018) 1406–1416.
- [86] K. N. Brejnrod, P. Kalbar, S. Petersen, M. Birkved, The absolute environmental performance of buildings, *Building and environment* 119 (2017) 87–98.
- [87] H. Hoff, H. Tiina, C. Sarah, L. Paul, Bringing eu policy into line with the planetary boundaries (2017).
- [88] D. W. O'Neill, A. L. Fanning, W. F. Lamb, J. K. Steinberger, A good life for all within planetary boundaries, *Nature sustainability* 1 (2018) 88–95.
- [89] C. Knight, What is grandfathering?, *Environmental Politics* 22 (2013) 410–427.
- [90] Our World in Data, Global co<sub>2</sub> emissions from fossil fuels, <https://ourworldindata.org/co2-emissions>, (Accessed July 2023).
- [91] Intergovernmental Panel on Climate Change (IPCC), Global Warming of 1.5°C. An IPCC Special Report on the impacts of global warming of 1.5°C above pre-industrial levels and related global greenhouse gas emission pathways, in the context of strengthening the global response to the threat of climate change, sustainable development, and efforts to eradicate poverty, Technical Report, 2018.
- [92] IEA, Nuclear power and secure energy transitions, 2022. URL: <https://www.iea.org/reports/nuclear-power-and-secure-energy-transitions>, license: CC BY 4.0.
- [93] Eurostat, Share of energy from renewable sources, [https://ec.europa.eu/eurostat/databrowser/view/NRG\\_IND\\_REN\\_\\_custom\\_4442440/default/table?lang=en](https://ec.europa.eu/eurostat/databrowser/view/NRG_IND_REN__custom_4442440/default/table?lang=en), (Accessed April 2023).
- [94] P. Turati, N. Pedroni, E. Zio, Simulation-based exploration of high-dimensional system models for identifying unexpected events, *Reliability Engineering and System Safety* 165 (2017) 317–330.
- [95] World Nuclear Association, Economics of nuclear power, August 2022. URL: <https://world-nuclear.org/information-library/economic-aspects/economics-of-nuclear-power.aspx>.
- [96] D. Coppitters, F. Contino, Optimizing upside variability and antifragility in renewable energy system design, *Scientific Reports* 13 (2023) 9138.

- [97] B. Pickering, F. Lombardi, S. Pfenninger, Diversity of options to eliminate fossil fuels and reach carbon neutrality across the entire european energy system, Joule 6 (2022) 1253–1276.
- [98] B. S. Palmintier, Incorporating operational flexibility into electric generation planning: Impacts and methods for system design and policy analysis, Ph.D. thesis, Massachusetts Institute of Technology, 2013.
- [99] D. Connolly, H. Lund, B. V. Mathiesen, M. Leahy, A review of computer tools for analysing the integration of renewable energy into various energy systems, Applied Energy 87 (2010) 1059–1082. doi:10.1016/j.apenergy.2009.09.026.
- [100] M. G. Prina, M. Lionetti, G. Manzolini, W. Sparber, D. Moser, Transition pathways optimization methodology through EnergyPLAN software for long-term energy planning, Applied Energy 235 (2019) 356–368. doi:10.1016/j.apenergy.2018.10.099.
- [101] M. G. Prina, G. Manzolini, D. Moser, B. Nastasi, W. Sparber, Classification and challenges of bottom-up energy system models - a review, Renewable and Sustainable Energy Reviews 129 (2020) 109917.
- [102] M. Chang, J. Z. Thellufsen, B. Zakeri, B. Pickering, S. Pfenninger, H. Lund, P. A. Østergaard, Trends in tools and approaches for modelling the energy transition, Applied Energy 290 (2021) 116731.
- [103] R. Atlason, R. Unnþorsson, Ideal EROI (energy return on investment) deepens the understanding of energy systems, Energy 67 (2014) 241–245. doi:10.1016/j.energy.2014.01.096.
- [104] Pfenninger and Pickering, Calliope - a multi-scale energy systems modelling framework, Accessed 2023. URL: <https://www.calliope.net/>.
- [105] A. University, EnergyInteractive.NET, Accessed July 17th, 2018. URL: <http://energyinteractive.net/>.
- [106] Ž. Popović, B. Brbaklić, S. Knežević, A mixed integer linear programming based approach for optimal placement of different types of automation devices in distribution networks, Electric Power Systems Research 148 (2017) 136–146.
- [107] Berkeley Lab, Der-cam, Accessed June 12th, 2023. URL: <https://gridintegration.lbl.gov/der-cam>.

- [108] A. Zerrahn, W.-P. Schill, Long-run power storage requirements for high shares of renewables: review and a new model, *Renewable and Sustainable Energy Reviews* 79 (2017) 1518–1534.
- [109] University of Stuttgart, European Electricity Market Model, Accessed June 12th, 2023. URL: <https://www.ier.uni-stuttgart.de/forschung/modelle/E2M2/>.
- [110] S. Backe, C. Skar, P. C. del Granado, O. Turgut, A. Tomasdard, Empire: An open-source model based on multi-horizon programming for energy transition analyses, *SoftwareX* 17 (2022) 100877.
- [111] Quintel Intelligence, Energy transition model, Accessed September 17th, 2023. URL: <https://docs.energytransitionmodel.com/main/intro/>.
- [112] H. Lund, J. Z. Thellufsen, Energyplan - advanced energy systems analysis computer model (version 15.1), <https://doi.org/10.5281/zenodo.4001540>, 2020. [Accessed September 17, 2020].
- [113] O. Lugovoy, V. Potashnikov, energyRt: Energy systems modeling toolbox in R, development version, 2022. URL: <https://github.com/energyRt/energyRt>, r package version 0.01.21.9003.
- [114] Fraunhofer ISI, Enertile, Accessed June 12th, 2023. URL: <https://www.enertile.eu/enertile-en>.
- [115] C. F. Heuberger, Electricity systems optimisation with capacity expansion and endogenous technology learning (eso-xel), *Zenodo* (2017).
- [116] K. Löffler, K. Hainsch, T. Burandt, P.-Y. Oei, C. Kemfert, C. Von Hirschhausen, Designing a model for the global energy system—genesys-mod: an application of the open-source energy modeling system (osemosys), *Energies* 10 (2017) 1468.
- [117] L. Herc, A. Pfeifer, F. Feijoo, N. Duić, Energy system transitions pathways with the new h2res model: a comparison with existing planning tool, e-Prime—Advances in Electrical Engineering, Electronics and Energy 1 (2021) 100024.
- [118] R. Dufo López, ihoga, Accessed June 12th, 2023. URL: <https://ihoga.unizar.es/en/>.

- [119] P. Kuhn, Iteratives Modell zur Optimierung von Speicherausbau und-betrieb in einem Stromsystem mit zunehmend fluktuerender Erzeugung, Ph.D. thesis, Technische Universität München, 2012.
- [120] Electric Power Research Institute, Open distribution system simulator (opendss), Accessed June 12th, 2023. URL: <https://sourceforge.net/projects/electricdss/>.
- [121] Energy Exemplar, Plexos (version 9.0), 2023. URL: <https://plexos9.com/>.
- [122] V. Waucquez, Validation of the cost optimization model, pathway energyscope, for scenario analysis, 2023. URL: <http://hdl.handle.net/2078.1/thesis:40534>.
- [123] T. Brown, J. Hörsch, D. Schlachtberger, Pypsa: Python for power system analysis, arXiv preprint arXiv:1707.09913 (2017).
- [124] T. Brown, J. Hörsch, D. Schlachtberger, PyPSA: Python for Power System Analysis, 2018. URL: <https://pypsa.org/>.
- [125] T. T. Pedersen, E. K. Gøtske, A. Dvorak, G. B. Andresen, M. Victoria, Long-term implications of reduced gas imports on the decarbonization of the european energy system, Joule 6 (2022) 1566–1580.
- [126] Energistyrelsen, Modelldokumentation – Ramses energisystemmodel , Technical Report, 2023. URL: [https://ens.dk/sites/ens.dk/files/Analyser/ramses\\_energisystemmodel.pdf](https://ens.dk/sites/ens.dk/files/Analyser/ramses_energisystemmodel.pdf).
- [127] W. Short, P. Sullivan, T. Mai, M. Mowers, C. Uriarte, N. Blair, D. Heimiller, A. Martinez, Regional energy deployment system (ReEDS), Technical Report, National Renewable Energy Lab.(NREL), Golden, CO (United States), 2011.
- [128] R. Loulou, U. Remme, A. Kanudia, A. Lehtila, G. Goldstein, Documentation for the times model part ii, Energy technology systems analysis programme (2005).
- [129] IEA-ETSAP, Times model description, 2021. URL: <https://wiki.openmod-initiative.org/wiki/TIMES>.
- [130] G. Haydt, V. Leal, A. Pina, C. A. Silva, The relevance of the energy resource dynamics in the mid/long-term energy planning models, Renewable energy 36 (2011) 3068–3074.

- [131] S. Pfenninger, J. Keirstead, Renewables, nuclear, or fossil fuels? Scenarios for Great Britain's power system considering costs, emissions and energy security, *Applied Energy* 152 (2015) 83–93. doi:10.1016/j.apenergy.2015.04.102.
- [132] B. Pickering, R. Choudhary, Quantifying resilience in energy systems with out-of-sample testing, *Applied Energy* 285 (2021) 116465.
- [133] S. Pfenninger, Dealing with multiple decades of hourly wind and pv time series in energy models: A comparison of methods to reduce time resolution and the planning implications of inter-annual variability, *Applied energy* 197 (2017) 1–13.
- [134] H.-K. Bartholdsen, A. Eidens, K. Löffler, F. Seehaus, F. Wejda, T. Burandt, P.-Y. Oei, C. Kemfert, C. v. Hirschhausen, Pathways for germany's low-carbon energy transformation towards 2050, *Energies* 12 (2019) 2988.
- [135] M. Welsch, P. Deane, M. Howells, B. Ó. Gallachóir, F. Rogan, M. Bazilian, H.-H. Rogner, Incorporating flexibility requirements into long-term energy system models—a case study on high levels of renewable electricity penetration in ireland, *Applied Energy* 135 (2014) 600–615.
- [136] G. Limpens, Pathway extension of model EnergyScope TD, Accessed 2023.  
URL: [https://github.com/energyscope/EnergyScope\\_pathway/tree/v1.1](https://github.com/energyscope/EnergyScope_pathway/tree/v1.1).
- [137] V. Codina Gironès, S. Moret, F. Maréchal, D. Favrat, Strategic energy planning for large-scale energy systems: A modelling framework to aid decision-making, *Energy* 90, Part 1 (2015) 173–186. doi:10.1016/j.energy.2015.06.008.
- [138] F. Y. Kuo, I. H. Sloan, Lifting the curse of dimensionality, *Notices of the AMS* 52 (2005) 1320–1328.
- [139] P. Gabrielli, M. Gazzani, E. Martelli, M. Mazzotti, Corrigendum to “Optimal design of multi-energy systems with seasonal storage” [Appl. Energy (2017)], *Applied Energy* 212 (2018) 720. doi:10.1016/j.apenergy.2017.12.070.
- [140] J. Després, S. Mima, A. Kitous, P. Criqui, N. Hadjsaid, I. Noirot, Storage as a flexibility option in power systems with high shares of variable renewable energy sources: a POLES-based analysis, *Energy Economics* 64 (2017) 638–650. doi:10.1016/j.eneco.2016.03.006.

- [141] P. Nahmmacher, E. Schmid, L. Hirth, B. Knopf, Carpe diem: A novel approach to select representative days for long-term power system modeling, *Energy* 112 (2016) 430–442.
- [142] J. E. Gentle, L. Kaufman, P. J. Rousseeuw, *Finding Groups in Data: An Introduction to Cluster Analysis.*, John Wiley & Sons 47 (2006) 788. doi:10.2307/2532178.
- [143] H. S. Park, C. H. Jun, A simple and fast algorithm for K-medoids clustering, *Expert Systems with Applications* 36 (2009) 3336–3341. doi:10.1016/j.eswa.2008.01.039.
- [144] F. Contino, S. Moret, G. Limpens, H. Jeanmart, Whole-energy system models: The advisors for the energy transition, *Progress in Energy and Combustion Science* 81 (2020) 100872. URL: <https://doi.org/10.1016/j.pecs.2020.100872>.
- [145] G. Limpens, S. Moret, G. Guidati, X. Li, F. Maréchal, H. Jeanmart, The role of storage in the Swiss energy transition, in: proceedings of ECOS 2019 conference, 2019, pp. 761–774.
- [146] M. Borasio, S. Moret, Deep decarbonisation of regional energy systems: A novel modelling approach and its application to the italian energy transition, *Renewable and Sustainable Energy Reviews* 153 (2022) 111730.
- [147] P. Thiran, H. Jeanmart, F. Contino, Validation of a method to select a priori the number of typical days for energy system optimisation models, *Energies* 16 (2023) 2772.
- [148] M. Pavičević, P. Thiran, G. Limpens, F. Contino, H. Jeanmart, S. Quoilin, Bi-directional soft-linking between a whole energy system model and a power systems model, in: 2022 IEEE PES/IAS PowerAfrica, IEEE, 2022, pp. 1–5.
- [149] J. Schnidrig, R. Cherkaoui, Y. Calisesi, M. Margni, F. Maréchal, On the role of energy infrastructure in the energy transition. case study of an energy independent and co2 neutral energy system for switzerland, *Frontiers in Energy Research* 11 (2023) 1164813. URL: <https://doi.org/10.3389/fenrg.2023.1164813>. doi:10.3389/fenrg.2023.1164813.
- [150] G. Limpens, EnergyScope TD documentation, Accessed 2023. URL: <https://energyscope.readthedocs.io/en/v2.2/>.

- [151] IPCC, Climate Change 2013 - The Physical Science Basis, 2014. URL: <https://www.ipcc.ch/report/ar5/wg1/>.
- [152] SPF Economie, Energy - key data - edition february 2022, Brussels, Februrary 2022.
- [153] D. Devogelaer, J. Duerinck, D. Gusbin, Y. Marenne, W. Nijs, M. Orsini, M. Pairon, “Towards 100% renewable energy in Belgium by 2050”, Technical Report, 2013.
- [154] M. Cornet, J. Duerinck, E. Laes, P. Lodewijks, E. Meynaerts, J. Pestiaux, N. Renders, P. Vermeulen, Scenarios for a Low Carbon Belgium by 2050, Technical Report November, Climact, VITO, 2013.
- [155] Climact, VITO, New scenarios for a climate neutral Belgium by 2050, Technical Report, 2021. URL: <https://klimaat.be/doc/climate-neutral-belgium-by-2050-report.pdf>.
- [156] Société Française d'énergie nucléaire, La belgique repousse de 10 ans sa sortie du nucléaire, <https://www.sfen.org/rgn/la-belgique-repousse-de-10-ans-sa-sortie-du-nucleaire/>, January 2023 (accessed April 17, 2023).
- [157] A. Dubois, J. Dumas, P. Thiran, G. Limpens, D. Ernst, Multi-objective near-optimal necessary conditions for multi-sectoral planning, arXiv preprint arXiv:2302.12654 (2023).
- [158] Fédération Belge et Luxembourgeoise de l'automobile et du cycle, Automotive Pocket Guide Belgium - Chiffres clefs, Technical Report, 2021. URL: <https://www.febiac.be/public/statistics.aspx?FID=23>.
- [159] I. Keppo, M. Strubegger, Short term decisions for long term problems—the effect of foresight on model based energy systems analysis, Energy 35 (2010) 2033–2042.
- [160] B. Nyqvist, Limited foresight in a linear cost minimisation model of the global energy system, Gothenburg: Master's Thesis in Complex Adaptive Systems, Physical Resource Theory, Chalmers University of Technology (2005).
- [161] F. Hedenus, C. Azar, K. Lindgren, Induced technological change in a limited foresight optimization model, The Energy Journal (2006).

- [162] SPF Economie, Vision and strategy hydrogen, October 2022. URL: <https://economie.fgov.be/sites/default/files/Files/Energy/View-strategy-hydrogen.pdf>.

---

---

## Appendix A

# EnergyScope Pathway: Its choice and its formulation

### A.1 EnergyScope Pathway: The right model to choose

Energy system models of varying complexity are valuable tools for guiding policy-makers and projecting future trends. These models enable the exploration of different energy scenarios and the assessment of their consequences based on the underlying assumptions. Specifically, techno-economic models play a crucial role in identifying technically feasible pathways for the energy transition while considering the associated economic costs. These models can be classified based on two key factors: technical resolution and simulation horizon, as illustrated in Figure A.1.

Increasing the technical resolution of energy system models often comes at the expense of a shorter simulation horizon, and vice versa. For instance, day-ahead grid operation models prioritise accurate grid resolution and capacity reserves in case of foreseeable deviations, but they may not incorporate long-term market trends. Different model classes cater to various needs, with decreasing technical resolution. These include machine-level control, network dispatch, unit commitment, maintenance, power plant expansion, planning for new infrastructure, and scenario analysis. Each class serves a specific purpose, from fine-grained control within a machine to the exploration of multiple assumptions across different scenarios.

In accordance with the previous classification, models aimed at aiding decision-makers in the energy transition primarily fall under the categories of planning and scenario analysis, with a lower technical resolution than the other classes of model (see Figure A.1). Nonetheless, ensuring technical accuracy is of paramount importance

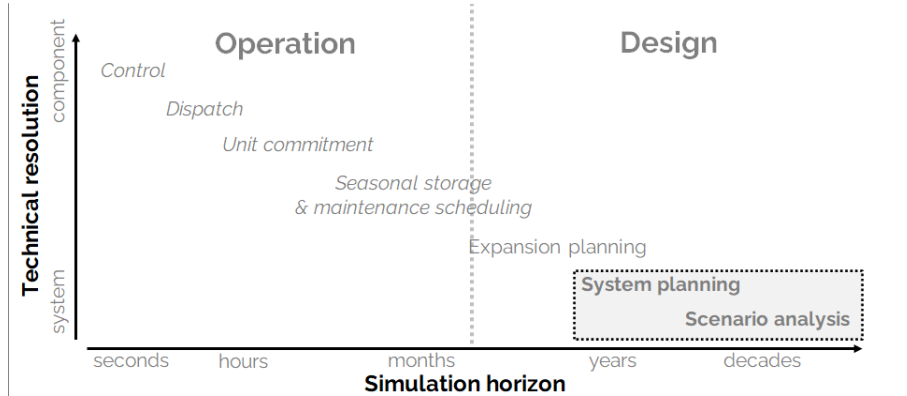


**Figure A.1.** Model can be classified by their core focus: **Operation** or **Design**. These categories can be broken down into subcategories. This paper focuses on the system planning and scenario analysis models. Inspired from [98].

to ensure the effective functionality of future energy systems. Hence, these models should meet the following requirements as a minimum: (i) assessment of intermittent renewable energy integration thanks to an **hourly resolution** spanning a one-year time horizon; (ii) accounting for the **whole-energy system** as including all energy (i.e. heat, electricity, mobility) and non-energy flows in different sectors, accounting for their respective greenhouse gas emissions, as well as all resources, conversion processes, and storage technologies; (iii) exploration of all available options through the **optimisation of investments and operations**; (iv) consideration of long-term investments throughout the **transition pathway** process (i.e. 30 years up to 2050, in our case); and (v) ensuring a reasonable **computational time** (i.e. less than one hour on a personal laptop 15 minutes) for analysing different trajectories. Additionally, to enhance result reproducibility and user understanding, it is advantageous for such models to: (vi) maintain transparency and preferably be **open-source**, with accessible data and accompanied by collaborative documentation.

These requirements are commonly found in reviews of energy system models. In 2010, Connolly et al. [99] reviewed 68 tools, considering similar criteria (i.e. (i-iv) and (vi)), along with others such as the number of users and market equilibrium. In 2019, Prina et al. [100] reviewed 12 “*most established*” models, focusing on criteria (i-ii) and (iv). This review was followed by a classification where criteria (i-iv) were taken into account [101]. In 2021, Chang et al. [102] conducted a survey-based review of 42 models for energy transition modelling, covering all criteria except computational

time. Based on these reviews, Table A.1 compares models based on all the previous criteria except the computational time (v). Indeed, the latter is hard to compare as models are not applied to the same case study and the information is rarely given. The table includes only the models that achieved partially at least four out of the five criteria. We endeavored to refresh the model's information by consulting the model's website and repository, yet there is a possibility that some information might have been overlooked or omitted inadvertently.

From Table A.1, four models almost check all the boxes (partially the pathway one): Calliope, GENeSYS-MOD, PyPSA and TIMES.

### **TIMES**

The TIMES model, short for The Integrated MARKAL-EFOM System, is a well-established framework renowned for its capacity to generate comprehensive energy models. It encompasses a rich array of features, including support for multi-cell modeling, pathway analysis, full-scale representation of energy systems, and the consideration of market equilibrium dynamics, all of which facilitate thorough scenario exploration. This model has a widespread adoption and has been utilized by worldwide institutions such as the International Energy Agency (IEA) or technical ones such as VITO (Vlaamse Instelling voor Technologisch Onderzoek) research institute in their research endeavors. Notably, TIMES was reported as commercial (i.e. not free to download) in 2010 [99]. A more recent survey conducted in 2020-2021 confirmed that the model was using a commercial interface [102]. Recent developments by the IEA-ETSAP have resulted in a version that is compatible with open-source solver CBC. In various studies conducted in different regions, including Canada, Sweden, the EU, and Denmark, TIMES has been shown to utilize 12 to 32 time-slices annually [101]. It is noteworthy that Haydt et al. [130] conducted a study focusing on the electrical sector, using 12 typical days with an hourly resolution, highlighting the sensitivity of results to time resolution. Regarding data accessibility, while some publications partially present the used dataset, the overall accessibility of TIMES data remains an area of ongoing inquiry [129].

### **Calliope**

Calliope is a “*tool that makes it easy to build energy system models*” at different geographical scale. Even if the framework offers the possibility of modelling multi-year systems, we did not find a relevant publication on this topic. In fact, the model is typically employed for scenario analysis. Previous studies have used the model to

**Table A.1.** Comparison of existing models that partially satisfy at least four of the five criteria (in alphabetical order). Legend: ✓ criterion satisfied; √ criterion partially satisfied; ✗ criterion not satisfied. Data from [99–102]

Model	Ref.	Hourly	Whole-energy	Optimis. invest. & operation	Pathway	Open-source
Calliope	[103, 104]	✓	✓	✓	✗ <sup>a</sup>	✓
COMPOSE	[105]	✓	✓	✓	✓	✓ <sup>b</sup>
DER-CAM	[106, 107]	✓	✓ <sup>c,d</sup>	✓	✗ <sup>e</sup>	✓ <sup>f</sup>
DIETER	[108]	✓	✓ <sup>d,g</sup>	✓	✗ <sup>e</sup>	✓
E2M2	[109]	✓	✓ <sup>c,d,h</sup>	✓	✓	✗ <sup>i</sup>
EMPIRE	[110]	✓	✗ <sup>c,d,g,h</sup>	✓	✓	✓ <sup>b</sup>
Ener. Trans. Model	[111]	✓	✓	✗ <sup>j</sup>	✓	✓
EnergyPLAN	[112]	✓	✓	✗ <sup>k</sup>	✗ <sup>l</sup>	✓ <sup>f</sup>
energyRt	[113]	✓	✓	✓ <sup>m</sup>	✓	✓
EnergyScope TD	[8]	✓	✓	✓	✗ <sup>l</sup>	✓
Enertile	[114]	✓	✓ <sup>d</sup>	✓	✓	✗ <sup>n</sup>
ESO-XEL	[115]	✓	✗ <sup>c,d,g,h</sup>	✓	✓	✓
GENeSYS-MOD	[116]	✓	✓	✓	✓	✓
H2RES	[117]	✓	✗	✓ <sup>??</sup>	✓	✓
iHOGA	[118]	✓	✗ <sup>c,d,g,h</sup>	✓ <sup>m</sup>	✓	✓ <sup>b</sup>
IMAKUS	[119]	✓	✓ <sup>c,d</sup>	✓	✓	✗ <sup>i</sup>
OpenDSS	[120]	✓	✓	✗ <sup>k</sup>	✓	✓
Plexos	[121]	✓	✓ <sup>o</sup>	✓	✓	✗ <sup>i</sup>
PyPSA	[123, 124]	✓	✓	✓	✓ <sup>p</sup>	✓
RamsesR	[126]	✓	✓ <sup>c,d,h</sup>	✓	✓	✓
ReEDS	[127]	✗ <sup>q</sup>	✓ <sup>d,g,h</sup>	✓	✓	✓ <sup>b</sup>
TIMES	[128]	✓	✓	✓	✓	✓ <sup>r</sup>

<sup>a</sup>Topic is being discussed in the chat of their repository but not yet included in their documentation.

<sup>b</sup>‘Free under some special conditions’.

<sup>c</sup> Transport not accounted.

<sup>d</sup> Industry not accounted

<sup>e</sup> Not specified but time horizon is 1 year.

<sup>f</sup> Freeware.

<sup>g</sup> DHN not accounted.

<sup>h</sup> individual heating not accounted.

<sup>i</sup> Commercially (paid) licensed.

<sup>j</sup>The ETM is a simulation model with a simple merit order ‘optimisation’ for electricity, flex and heat.

<sup>k</sup> Simulation model.

<sup>l</sup> Yearly horizon without pathway.

<sup>m</sup> EnergyRT optimises investments only.

<sup>n</sup>Only for internal use.

<sup>o</sup>Does not account for all sectors but allow to implement them according to Waucquez [122].

<sup>p</sup>Pedersen et al. [125] applied PyPSA to a whole energy system split in 37 nodes. Using a myopic approach, the model optimises the energy transition with a 3-hours resolution).

<sup>q</sup>Seasonal time slice.

<sup>r</sup>Model is now open-source with limited access to data [129].

investigate the phasing out of fossil and nuclear energies in a multi-regional UK power system [131]. More recently, the model has been applied to analyse a scenario of a multi-energy district in Switzerland [132]. Moreover, the model has been used with decades of weather data. However, its application has been limited to assessing the impact of inter-year variability in wind and PV on the results, rather than evaluating a transition pathway [133].

### GENeSYS-MOD

Similarly GENeSYS-MOD presents some limitations. This model is an application of the open-source energy modelling system (OSeMOSYS), itself represented as a model with a poor time discretisation and a heavy computational burden according to [100]. Löffler et al. [116] applied the model to the world by splitting it into 10 regions and most of the energy demand sectors, the time disaggregation being chosen by the user. For their application they used representative years with three days and two time slice per day.

### PyPSA

Among the open-source models with an active community, PyPSA is one of the best-performing, with a large and active community, development at the state of the art, worldwide applications, and usage not only limited to academia. A study conducted by Bartholdsen et al. [134] centered on Germany employed a representation comprising 16 time slices for representative years. This choice was substantiated by the work of Welsch et al. [135], which demonstrated that this level of temporal granularity yields consistent results in comparison to hourly time resolution over a year. However, it is noteworthy that the utilization of a limited number of time slices may simplify the optimization of storage technologies, especially those designed for inter-month energy storage. This simplification can be viewed as a pragmatic approach to reduce the computational burden while over-simplifying the challenge of accurately integrating intermittent renewable energy sources. Furthermore, PyPSA, a modeling framework recognized for its robustness and active user community, has also been employed to investigate scenarios related to myopic transitions [125].

Hence, it is worth noting that while Calliope, OSeMOSYS, PyPSA and TIMES frameworks have the potential to be used for evaluating a transition pathway, we have not come across any publication that explicitly demonstrates their application to such cases with an hourly time resolution over significant time slices. Hence, it appears

that none of the models of Table A.1 fully meets all five criteria outlined in the table, topped with the additional consideration of acceptable computational time. This observation is consistent with the findings presented by Prina et al. [100] who identified two approaches for optimising the energy transition pathway based on the six criteria. The first approach involves running a snapshot model multiple times using an algorithm that optimises the transition path and validates the operability of the system. The second approach aims to extend a snapshot model to represent the entire transition pathway. However, they excluded this option due to the lack of models that met the requirements of being fast enough and easily adaptable. Therefore, they developed a new model based on the first methodology, named EPLANoptTP. It uses a multi-objective evolutionary algorithm to optimise the EnergyPLAN model [112]. To manage computational time, the number of decision variables is limited to three: PV, wind turbine and battery capacities. Thus, the model does not investigate all the options (i.e. criteria (iii)).

For the aforementioned reasons, the current work opted for EnergyScope Pathway, an extension of the open-source and documented EnergyScope TD model [8] listed in Table A.1. The latter has an horizon time of one year and does not account for the pathway from an existing energy system to a long-term target. The pathway version extends the time horizon to decades and accounts for the pathway transition from an existing energy system to a long term target. The computational time is kept low (i.e. around a 15 minutes on a personal laptop), mostly due to keeping the linear formulation after extending the snapshot model. Limpens et al. [9] provides more detailed insights into the modeling choices made during methodological development. In the spirit of the EnergyScope project, the code is fully open-source (under the License Apache 2.0, see repo [136]) with a collaborative documentation [11]. Compared to existing models, EnergyScope Pathway introduces a rapid computational optimisation tool for exploring diverse transition pathways within an entire energy system while maintaining high temporal precision to accurately capture the integration of intermittent renewables. To the best of our knowledge, there are potentially frameworks that could be extended to similar capabilities, but their computational time for similar case study have not been found.

## A.2 EnergyScope Pathway and its linear formulation

EnergyScope Pathway is the extension of EnergyScope TD [8] that follows the snapshot approach [137]. The objective of this section is to present the fundamental variables and constraints of the latter based on which the former was developed. There

have been formulation choices to be made but they are not discussed in the current manuscript. However, the interested reader is invited to refer to the Appendix B of [9] for further information in this regard.

### A.2.1 The starting point: a scenario analysis model

#### Typical days to break the curse of dimensionality

In the field of bottom-up energy system modelling<sup>1</sup>, one of the biggest challenges is the time resolution [101]. With the rise of VRES, being able to integrate them and capture their interactions with the rest of the energy system requires an hourly time resolution while optimising a whole year (i.e. 8760 hours), if not a whole transition (i.e. several decades). This long-term target combined with a fine time resolution usually leads to the so-called “curse of dimensionality” [138]. As an example, running EnergyScope TD over each of the 8760 hours to optimise a single target year takes more than 19h [8].

To break this curse, EnergyScope TD, like other models [139–141], relies on a subset representative days called typical days (TDs). This more limited number of days, i.e. 12 in the rest of this thesis, cluster the days of the year that have similar time series of demands (i.e. varying electricity and heat demands) and weather data (i.e. sun, onshore and offshore wind). This way, each day of the year is associated to one of these typical days (see Figure A.2).

Finally, to properly capture the inter days dynamics, EnergyScope TD uses the “Coupling typical days” method from Gabrielli et al. [139]. Among others, this allows representing the dynamics and the seasonality of storage capacities. This method as well as the clustering approach selected in our case, i.e. k-medoids [142, 143], extensively detailed and compared to other methods, in the work of Limpens et al. [8].

#### Overview of the snapshot model

EnergyScope TD [8] is a model that optimises both the investment and operating strategy of a ‘whole’-energy system, encompassing electricity, heating, mobility, and non-energy sectors. According to Contino et al. [144], a model qualifies as a ‘whole-energy’ system when it considers all energy sectors, including the non-energy demand such as

<sup>1</sup> As detailed by Prina et al. [101], bottom-up models offer a detailed analysis of components and interconnections within different energy sectors, allowing for a techno-economic comparison of technologies and assessment of alternatives for achieving energy targets and reducing greenhouse gas emissions. On the contrary, top-down modes, mostly used by economists and administrations, integrate a simplified representation of the energy system as interacting with the other macro-economic sectors.

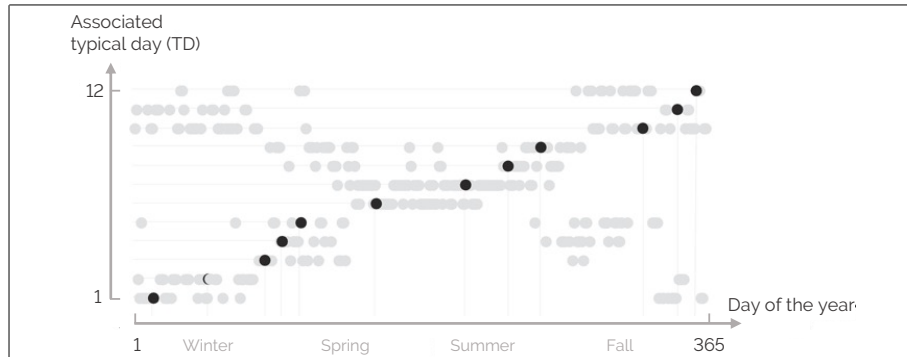


**Figure A.2.** Association of each day of the year (grays) to one of the 12 typical days (TDs) (black dots). Graph adapted from Limpens et al. [8].

the production of plastics and other materials using feedstocks that are also considered as energy carriers, with the same level of detail.

The model's hourly resolution over a year makes it well-suited for integrating intermittent renewables. Its formulation incorporates typical days and a reconstruction method that captures different time scales from the hour to the season while accounting for the inter-weeks patterns of wind. The model investigates all the possibilities by optimising the investment decisions and hourly operations over a year, with a computational time of less than a minute on a personal laptop. This characteristic was intentionally incorporated into the model design to facilitate uncertainty quantification and other studies that require numerous iterations [5].

EnergyScope TD has been successfully applied to various national energy systems, including Switzerland [8, 145], Belgium [54], Italy [146], and other European countries [51]. Furthermore, it has been extended to a multi-region energy system model [147], coupled with other energy models [148], or employed to focus on specific sectors such as the power networks of electricity, gas, and hydrogen [149].

### Formulation of the snapshot model

The conceptual structure of the model is illustrated in Figure A.3: given the end-use energy demand, the efficiency and cost of energy conversion technologies, the availability and cost of energy resources, the model identifies the optimal investment and hourly operation strategies to meet the demand and minimise the total annual cost and greenhouse gas emissions of the energy system. Typically, the two objectives are in-

integrated by placing a limit on emissions while simultaneously striving to minimize costs.

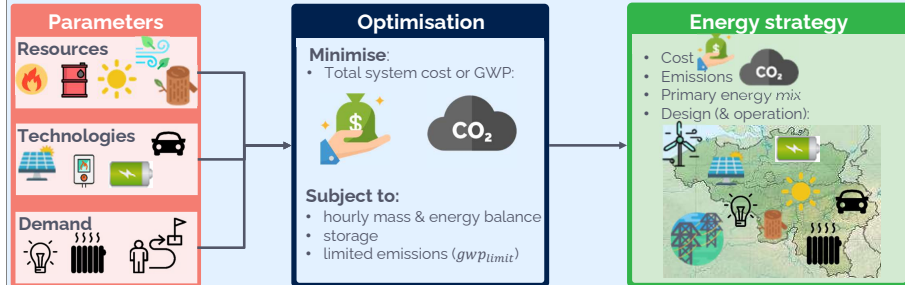


**Figure A.3.** EnergyScope TD model is a flow model with inputs (Parameters), an optimizing model (Optimisation) and results (Energy strategy). The image illustrates what is included (non-exhaustively).

### Linear formulation

The following section illustrates the main constraints of the original EnergyScope TD model. The objective function, cost and GHG formulation will be detailed. The rest of the formulation is detailed and available in previous works [1]. This work uses the following nomenclature: SETs are in capital letters, **Variables** are in bold and with first letter capital, and *parameters* are in italic.

$$\min \mathbf{C}_{\text{tot}} = \sum_{j \in TECH} \left( \tau(j) \mathbf{C}_{\text{inv}}(j) + \mathbf{C}_{\text{maint}}(j) \right) + \sum_{i \in RES} \mathbf{C}_{\text{op}}(i) \quad (\text{A.1})$$

$$\text{s.t. } \tau(j) = \frac{i_{rate}(i_{rate} + 1)^{\text{lifetime}(j)}}{\left( (i_{rate} + 1)^{\text{lifetime}(j)} \right) - 1} \quad \forall j \in TECH \quad (\text{A.2})$$

The objective, Eq. (A.1), is the minimisation of the total annual cost of the energy system ( $\mathbf{C}_{\text{tot}}$ ), defined as the sum of the annualised investment cost of the technologies ( $\tau \cdot \mathbf{C}_{\text{inv}}$ ), the operating and maintenance costs of the technologies ( $\mathbf{C}_{\text{maint}}$ ) and the operating cost of the resources ( $\mathbf{C}_{\text{op}}$ ). The annualised factor  $\tau$  is computed *a priori* based on the interest rate ( $i_{rate}$ ) and the technology lifetime, ( $\text{lifetime}$ ), Eq. (A.2).

$$\mathbf{C}_{\text{inv}}(j) = c_{\text{inv}}(j) \mathbf{F}(j) \quad \forall j \in TECH \quad (\text{A.3})$$

$$\mathbf{C}_{\text{maint}}(j) = c_{\text{maint}}(j) \mathbf{F}(j) \quad \forall j \in TECH \quad (\text{A.4})$$

The total investment cost ( $\mathbf{C}_{\text{inv}}$ ) of each technology results from the multiplication of its specific investment cost ( $c_{\text{inv}}$ ) and its installed capacity ( $\mathbf{F}$ ), see Eq. (A.3).

The installed capacity is defined with respect to the main end-uses output type, such as electricity for PV or heat for a boiler. The total operation and maintenance costs ( $\mathbf{C}_{\text{maint}}$ ) are calculated in the same way, Eq. (A.4).

$$\mathbf{C}_{\text{op}}(i) = \sum_{t \in T} c_{op}(i) \mathbf{F}_t(i, t) t_{op}(t) \quad \forall i \in RES \quad (\text{A.5})$$

The total cost of the resources ( $\mathbf{C}_{\text{op}}$ ) is calculated as the sum of the end-use over different periods multiplied by the period duration ( $t_{op}$ ) and the specific cost of the resources ( $c_{op}$ ), Eq. (A.5). To simplify the reading, we write the sum over typical days as  $t \in T$  such as in Eq. (A.5) and following equations. The period  $T$  represents the sequence of hours and typical days over a year (8760h)<sup>2</sup>. The full formulation is detailed in [8] or in the documentation [150].

$$\mathbf{GWP}_{\text{tot}} = \sum_{i \in RES} \mathbf{GWP}_{\text{op}}(i) \quad (\text{A.6})$$

$$\mathbf{GWP}_{\text{op}}(i) = \sum_{t \in T} gwp_{op}(i) \mathbf{F}_t(i, t) t_{op}(t) \quad \forall i \in RES \quad (\text{A.7})$$

The global annual GHG emissions are calculated using a LCA approach, i.e. taking into account emissions of the resources '*from cradle to use*'. It is based on the indicator '*GWP100a-IPCC2013*' developed by the intergovernmental panel for climate change (IPCC) [151]. For climate change, the natural choice as indicator is the global warming potential, expressed in ktCO<sub>2</sub>-eq./year. In Eq. (A.6), the total yearly emissions of the system ( $\mathbf{GWP}_{\text{tot}}$ ) are defined as the emissions related to resources ( $\mathbf{GWP}_{\text{op}}$ ). The total emissions of the resources are the emissions associated to fuels (from cradle to combustion) and imports of electricity ( $gwp_{op}$ ) multiplied by the period duration ( $t_{op}$ ), Eq. (A.7). Thus, this version accounts only for operation without accounting for the GWP emitted during the construction of the technologies. This makes the results comparable with metrics used in the reports by the European Commission and the International Energy Agency (IEA).

The above equations (Eqs. (A.1) - (A.7)) represent only a part of the formulation and illustrate the syntax that is used. Those representing the energy balance, network implementation, sectors representation, etc. are not presented in this work but are detailed in the latest version of the model, see [1] and on the documentation [150].

Finally, energy storage has two dimensions to be optimised: the stored energy quantity (also referred to as 'storage level') and the hourly power flow, encompassing both charging and discharging. EnergyScope TD optimises the hourly charge and

<sup>2</sup>The exception is storage level which is optimised over the 365 days of the year instead of typical days.

discharge operations based on the hourly resolution of the typical days. In contrast, the optimisation of stored energy is conducted over the entire span of 8760 hours in a year. This formulation allows for the effective integration of a wide range of energy storage technologies, spanning short-term solutions like small thermal storage units and daily-use batteries, to longer-term options such as hydro-dam storage for seasonal storage, and even large-scale thermal storage for intra-week patterns. A previous study delved into the roles of various storage technologies, considering their sectoral applications and temporal aspects, within the context of the Swiss energy system [145].

### A.2.2 Extending the model for pathway optimisation

In this section, we delve into the extension of EnergyScope TD from a static yearly snapshot model to a comprehensive pathway model. While snapshot models provide insights into the energy system for individual years, they lack the capacity to capture the dynamics inherent in investment strategies throughout a transition period. The proposed approach involves segmenting the transition into five-year intervals. This approach results in seven instances of EnergyScope TD – called representative years – spanning the 30-year transition period, covering the years from 2020 to 2050. To bridge these representative years, we introduce additional constraints that capture the investments changes between consecutive periods, accounting for societal inertia and evaluating both the cost implications and emissions of the transition (see Figure A.4). Overall, these constraints are integrated into a linear framework, ensuring computational efficiency, with an approximate computational time of 14 minutes on a personal laptop (2.4 GHz Intel Core i5 quad-core). Simplification and choices were necessary to implement linearly the problem while keeping a tractable computational time. In this section, we present the formulation retained.

The proposed formulation relies on representative years, selected every 5 years from 2020 to 2050. The period between two of them is called ‘*PHASE*’. For each of these 7 representative years, the EnergyScope TD model is run using the relevant data (such as energy demand, technology costs or GHG emissions constraints).

As a consequence, a new dimension ‘*year*’ is added to all **Variables** and parameters, except the interest rate ( $i_{rate}$ ) assumed constant during the transition. This new dimension is necessary to represent the changes of technology and resource characteristics over the representative years. As an example, the investment cost ( $c_{inv}$ ) of a solar photovoltaic panels could drastically vary in the next decades (e.g. data used ranges between 1220 to 870 [ $\text{€}_{2015}/\text{kW}$ ] between 2020 and 2035).

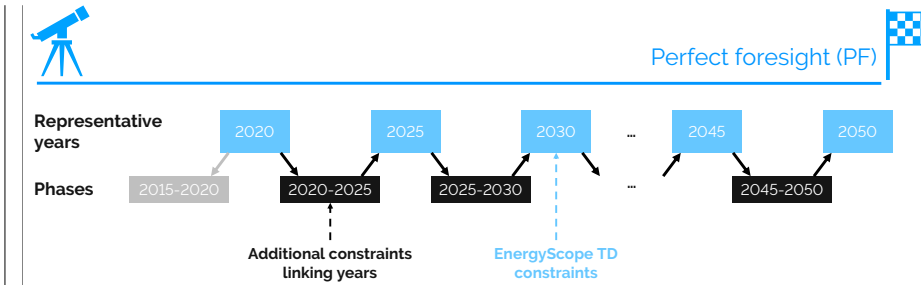


**Figure A.4.** The pathway methodology relies on 7 representative years (blue boxes) where the model EnergyScope TD is applied. Moreover, the formulation accounts for linking constraints (black boxes) and an initial condition (grey box). The overall problem is the pathway model.

### Linking years

At this stage, all years are independent. In the following, we introduce new constraints to link representative years. The formulation allows to install new capacity ( $F_{\text{new}}$ ), remove a capacity that has reached its lifespan ( $F_{\text{old}}$ ) or decommission a technology prematurely ( $F_{\text{decom}}$ ). These capacity changes occur during a phase, this implies that there is no capacity change during a representative year. Figure A.5 illustrates the concept.

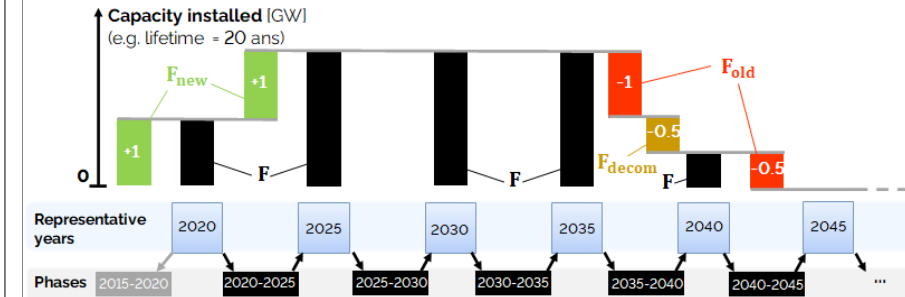


**Figure A.5.** Example of how the technologies capacity and associated variables are evolving. The example uses a technology with a 20 years lifetime. Initially 1 GW of capacity exists ( $F_{\text{new}}$  during phase 2015\_2020). Then another 1 GW is deployed ( $F_{\text{new}}$  during phase 2020\_2025). 15 years later, a part of the capacity reaches its lifetime limit and is removed ( $F_{\text{old}}$  phase 2035\_2040). Moreover, during the latter phase, additional capacity is decommissioned prematurely ( $F_{\text{decom}}$ ). Finally, the technology reaches its expected lifetime and is fully withdrawn ( $F_{\text{old}}$ ).

$$\mathbf{F}(y_{stop}, i) = \mathbf{F}(y_{start}, i) + \mathbf{F}_{\text{new}}(p, i) - \mathbf{F}_{\text{old}}(p, i) - \sum_{p2 \in \text{PHASE} \cup \{2015\_2020\}} \mathbf{F}_{\text{decom}}(p, p2, i)$$

$$\forall p \in \text{PHASE}, y_{stop} \in Y\_STOP(p), y_{start} \in Y\_START(p), i \in \text{TECH} \quad (\text{A.8})$$

Similarly to a mass balance, Eq. (A.8) is the technology capacity balance. The constraint forces the installation or withdrawing of capacities between two representative years: at the end of the phase ( $y_{stop}$ ), the available capacity is the one used in the next representative year ( $\mathbf{F}(y_{stop})$ ). This capacity is equal to the one available in the previous representative year ( $\mathbf{F}(y_{start})$ ) plus the new installed capacity ( $\mathbf{F}_{\text{new}}$ ) minus the capacity that has reached its lifetime ( $\mathbf{F}_{\text{old}}$ ) minus the early decommissioned capacity ( $\mathbf{F}_{\text{decom}}$ ). One notices that the capacity available for each representative year depends on a year ( $y_{start}$  or  $y_{stop}$ ), while the other capacity changes depend on a phase ( $p$  or  $p2$ ). Moreover, the decommissioning term depends on another phase, which is the one when the technology decommissioned has been built. As an illustration, Figure A.5 gives an example where 0.5 GW of a capacity built in 2015\_2020 is decommissioned in 2030\_2035 ( $\mathbf{F}_{\text{decom}}(2030\_2035, 2015\_2020, i)$ ).

$$\mathbf{F}_{\text{decom}}(p, p2, i) = 0$$

$$\forall i \in \text{TECH}, p \in \text{PHASE}, p2 \in \text{PHASE} \cup \{2015\_2020\} | \text{decom}_{\text{allowed}}(p, p2) = 0 \quad (\text{A.9})$$

$$\mathbf{F}_{\text{old}}(p, i) = \begin{cases} \text{if}(age = \text{\{STILL\_IN\_USE'\}}) \text{ then } 0 \\ \text{else } \left( \mathbf{F}_{\text{new}}(age, i) - \sum_{p2 \in \text{PHASE}} \mathbf{F}_{\text{decom}}(p2, age, i) \right) \end{cases}$$

$$\forall p \in \text{PHASE}, \forall j \in \text{TECH} | age \in AGE(p, j) \quad (\text{A.10})$$

In linear programming, a solution might be mathematically correct, while not making sense in practice. As an example, a technology could be decommissioned before being built ( $p < p_{\text{built}}$ ). Eqs. (A.9-A.10) allow preventing these non-sense while keeping the formulation linear. Eq. (A.9) forces the decommissioned capacity to zero when technology will be built after. To do so, a parameter ( $\text{decom}_{\text{allowed}}$ ) is defined *a priori* and is equal to 0 or 1 when decommissioning is not possible or possible, respectively. Eq. (A.10) defines the capacity reaching its lifetime limit at a certain phase, the concept is illustrated in Figure A.5. For each phase, a set ( $AGE$ ) is calculated *a priori*. It relates, for a given phase and technology, when the technology should have been built. In the case the technology has already reached its lifetime limit, the set ( $AGE$ ) returns the phase when the technology has been built. The first part of Eq. (A.10) indicates

that the technology is still available, and thus no capacity needs to be removed. The second part of the equation represents the capacity that reached its expected lifetime minus a part of the capacity that would have been decommissioned. As an example, Figure A.5 shows a 20 years lifetime technology with 1 GW of capacity installed before 2020. Ones will highlight the use of a ‘if’ in Eq. (A.10), this formulation is linear as the if is applied to a parameter and not a variable.

$$\mathbf{F}_{\text{new}}(2015\_2020, i) = \mathbf{F}(\text{YEAR\_2020}, i) \quad \forall i \in \text{TECH} \quad (\text{A.11})$$

To initialise the problem in 2020 with the existing design, an additional phase ‘2015\_2020’ is created. Eq. (A.11) requires that the capacity used in 2020 is installed in the previous phase.

### Society inertia

To avoid unrealistically fast changes in the system, additional constraints are needed during the phases for the mobility and low temperature heat sectors. Without the following constraints, the model would eliminate certain technologies in one phase, such as oil and gas decentralised boilers. Even if this result is mathematically and physically correct, (i.e. fuels are expensive and investing in more efficient technology is economically and environmentally more profitable), this swap of technology cannot occur in one phase (i.e. 5 years). Indeed, society inertia to change, available manpower, supply chains and manufacturers limit the change.

$$\Delta_{\text{change}}(p, i) \geq \sum_{t \in T} (\mathbf{F}_t(y_{\text{start}}, i, t)) - \sum_{t \in T} (\mathbf{F}_t(y_{\text{stop}}, i, t)) \quad \forall j \in \text{TECH}, p \in \text{PHASE}, y_{\text{start}} \in Y_{\text{START}}(p), y_{\text{stop}} \in Y_{\text{STOP}}(p) \quad (\text{A.12})$$

$$\sum_{i \in \text{TECH}(\text{HeatLowT})} \Delta_{\text{change}}(p, i) \leq \lim_{LT,ren} \cdot (eui(y_{\text{start}}, \text{HotWater}) + eui(y_{\text{start}}, \text{SpaceHeat})) \quad \forall p \in \text{PHASE}, y_{\text{start}} \in Y_{\text{START}}(p) \quad (\text{A.13})$$

$$\sum_{i \in \text{TECH}(\text{MobPass})} \Delta_{\text{change}}(p, i) \leq \lim_{MobPass} \cdot eui(y_{\text{start}}, \text{MobPass}) \quad \forall p \in \text{PHASE}, y_{\text{start}} \in Y_{\text{START}}(p) \quad (\text{A.14})$$

$$\sum_{i \in \text{TECH}(\text{MobFreight})} \Delta_{\text{change}}(p, i) \leq \lim_{MobFreight} \cdot eui(y_{\text{start}}, \text{MobFreight}) \quad \forall p \in \text{PHASE}, y_{\text{start}} \in Y_{\text{START}}(p) \quad (\text{A.15})$$

Eq. (A.12) calculates the upper limit of change ( $\Delta_{\text{change}}$ ) in terms of supplied demand instead of installed capacity. Based on this quantification, the amount of change per phase is limited for low temperature heat ( $lim_{LT,ren}$ ), Eq. (A.13), passenger mobility ( $lim_{MobPass}$ ), Eq. (A.14) and freight mobility ( $lim_{MobFreight}$ ), Eq. (A.15). For instance, if the maximum allowable variation in supplied low temperature heat is set at 25%, it would restrict the technology-related changes in low temperature heat to 25% within a given phase. Consequently, if a technology supplies more than 25% of the low temperature heat, it would require multiple phases to replace it with a different technology.

### Cost and emissions of the transition

To optimise the energy system, two key metrics must be adapted: the transition cost and the total global warming potential (GWP). Concerning the first one, all costs are expressed in €<sub>2015</sub> and an annualisation factor is used to distinguish investments over the transition. For the GWP, the metric used is based on the contributions of the gases over 100 years. It is assumed that the impact of emitting at the beginning or the end of transition are equivalent and thus no annualisation is used.

$$\min \mathbf{C}_{\text{tot,trans}} = \mathbf{C}_{\text{tot,capex}} + \mathbf{C}_{\text{tot,opex}} \quad (\text{A.16})$$

$$\mathbf{C}_{\text{tot,capex}} = \sum_{p \in \text{PHASE} \cup \{2015\_2020\}} \mathbf{C}_{\text{inv,phase}}(p) - \sum_{i \in \text{TECH}} \mathbf{C}_{\text{inv,return}}(i) \quad (\text{A.17})$$

$$\mathbf{C}_{\text{tot,opex}} = \mathbf{C}_{\text{opex}}(2020) + t_{\text{phase}} \cdot \tau_{\text{phase}}(p) \cdot \sum_{p \in \text{PHASE} | y_{\text{start}} \in P_{\text{START}}(p), y_{\text{stop}} \in P_{\text{STOP}}(p)} \left( \mathbf{C}_{\text{opex}}(y_{\text{start}}) + \mathbf{C}_{\text{opex}}(y_{\text{stop}}) \right) / 2 \quad (\text{A.18})$$

$$\tau_{\text{phase}}(p) = 1 / (1 + i_{\text{rate}})^{\text{diff\_2015\_year}(p)} \quad (\text{A.19})$$

The objective function to be minimised is the total transition cost of the energy system ( $\mathbf{C}_{\text{tot,trans}}$ ), defined as the sum of the total capital expenditure (CAPEX) ( $\mathbf{C}_{\text{tot,capex}}$ ) and the operational expenditure (OPEX) ( $\mathbf{C}_{\text{tot,opex}}$ ), according to Eq. (A.16). The total CAPEX ( $\mathbf{C}_{\text{tot,capex}}$ ) is the sum of the investment during each phase ( $\mathbf{C}_{\text{inv,phase}}$ ), Eq. (A.17), to which the residual asset investment cost in 2050 is withdrawn ( $\mathbf{C}_{\text{inv,return}}$ ). Thus, the investments account for the installation and dismantlement costs of the technologies. The total OPEX ( $\mathbf{C}_{\text{tot,opex}}$ ) is the sum of the OPEX in 2020 and the annualised sum of the OPEX during each phase ( $\mathbf{C}_{\text{opex}}$ ), Eq. (A.18). During a phase, the system OPEX is the product of the annualised phase factor, defined in Eq. (A.19), and the arithmetic average of OPEX cost for the representative years before and after the phase. The annualised phase factor is defined based on an average interest rate during the transition.

$$\mathbf{C}_{\text{opex}}(y) = \sum_{i \in \text{TECH}} \mathbf{C}_{\text{maint}}(y, i) + \sum_{j \in \text{RES}} \mathbf{C}_{\text{op}}(y, j) \quad \forall y \in \text{YEARS} \quad (\text{A.20})$$

For each year, the yearly OPEX ( $\mathbf{C}_{\text{opex}}$ ) is the sum of the operating and maintenance costs of technologies ( $\mathbf{C}_{\text{maint}}$ ) and the operating cost of the resources ( $\mathbf{C}_{\text{op}}$ ), Eq. (A.20).

$$\mathbf{C}_{\text{inv,phase}}(p) = \sum_{j \in \text{TECH}} \mathbf{F}_{\text{new}}(p, j) \cdot \tau_{\text{phase}}(p) \cdot (c_{\text{inv}}(y_{\text{start}}, j) + c_{\text{inv}}(y_{\text{stop}}, j)) / 2$$

$$\forall p \in \text{PHASE} | y_{\text{start}} \in P\_START(p), y_{\text{stop}} \in P\_STOP(p) \quad (\text{A.21})$$

The investment during a phase ( $\mathbf{C}_{\text{inv,phase}}$ ) results from the multiplication of the newly built technologies ( $\mathbf{F}_{\text{new}}$ ) with their annualised arithmetic averaged specific cost, Eq. (A.21). The annualised phase factor (defined by Eq. (A.19)) is used. The specific cost during the phase is defined as the average between the investment cost for the first and last year of the period.

$$\begin{aligned} \mathbf{C}_{\text{inv,return}}(i) = & \sum_{p \in \text{PHASE} \cup \{2015\_2020\} | y_{\text{start}} \in Y\_START(p), y_{\text{stop}} \in Y\_STOP(p)} \tau_{\text{phase}}(p) \cdot (c_{\text{inv}}(y_{\text{start}}, i) + c_{\text{inv}}(y_{\text{stop}}, i)) / 2 \cdot \\ & \frac{\text{remaining\_years}(i, p)}{\text{lifetime}(y_{\text{start}}, i)} \left( \mathbf{F}_{\text{new}}(p, i) - \sum_{p2 \in \text{PHASE}} \mathbf{F}_{\text{decom}}(p2, p, i) \right) \quad \forall i \in \text{TECH} \end{aligned} \quad (\text{A.22})$$

A part of the investment will remain after 2050. This residual investment, also called salvage value, can be calculated for each technology. A parameter, calculated *a priori*, gives for each technology and construction phase, the remaining amount of years (*remaining\_years*). As an example, if a PV panel has been built in 2045 and has a 20 years lifetime, the parameter will equal to 15 years. Thus, the salvage value is a fraction of the investment cost of this technology when it has been built. This fraction is the ratio between the number of remaining years and the lifetime of the technology. In the previous example, the residual investment of the PV built is 75%. Eq. (A.22) computes, for each technology, the residual value that must be deducted from the total cost. The residual value reflects the fact that the technology can still be used after the horizon of the model and is not fully amortised. The residual value is not applied to technologies that are removed prematurely. This differ from other models, such as Plexos where a technology removed prematurely will benefit from its salvage value (see analysis of [122]).

$$\mathbf{GWP}_{\text{tot,trans}} = \mathbf{GWP}_{\text{tot}}(2020) + t_{\text{phase}} \sum_{p \in \text{PHASE} | y_{\text{start}} \in Y_{\text{START}(p)}, y_{\text{stop}} \in Y_{\text{STOP}(p)}} /2 (\mathbf{GWP}_{\text{tot}}(y_{\text{start}}) + \mathbf{GWP}_{\text{tot}}(y_{\text{stop}})) \quad (\text{A.23})$$

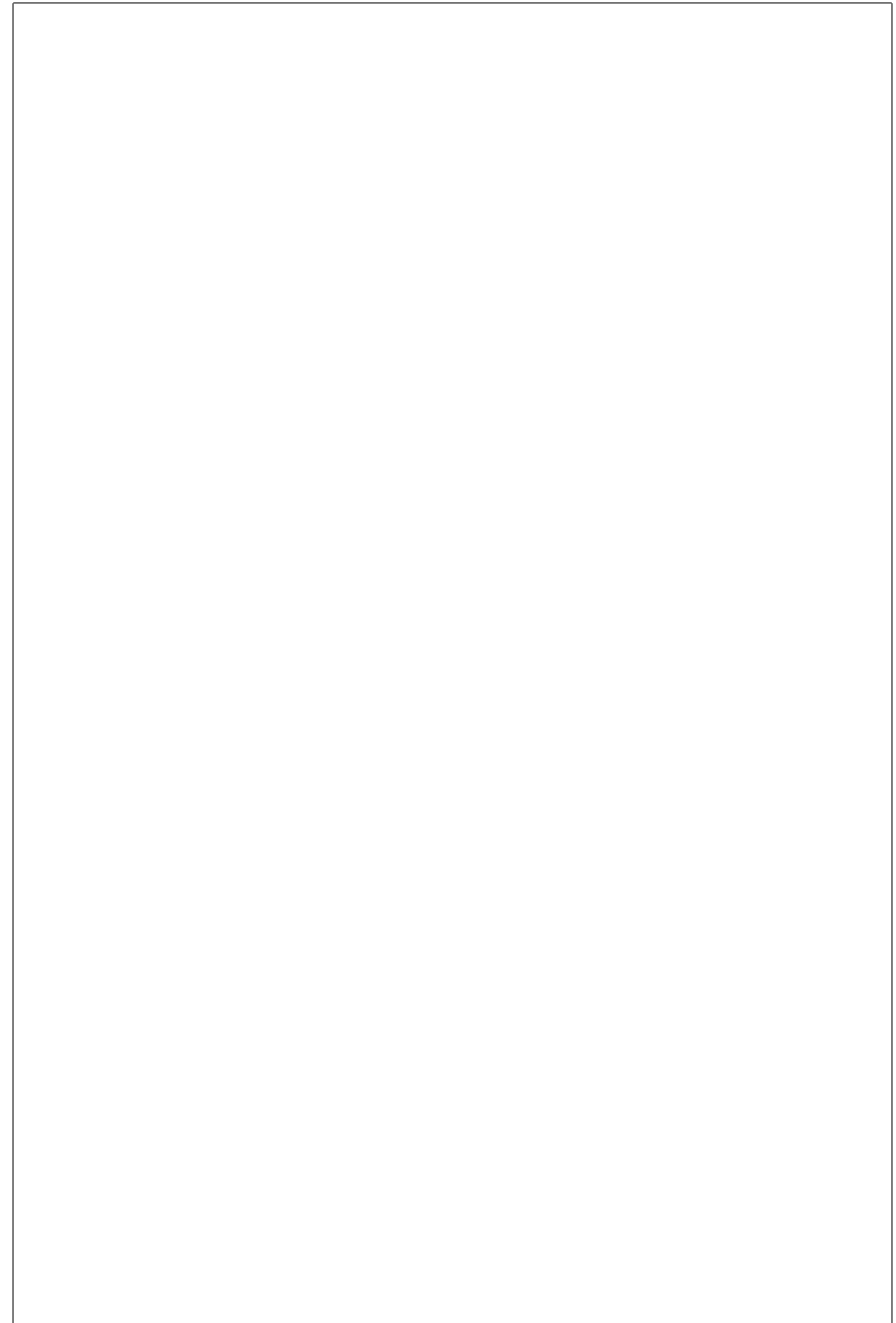
$$\mathbf{GWP}_{\text{tot,trans}} \leq gwp_{\text{lim,trans}} \quad (\text{A.24})$$

The total global warming potential (GWP) emissions during the transition ( $\mathbf{GWP}_{\text{tot,trans}}$ ) are equal to the sum of the total emissions per period ( $\mathbf{GWP}_{\text{tot}}$ ), Eq. (A.23). The emissions during a phase is estimated as the arithmetic average of the representative years before and after the phase. Eq. (A.24) limits the total GWP emissions during the transition by a maximum ( $gwp_{\text{lim,trans}}$ ).

– Appendix 2 - Case study

---

---



---

---

---

## Appendix B

# Case study: the Belgian energy system

### B.1 Belgian energy system in 2020

The Belgian whole-energy system of 2020 was largely based (88.6% of the primary energy mix) on “conventional fuels”(i.e. oil and oil products (38.2%), natural gas (29.5%), uranium (16.3%) and solid fossil fuels (4.6%) while the rest mainly accounts for 26.7 TWh of lignocellulosic and wet biomass, 12.8 TWh of wind and 5.1 TWh of solar [152]. Given the data available in the literature (mostly for the power sector) and, when not available, following the assumptions made by Limpens et al. [54], Table B.1 gives the major technologies used in 2020 to supply the different demands of Figure 2.1.

### B.2 Belgian energy transition pathway towards carbon-neutrality in 2050

This section presents the results of the deterministic (i.e. all parameters at their respective nominal value) perfect foresight optimisation of the Belgian energy transition pathway constrained to a linear decrease of the GHG emissions from 2020 (121 MtCO<sub>2,eq</sub>) to carbon-neutrality in 2050. After performing a technical investigation of the pathway by checking the greenhouse gas breakdown by energy sectors, the primary energy mix is analysed. To illustrate the sector coupling, a focus is made on the electrification of other sectors. Then, the cost implications in terms of investments and operations are discussed.

**Table B.1.** Major technologies used to supply the 2020-demands of Figure 2.1 in terms of share of production and installed capacity.

End-use demand	Major technologies	Share of supply	Installed capacity
Electricity	Nuclear	39%	5.9 GW
	CCGT	21%	3.9 GW
	Wind turbines	14%	5.0 GW
Heat High-Temp.	Gas boiler	36%	3.3 GW
	Coal boiler	30%	2.3 GW
	Oil boiler	20%	1.5 GW
Heat Low-Temp. (DEC) <sup>a</sup>	Oil boiler	48%	21.4 GW
	Gas boiler	40%	17.5 GW
	Wood boiler	10%	4.4 GW
Heat Low-Temp. (DHN)	Gas CHP	59%	0.3 GW
	Gas boiler	15%	0.3 GW
	Waste CHP	15%	0.1 GW
Private mobility <sup>b</sup>	Diesel car	49%	93.5 Mpass.-km/h
	Gasoline car	49%	94.7 Mpass.-km/h
	HEV	2%	5.9 Mpass.-km/h
Public mobility	Diesel bus	43%	3.6 Mpass.-km/h
	Train	43%	3.9 Mpass.-km/h
	CNG bus	5%	0.8 Mpass.-km/h
Freight mobility	Diesel truck	74%	62.7 Mt.-km/h
	Diesel boat	15%	10.8 Mt.-km/h
	Train	11%	2.5 Mt.-km/h
HVC	Naphtha/LPG cracking	100%	4.6 GW
Ammonia	Haber-Bosch	100%	1 GW
Methanol	Import	100%	-

<sup>a</sup>The decentralised heating units provide 98% of the low-temperature heat demand.

<sup>b</sup>The private mobility accounts for 80% of the passengers mobility.

### B.2.1 Greenhouse gases and primary energy

Figure B.1 shows the greenhouse gases (GHG) per sector. The system reaches its upper bound (i.e. maximum emissions) every year.

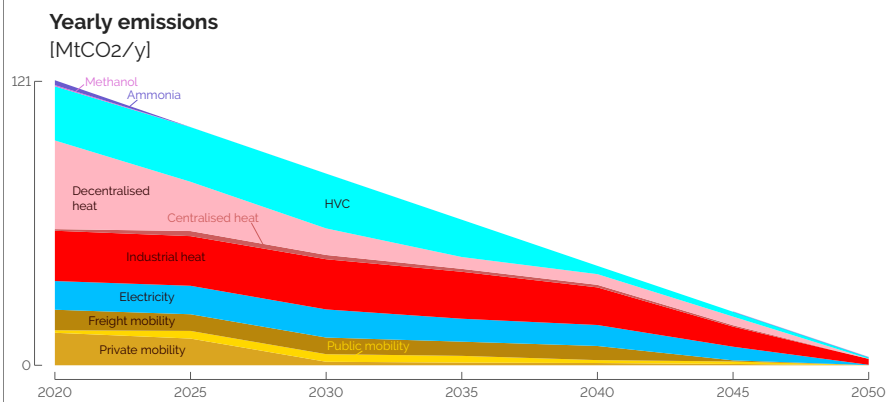


**Figure B.1.** Energy sectors have different speed to reduce GHG emissions over the transition. The system uses all the allowed GHG prescribed by the linear decrease from the emissions in 2020 until carbon-neutrality in 2050.

The defossilisation of the different sectors are not performed at the same rate. The non-energy demand of methanol and ammonia are substituted by electrofuels. These are the first use of electrofuels as e-ammonia is the cheapest electrofuel thanks to the high maturity of the Haber-Bosch process. The decentralised heat and mobility sectors are also dropping first. This is a combination of efficiency and substitution of fossil fuels with electricity. Efficiency comes mainly from district heating networks and electrical heat pumps for the heat sector, and public mobility and electric cars for the mobility sector. From 2040 onward, the decreases are mainly due to the substitution of the remaining fossil fuels by electrofuels as illustrated in Figure B.2.

Figure B.2 shows the primary energy mix for the different representative years. The pathway verifies five trends: (i) reduction of primary energy thanks to energy efficiency; (ii) massive integration of endogenous renewable energies; (iii) importance of electrification; (iv) the usage of gas as the last fossil resource; and (v) the obligation to rely on renewable fuels to achieve carbon neutrality.

The energy supply decreases from 554 TWh/y in 2020 down to 368 TWh/y in 2050 (i.e. -34%) whereas, in the meantime, the demands have increased by 19%, on average. This drop of primary energy consumption reflects the penetration of efficient measures and technologies, such as the previously mentioned public mobility, DHN or

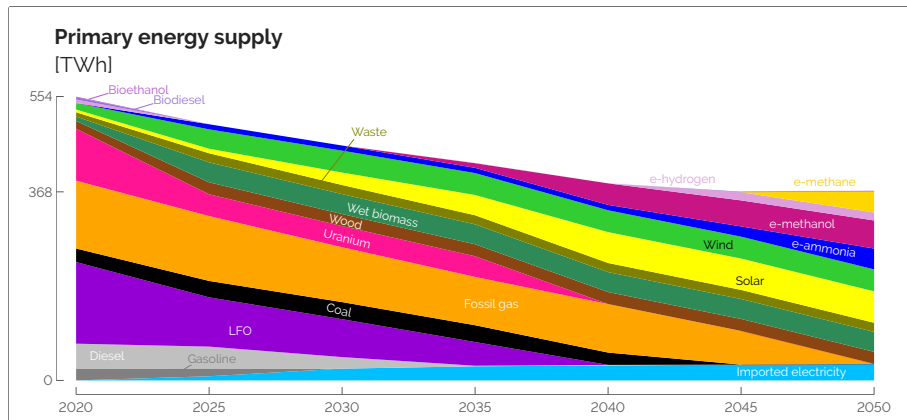


**Figure B.2.** Primary energy emitting GHG (below Uranium) are reducing linearly with fossil gas remaining until 2045. A part of this energy is replaced by renewable ones and starting from 2040, a significant share of electrofuels. As end-use demands slightly increase (see Figure 2.1), the drop represents energy efficiency (i.e. providing the same services with less primary energy).

heat pumps. The results in 2050 are aligned with other studies, such as Devogelaer et al. [153]<sup>1</sup> and My2050<sup>2</sup> [155] which estimates respectively a range of 305-417 TWh/y and 307-364 TWh/y for their central scenarios.

The first fossil energy to phase out is gasoline, which is exclusively used for private cars. Indeed, private mobility is partially replaced by public one<sup>3</sup>; and the cars are switching from gasoline and diesel to electricity. Then, diesel and LFO are decreasing. As diesel is used for trucks and buses mobility, it is harder to phase out compared to gasoline exclusively burned in cars. The first drop of LFO reflects the switch from oil boilers to other technologies: heat pumps and gas cogeneration mainly. Then, it is mainly used for the production of HVC, this reflects that HVC is a feedstock hard to defossilise. Finally, coal is kept mainly for industrial usage because it is a cheap fossil fuel (mainly for industrial usage). To phase it out beforehand, a penalty mechanism, such as a carbon tax, would be required, or its strict ban should be put in place. The last

<sup>1</sup>This study was ordered by the National Planning Bureau in 2013. Five scenarios are proposed.

<sup>2</sup>The Climate Change Service of the Federal Public Service Health launched an initiative in 2012 entitled ‘Low Carbon Belgium by 2050’. This initiative resulted in a report and a calculator in 2013 [154]. The Belgian calculator has been improved since then into a recent expert version called **My2050** [155]. From this study, the results of two scenarios will be used: one based on an optimistic evolution of technologies (Technology), and one focusing on an increased dependence on neighbouring countries (EU integration).

<sup>3</sup>Given the major role played by private cars in the Belgian passenger mobility nowadays (i.e. around 80% [58]), public transport (e.g. tramways, buses and trains) is assumed to be able to supply only half of it.

fossil energy present in the system is fossil gas, used for the production of electricity and heat, through cogeneration mainly. Indeed, gas plays a key role to balance the intermittency of solar and wind.

The consumption of uranium declines in 2025, dropping to 2 GW, primarily due to the political framework aimed at phasing out nuclear energy [156]. In the initial stages, significant deployment of endogenous energies takes place. This includes the utilization of wood, wet biomass, and wind energy, followed by the introduction of solar energy. However, solar energy is not fully deployed during this period due to higher integration costs. Starting from 2025, the importation of electrofuels begins, although their significant utilisation is observed from 2035 onwards. Initially, these fuels are predominantly employed as feedstocks in non-energy sectors. From 2040, e-methanol is additionally utilised for the production of High-Value Chemicals (HVCs), e-hydrogen is employed for mobility purposes, and both e-methane and e-ammonia are used for electricity generation through gas CHP and ammonia-based CCGT plants (see Figure B.3).

In 2020, Belgium has been a net-exporter of electricity, however with the shutdown of nuclear power plants and the increase of electricity consumption, Belgium will become a net importer of electricity. These imports reach their maximal allowed capacity by 2035 (i.e. 30% of electricity end use). This strong dependence on imported electricity illustrates the need for balancing intermittent renewables without relying on fossil fuels.

### B.2.2 Electricity sector: Capacities and yearly balance

To better understand the electricity sector, the installed production capacities are given in Figure B.3, while the supply-demand yearly balance is illustrated in Figure B.4.

As introduced in the primary energy analysis (see Figure B.2), renewable capacities soar. By 2050, wind and solar technologies deployments are 60 GW of PV, 10 GW of onshore wind turbines and 6 GW of offshore wind turbines. To compensate the intermittency, the system relies on imported electricity, gas CCGT, sector coupling and storage. As an illustration, in 2050, 176.8 TWh of electricity transit on the grid which includes 32.4 TWh of electricity imported and 15.4 TWh of electricity from CCGT. This result is aligned with other studies that estimates different ranges: 180-310 TWh/y [153], 126-140 TWh/y [155] and in a more recent study using the TIMES-BE model, 185-196 TWh/y [73]. Higher values from Devogelaer et al. [153] illustrate an almost exclusively electrified energy system. The differences between the study ranges reflect the different assumptions in terms of renewable potentials and availability of nuclear

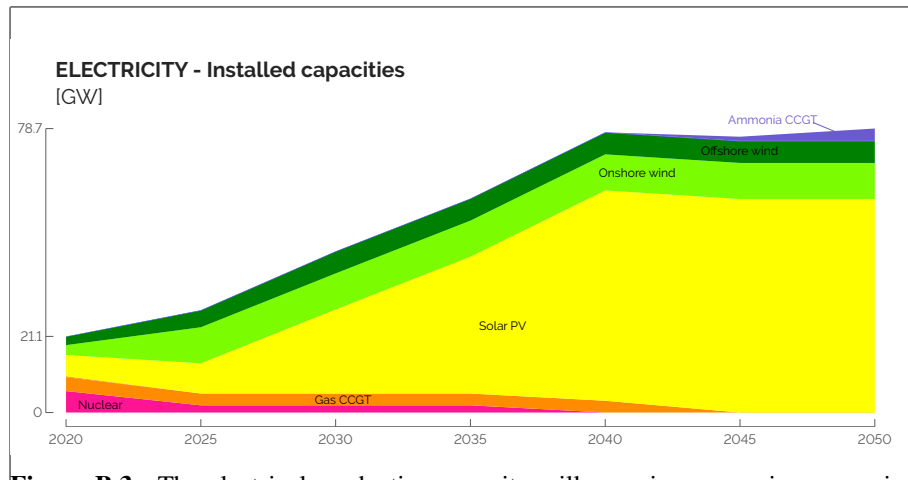


**Figure B.3.** The electrical production capacity will experience massive expansion of wind turbines (onshore and then offshore) and a soaring installed capacity of PV. Ammonia CCGT are installed at the end of the transition to provide a flexible capacity as gas CCGT are phased out.

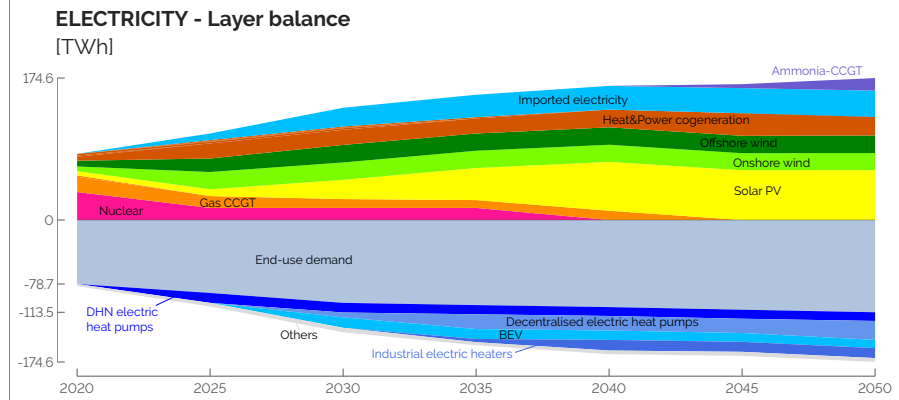


**Figure B.4.** The electricity supply (positive values) will remain a mix of different technologies where backup is first mainly provided by gas-CCGT and then imported electricity, heat and power cogeneration and later ammonia-CCGT. The electricity demand (negative values) is led by the electricity end-use demand, but the share used to electrify heat (heat pumps), vehicles (cars, trains, trams, ...) and industrial heaters drastically increase. This enables a flexible demand that can facilitate the integration of intermittent renewables.

energy. A general trend is that Belgium should maximise its use of endogenous renewable resources, which Dubois et al. [157] identified as a cheaper option than importing additional renewable energies from abroad. Demand management reflects the flexible use of electricity, mainly through heat pumps that uncouple the heat demand and the electricity consumption when combined with thermal storage. Gas CCGT is also a useful asset to compensate intermittent renewables. However, its capacity remains the same as the one installed in 2020. These results are verifying an hourly adequacy of the power demand. Moreover, in a previous study by Pavičević et al. [148], the snapshot version of the model has been coupled with Dispa-SET, a dispatch optimisation model. Results showed that the backup capacity was underestimated by less than 20% to respect reserve capacity, mainly due the lack of reserve capacity for grid stability.

From 2025, the electricity mix has a strong renewable share that rises up to 60% in 2050. The remaining 40% are mainly gas (or ammonia) in CCGT and cogeneration and imported electricity. From a demand perspective, the electrification first starts with DHN heat pumps, then electric cars, then decentralised heat pumps and finally industrial heaters. The latter reflects the usage of cheap PV production peaks.

### B.2.3 Costs: Investments and operation

In the following paragraphs, the results are analysed from an economic perspective to decipher the choices made by the model, as the overall cost of the transition is 1 004 b€<sub>2015</sub> split unequally among the sectors.

Figure B.5 illustrates the cumulative investments made throughout the transition, amounting to a total of 377.8 b€<sub>2015</sub>. Initially, the infrastructure, transport, and electricity sectors each account for approximately one-third of the investments. The investments in infrastructure are primarily driven by the electricity grid and the district heating network (DHN), representing a combined investment of 73 b€<sub>2015</sub>. The electricity sector's investment is led by power plants, totalling 31.5 b€. Notably, the investment costs in the mobility sector are primarily attributed to private cars, constituting 71% of the total. A rough estimation confirms the significant investment in cars, with an average of 500,000 vehicles registered annually in Belgium over the last decade [158] and assuming an average cost of 20 k€ per car, the funds allocated to private cars amount to 10 b€ per year. This trend in private cars explains why the private mobility sector accounts for half of the investments required to achieve the transition by 2050. This finding aligns with other studies, such as Devogelaer et al. [153], which estimates cumulative investment expenditures of approximately 600 b€<sub>2005</sub> for the transport sector between 2013 and 2050, which confirms our conservative approach in the estimation.

As a comparison, the investments required to fully deploy the PV and wind potentials from 2020 to 2050 amount to 74.4 b€<sub>2015</sub>, with an additional 22.2 b€<sub>2015</sub> allocated to reinforce the grid. The electrification of the heating sectors necessitates investments of 29.2 b€<sub>2015</sub>, including 6.5 b€<sub>2015</sub> for the deployment of the DHN infrastructure. Storage investments, primarily focused on DHN seasonal storage, amount to 3.6 b€<sub>2015</sub>. Apart from the investment required to replace all private vehicles (accounting for 44% of the overall investments), the remaining sectors represent a total of 212 b€<sub>2015</sub>. To mitigate the cost of the transition, My2050 suggests deploying a fleet of no more than one million vehicles and implementing a car sharing system, distinct from car-pooling, as an inevitable measure [155].

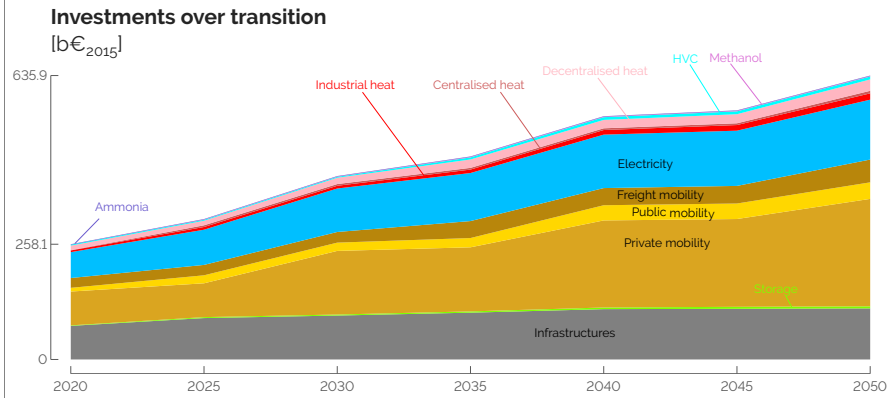


**Figure B.5.** The cumulative investments over the transition is unequally spread between the sectors. The energy system in 2020 is imposed to the existing energy system and its expenses are split in three main categories: mobility (mainly vehicles), infrastructure (mainly grids) and electricity (mainly thermal power plants). The investments required during the transition represents 150% the initial investment and mainly in the same three sectors.

A part of the investment will be recovered at the end of the transition based on the remaining lifespan of the technology after 2050. Figure B.6 illustrates the salvage value by sectors, calculated according to Eq. (1.5). Out of the 114.4 b€<sub>2015</sub> of investments in the infrastructure (i.e. mostly power grid and gas network), 55.9% remain available after 2050, due to their long lifetime. On the contrary, private mobility has a lower salvage value due to a major drop within the first four years and an average lifetime below 10 years [158].

In addition to investment decisions, the operational expenditure (OPEX), which accounts for resource utilisation and technology maintenance, are significant. Figure

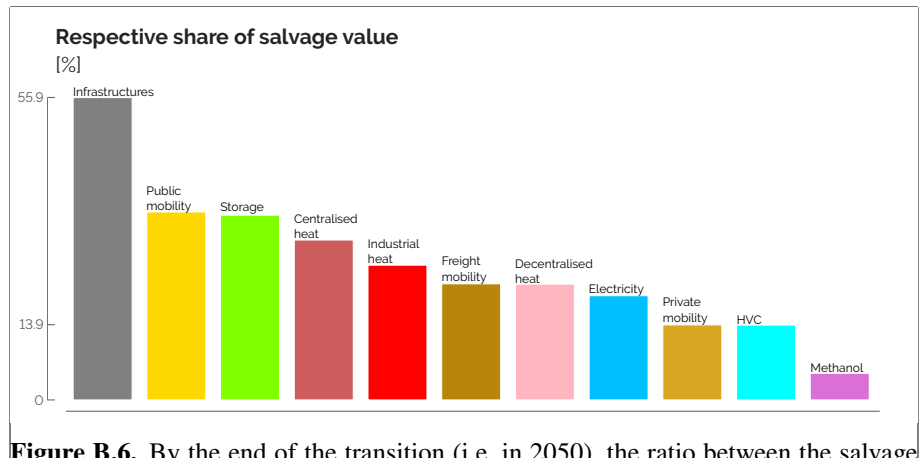


**Figure B.6.** By the end of the transition (i.e. in 2050), the ratio between the salvage value and its cumulative investment, per sector, is unequal. Investments in infrastructures, public mobility, storage and other long-lifetime technologies experience an important salvage value, at the contrary, investments in private mobility will not be recovered as vehicles have a short lifetime. All together, these salvage values represent 160.1 b€<sub>2015</sub>, 25% of the cumulative investment costs in 2050.

B.7 shows the yearly system cost for each sector except the OPEX related to resources that are grouped together. The latter dominates the OPEX, with a significant share of non-renewable resources (i.e. 63.6% in 2020) until 2040, followed by a steep increase in the share of renewable resources (i.e. 66.2% in 2050). The substantial reliance on non-renewable resources reflects the prevalent use of fossil fuels in our current energy system. The high cost-share of non-renewable fuels underscores the economic challenges of simply substituting fossil fuels with renewables, particularly evident when emphasizing that electrofuels are 2-3 times more expensive. Maintenance expenses in the private mobility sector rank second in terms of expenditure. On the other hand, maintenance expenses in other sectors are relatively small compared to the aforementioned sectors.

The annualised cost of the energy system in 2020 is estimated to 44.3 b€/y and increases by 5.5 b€/y to reach 49.8 b€/y by 2050. The work of Climact and VITO [155] estimates the annualised cost in 2050 between 63 and 82 b€/y, while the other studies just indicate the cost increase compared to 2015 (+11.7 to +21) [73, 153]. The differences come from the scope of the energy system: as an example Climact and VITO [155] also account for the agriculture sector. These differences highlight the difficulty to compare different studies due to difference of scope and partial availability

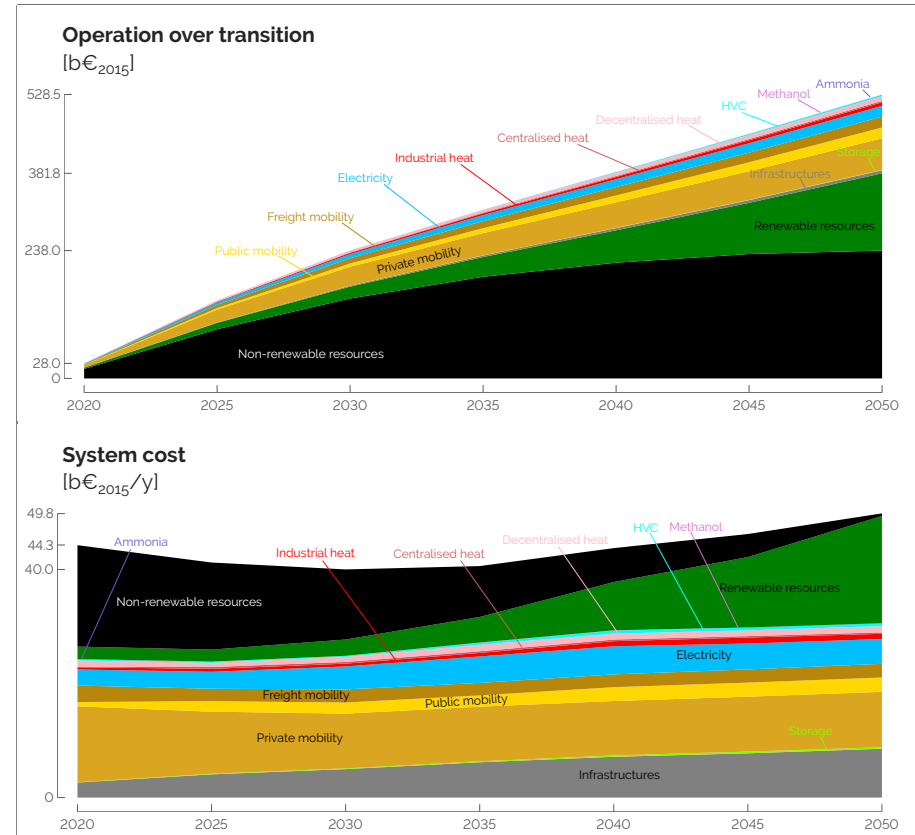


**Figure B.7.** The yearly system cost shows the shift from non-renewable to renewable resources (mainly electrofuels). Operation cost and maintenance represents almost 50% of the expenses.

of used data. Overall, comparing with existing studies shows the consistency of the results provided by EnergyScope Pathway.

### B.3 Myopic versus perfect foresight pathway optimisation

This section aims at digging more into the details of the differences observed between the myopic approaches and the reference case (i.e. hourly perfect foresight model).

Similarly to Nerini et al. [16], Figure B.8 shows that myopic optimisation ends up with a slightly more expensive energy transition by 2050 (i.e. +3.2 b€<sub>2015</sub>), compared to the perfect foresight, despite the savings done at the early stages. Even though this

**Table B.2.** Exhaustive general comparison between the two different foresight approaches: Perfect foresight (PF) and Myopic (MY). Differences with the reference case (PF) below 1% are not shown ( $\simeq$ ) and ones above 10% are in bold.

		PF	MY	Units
Computational time <sup>a</sup>		830	<b>373</b>	s
Costs in 2050	Total transition <sup>b</sup>	1004	$\simeq$	b€ <sub>2015</sub>
	Cumulative opex	528	$\simeq$	b€ <sub>2015</sub>
	Cumulative capex	636	$\simeq$	b€ <sub>2015</sub>
	Salvage value	160	-1%	b€ <sub>2015</sub>
Primary energy mix in 2050	Total	368.0	$\simeq$	TWh/y
	e-hydrogen	15.6	$\simeq$	TWh/y
	e-methane	41.0	+6%	TWh/y
	e-methanol	54.8	$\simeq$	TWh/y
	e-ammonia	40.7	-10%	TWh/y
Electrification in 2050 <sup>c</sup>	System <sup>d</sup>	63.3	$\simeq$	TWh <sub>e</sub>
	Industrial heat <sup>e</sup>	12.3	-7%	TWh <sub>th</sub>
	Decentralised heat <sup>e</sup>	73.9	$\simeq$	TWh <sub>th</sub>
Year of full VRES-deployment	PV	2045	<b>2040</b>	-
	Wind-offshore	2030	<b>2025</b>	-
	Wind-onshore	2025	2025	-

<sup>a</sup>These computational times were reached on a 2.4GHz 4-core machine.

<sup>b</sup>As detailed in Equation 1.1, the transition cost is the sum of the cumulative opex and capex, salvage value being deduced.

<sup>c</sup>The electrification of the other sectors (i.e. centralised heat (100%-heat pump), private (100%-BEV), public mobility (80%-train and tramway), freight mobility (25%-train) and non-energy demand (0%)) are identical between the three approaches and are, therefore, not presented in the table.

<sup>d</sup>The electrification of the system is computed as the difference between the total production of electricity and the end-use demand of electricity.

<sup>e</sup>The electrification of the industrial and decentralised heating sectors are expressed in terms of thermal energy (TWh<sub>th</sub>) provided by electrified processes, respectively industrial resistors and decentralised electric heat pumps.

over-cost is negligible compared to the overall cost of the transition (i.e.  $\sim 1000 \text{ b}\epsilon_{2015}$ ), this is explained by the early investments in renewable technologies (i.e. PVs and wind turbines) boosted by the significant salvage value retrieved from investing in the consequent reinforcement of the grid.

Figure B.9 highlights this as infrastructures and the electricity-technologies account respectively for 83.2 and 61.2  $\text{b}\epsilon_{2015}$  in 2030 whereas the overall cumulative investments, so far, are 421.3  $\text{b}\epsilon_{2015}$ . The significant lifetime (e.g. 80 years) and investment cost (i.e. 368M€/GW<sub>VRES</sub> [11]) of the power grid, and, on a smaller scale, the district heating network, explain why the myopic optimisation opts for a higher investment in these infrastructures, at early stages. Similarly to what Keppo and Strubegger [159] observed in their studies, these early investments consequently lead to more investments, later in the transition, to renew technologies that have become too old before 2050: during the phase between 2045 and 2050, the myopic approach needs to invest in 9.2GW of PVs that have been installed 25 years before whereas the perfect foresight, by smoothing its investments over the entire transition, has to renew only 2.5GW of PVs.

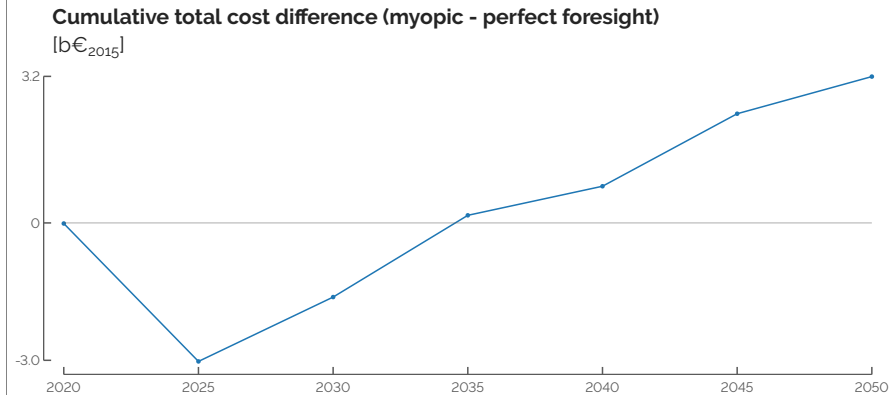


**Figure B.8.** Cumulative total cost (i.e. opex+capex-salvage value) difference between the myopic and perfect foresight (PF) approaches. Positive values mean that the myopic approach is higher than perfect foresight. Early savings of the myopic vision are overcompensated by late investments further on.

In 2050, the capacities installed in the different sectors, the design of the system in other words, are very similar between the two approaches. The passenger and freight mobility sectors are the same where differences smaller than 1GW are observed in other sectors. More interestingly, the myopic optimisation tends to postpone the de-

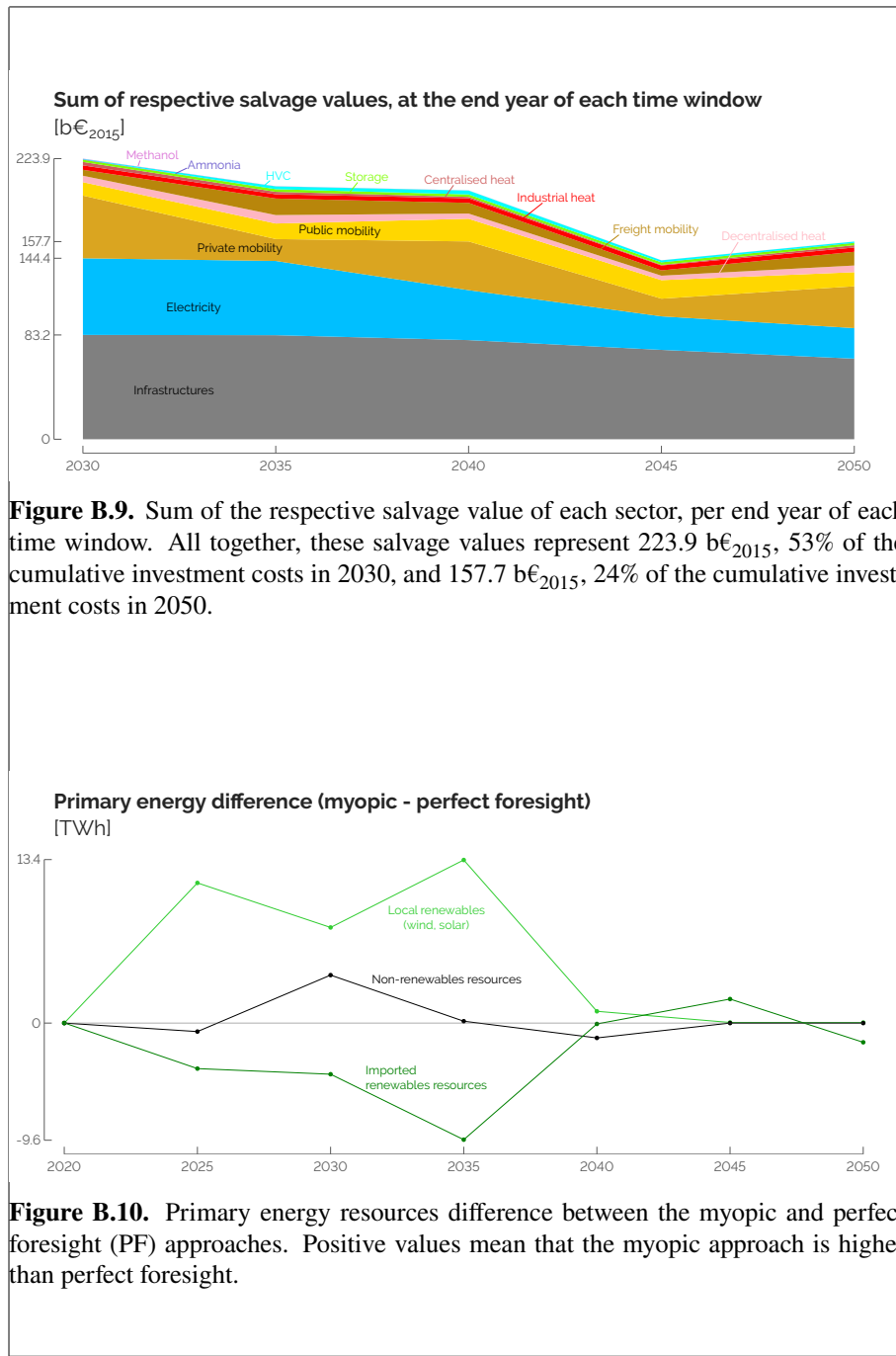
commissioning of capacities when the loss of salvage values at the end of an optimisation window would be bigger than the maintenance cost. For instance, in the myopic approach, 0.8GW of industrial coal boilers will remain installed in 2045 and 2050 or 3.6GW of naphtha-crackers to produce HVC in 2040, whereas these technologies are not used. This is comparable to the “lock-ins” detailed in other studies [17, 159] where technologies installed at early stages of the transition remain in place.

Highlighted in Figure B.10, the earlier availability of renewable (and intermittent) electricity consequently accelerates the electrification of the other sectors. For instance, in 2035, 3.7GW (+75%) more of industrial electric heaters to produce 5.1TWh/year (+130%) of additional industrial heat. In the low-temperature heat sector, decentralised and centralised electric heat pumps capacities are, respectively, 2.2GW (+19%) and 1GW (+8%) higher for each of the representative years between 2030 and 2045, to produce, around 7.8TWh/year (+23%) and 0.8TWh/year (+1%), at the expense of other technologies such as gas heat pumps. Finally, public trains substitute from 2035 a higher share of the CNG-buses.

In general, due to the formulation of the salvage value (see Eq. 1.5), the myopic approach is more techno-oriented as investing more in technologies is beneficial, especially at the early stages of the transition. Therefore, before converging to a similar energy mix in 2050, the myopic system relies more on local renewables (e.g. solar and wind) than on importing renewable energy carriers (e.g. e-ammonia, e-methanol, e-hydrogen or e-methane), see Figure B.10. In parallel, in the near term, the system relies on average more on conventional/non-renewable sources, like observed in other studies [159–161].

## B.4 Assessment of different emissions-trajectories

This section compare results of the optimisation subject to different emissions-trajectories with the REF case where the emissions are constrained to decrease linearly from the level in 2020 to carbon-neutrality in 2050. The first comparison is done with the trajectory subject to respect the CO<sub>2</sub>-budget prescribed in the RL-based pathway optimisation, i.e. 1.2GtCO<sub>2,eq</sub> (Section 2.5). Then, to assess the impact of the myopic approach on the optimisation of the transition, it is compared to perfect foresight results, alleviating the constraint on the emissions-trajectory.



### B.4.1 CO<sub>2</sub>-budget versus linear decrease of emissions

Figure B.11 shows the yearly emissions attributed for each sector in the REF case (i.e. imposed CO<sub>2</sub>-budget) and a case where the CO<sub>2</sub>-trajectory is constrained instead. Interestingly, these two transition pathways end up in a similar carbon-neutral whole-energy system in 2050. The two main sectors that significantly reduce their emissions in the REF case are the production of HVC and the high-temperature heat. In the former, this is linked to the extended use of oil products through naphtha-cracking. The latter is produced by industrial coal boilers for longer, until 2040. Overall, ending up to the same level of emissions in 2050, the REF case represents a 60% reduction of the cumulative emissions compared to the linear decrease, for a 7.5% more expensive transition.

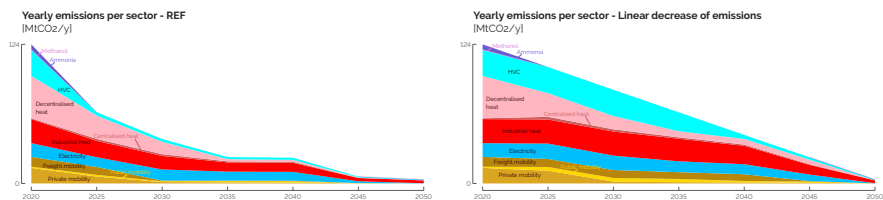


**Figure B.11.** Respecting the CO<sub>2</sub>-budget imposed in the REF case drastically cuts the emissions of the system, especially in the production of high value chemicals (HVC) and the high-temperature heating sector.

### B.4.2 Comparison without restriction on GHG

The outcomes of a model could be limited when the case study is too restrictive. Indeed, ones could argue that the comparison between myopic, monthly and perfect foresight are very similar as the energy system is strongly constrained in terms of GHG emissions.

In the following, we perform a similar comparison in the transition pathway without restricting the GHG emissions.

#### Reference case

Figure B.12 illustrates the transition taken by Belgium without restriction on the GHG emissions.

Similar trends that for the defossilisation are observed: primary energy mix reduces, renewable energy integration rises and an electro-fuel is imported. However,

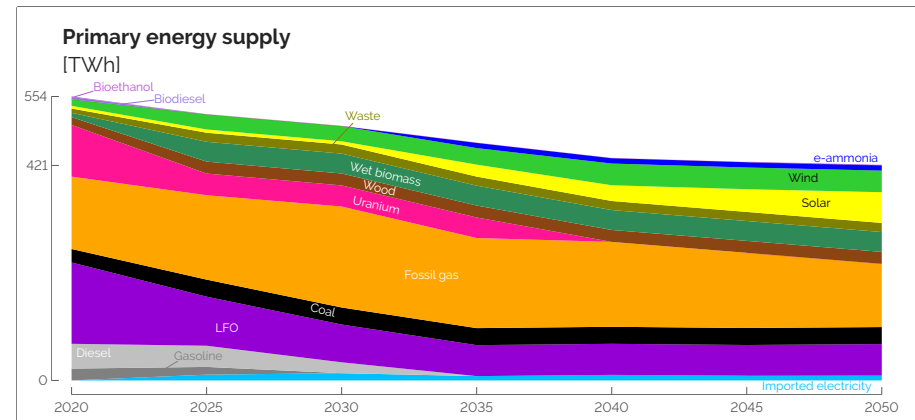


**Figure B.12.** Primary energy mix of a non-constrained energy transition. In this results, carbon neutrality is not reached in 2050. Some fossil fuels remain used.

some changes reflects the cheapest option that the system could utilise to reach a cheaper transition, such as using as little electrofuels as possible. In this case, only e-ammonia is used for its end use demand.

Instead of analysing the energy system in details, the following paragraphs will investigate if the comparison findings are consistent on a different case study.

#### Comparison with Myopic approach

Several key messages of the comparison have been summarised in Table B.2. In the following paragraph we analyse how these conclusions are affected when the constraint on the GHG-emissions trajectory is removed.

First, considering the overall transition cost, the myopic approach keeps on making short-term savings, i.e. down to -0.2%, before ending up with a more expensive transition by 2050, i.e. +0.2%. Similarly to the case with an imposed GHG-emissions trajectory, myopic optimisation invests more, compared to the perfect foresight, at early stages into VRES technologies to benefit from the significant salvage values of the related grid infrastructures. In 2030, the salvage value of the infrastructures and electricity-generation technologies account for 80.2 and 56.2 b€<sub>2015</sub>, respectively, whereas the overall CAPEX are 404.8 b€<sub>2015</sub> by then.

Then, in the case with a prescribed GHG-emissions trajectory, the myopic approach had to invest more by the end of the transition to renew PV installed more massively at early stages and that reached the end of their lifetime before the end of the transition. In the case without this emissions trajectory, there is less an urgency/need for

integrating renewables in the system. Consequently, in the latter case, there is not such an extra-investment to make to renew too old renewable assets. On top of this, the slower uprise of VRES in the case without emissions trajectory leads to a smaller difference of electrification of the other sectors between the perfect foresight and myopic approaches.

Finally, even though the way to get there differs between the perfect foresight and the myopic approaches, the system designs by 2050 are very similar between these two in most of the sectors. The main observed difference is in the freight transport where diesel boats are preferred to gas boats. This can be looked as a result of the lock-in effect where choices made at early stages, due to the limited foresight, remain in place in the longer term.

In essence, when comparing perfect foresight and myopic approaches, distinctions arise in minor aspects, while the fundamental conclusions of Table B.2 were verified. These variances have been elucidated in the preceding enumerated points and can primarily be attributed to the changes in the case study, rather than reflecting limitations inherent to the model or the comparative analysis itself.

## B.5 Uncertainty characterisation for the 5-year steps transition

Table B.3 summarises the uncertainty ranges for the different groups of technologies and resources, for the year 2025. Refer to [3, 35] for the methodology and sources. As the model optimises the system every 5 years,  $N = 5$  has been selected to get the final ranges of uncertainties of type II and III, based on the work of Moret [35]. For type III uncertainties (i.e. uncertainty ranges increasing with time), a 50% increase has been set arbitrarily between the ranges for 2025 and these same ranges for 2050. In other words, for these specific uncertainties, the ranges for 2050 are 50% larger than for 2025.

Rixhon et al. [5] analysed the impact of these parameters on the total cost of the snapshot Belgian whole-energy system in 2050 subject to different GWP limits. Based on this work, we have selected a subset of impacting uncertainties, added others due to the pathway formulation (e.g.  $\Delta_{\text{change,pass}}$ ), and listed them in Table B.3. The uncertainty characterisation gives the uncertainty ranges per parameter or group of parameters (category).

This work considers nine groups of uncertain parameters: (i) the cost of purchasing imported energy carriers; (ii) the investment cost (i.e. CAPEX) of some technologies, mostly related to the mobility sector and the integration of renewables; (iii) the maintenance cost (i.e. OPEX) of every technology; (iv) the consumption of electric and fuel

cells vehicles in the mobility sector; (v) the potential installed capacity of renewables; (vi) the hourly load factor of renewables accounting for variability of solar irradiance or wind speed; (vii) the availability of resources considered as limited (i.e. biomass and electricity); (viii) the end-use-demands split per sector of activities (i.e. households, services, passenger mobility and industry) and (ix) other parameters like the interest rate or the modal share change in different key sectors. For the specific case of SMR, the parameter  $f_{\max,SMR}$  will influence the maximum capacity (i.e. 6 GW) to install to translate somehow the readiness of this technology. If it is (i) smaller than 0.6, there is no possibility to install SMR during the transition; (ii) between 0.6 and 0.8, these 6 GW can be installed only in 2050; (iii) between 0.8 and 0.9, these can be installed from 2045 onward and; (iv) higher than 0.9, the prescribed maximum capacity can be installed from 2040 onward.

**Table B.3.** Application of the uncertainty characterization method to the EnergyScope Pathway model for the year 2025.

Category	Parameter	Meaning	Type <sup>a</sup>	Relative variation <sup>b</sup> min	max
<b>Cost of purchasing</b>	$c_{\text{op,fossil}}$	Purchase fossil fuels	II	-64.3%	179.8%
	$c_{\text{op,elec}}$	Purchase electricity	II	-64.3%	179.8%
	$c_{\text{op,electrofuels}}$	Purchase electrofuels	II	-64.3%	179.8%
	$c_{\text{op,biofuels}}$	Purchase biofuels	II	-64.3%	179.8%
<b>Investment cost</b>	$c_{\text{inv,car}}$	CAPEX car	I	-21.6%	25.0%
	$c_{\text{inv,bus}}$	CAPEX bus	I	-21.6%	25.0%
	$c_{\text{inv,ic\_prop}}$	CAPEX ICE	I	-21.6%	25.0%
	$c_{\text{inv,e\_prop}}$	CAPEX electric motor	I	-39.6%	39.6%
	$c_{\text{inv,fc\_prop}}$	CAPEX fuel cell engine	I	-39.6%	39.6%
	$c_{\text{inv,efficiency}}$	CAPEX efficiency measures	I	-39.3%	39.3%
	$c_{\text{inv,PV}}$	CAPEX PV	I	-39.6%	39.6%
	$c_{\text{inv,grid}}$	CAPEX power grid	I	-39.3%	39.3%
	$c_{\text{inv,grid\_enforce}}$	CAPEX grid reinforcement	I	-39.3%	39.3%
	$c_{\text{inv,nuclear\_SMR}}$	CAPEX SMR <sup>c</sup>	I	-40.0%	44.0%
<b>Maintenance cost</b>	$c_{\text{maint,var}}$	Variable OPEX of technologies	I	-48.2%	35.7%
<b>Consumption</b>	$\eta_{\text{e\_prop}}$	Consumption electric vehicles	I	-28.7%	28.7%
	$\eta_{\text{fc\_prop}}$	Consumption fuel cell vehicles	I	-28.7%	28.7%
<b>Potential installed capacity</b>	$f_{\text{max,PV}}$	Max capacity PV	I	-24.1%	24.1%
	$f_{\text{max,windon}}$	Max capacity onshore wind	I	-24.1%	24.1%
	$f_{\text{max,windoff}}$	Max capacity offshore wind	I	-24.1%	24.1%
<b>Hourly load factor</b>	$c_{\text{p,t,PV}}$	Hourly load factor PV	II	-22.1%	22.1%
	$c_{\text{p,t,winds}}$	Hourly load factor wind turbines	II	-22.1%	22.1%
<b>Resource availability</b>	$avail_{\text{elec}}$	Available electricity import	I	-32.1%	32.1%
	$avail_{\text{biomass}}$	Available local biomass	I	-32.1%	32.1%
<b>End-use demand</b>	$HH\_EUD$	Households EUD	III	-13.8%	11.2%
	$services\_EUD$	Services EUD	III	-14.3%	11%
	$pass\_EUD$	Passenger mobility EUD	III	-7.5%	7.5%
	$industry\_EUD$	Industry EUD	III	-20.5%	16.0%
<b>Miscellaneous</b>	$i_{\text{rate}}$	Interest rate	I	-46.2%	46.2%
	$\%_{\text{pub,max}}$	Max share of public transport	I	-10%	10%
	$\Delta_{\text{change,freight}}$	Modal share change freight mobility	-	-30%	30%
	$\Delta_{\text{change,pass}}$	Modal share change passenger mobility	-	-30%	30%
	$\Delta_{\text{change,LT\_heat}}$	Modal share change LT-heat	-	-30%	30%
	$f_{\text{max,SMR}}$	Potential capacity SMR	-	0	1

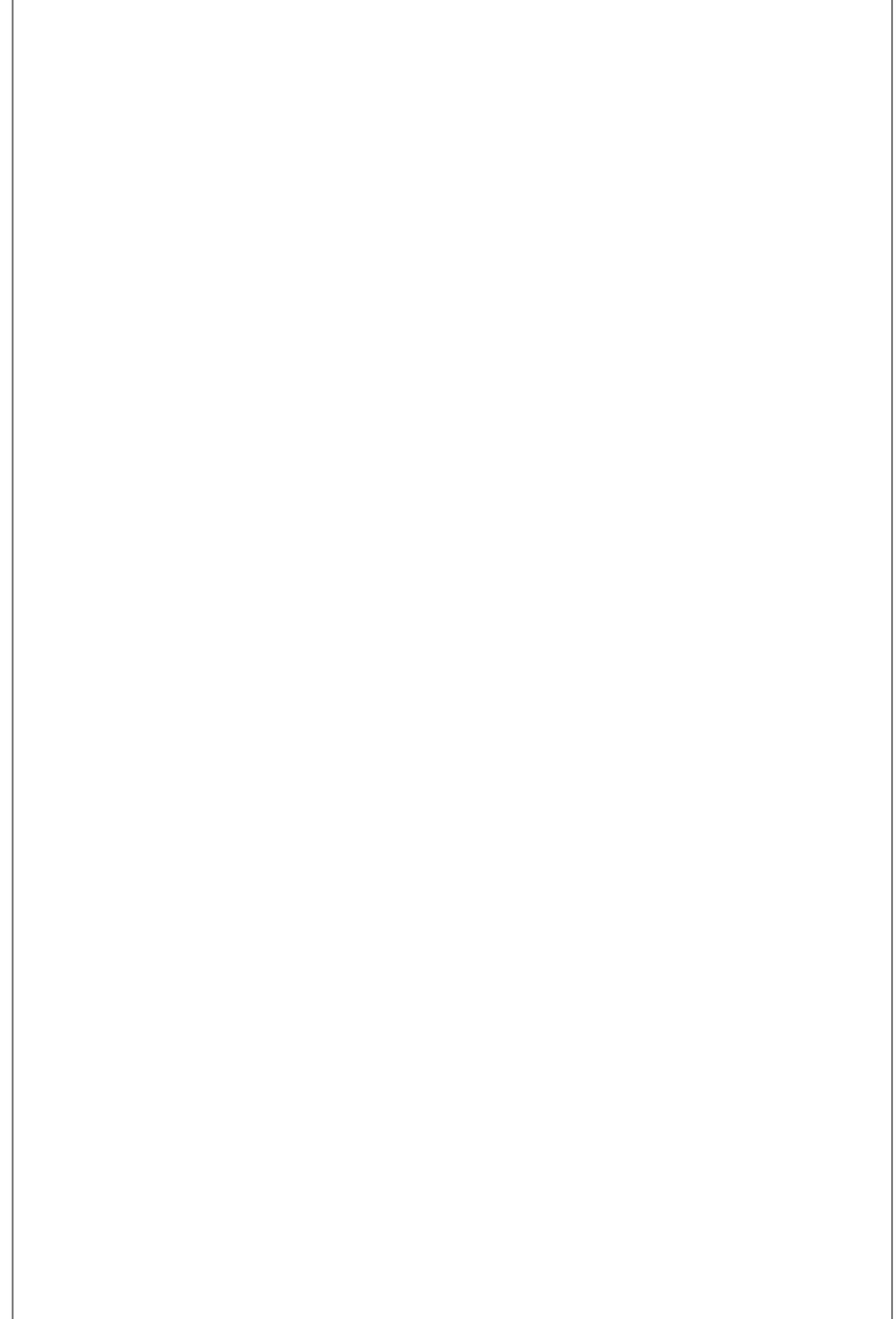
<sup>a</sup>Per Moret [35], “I: investment-type, II: operation-type (constant uncertainty over time), III: operation-type (uncertainty increasing over time)”.

<sup>b</sup>The nominal values of each of the parameters is 0, meaning no variation compared to the nominal values of the impacted parameter in the model.

<sup>c</sup>This range has been inferred from the local sensitivity analysis performed by EnergyVille [73].

---

---



---

---

---

## Appendix C

# Pathway optimisation under uncertainties

### C.1 Total transition cost

Table C.1 gives the ranking and total Sobol index over the total transition cost of each of the 34 parameters listed in Table B.3. The first column shows these indicators for the GSA applied on the monthly pathway model that has some limitations [?] but has the main advantage to run much faster. The second column gives the same indicators but for an uncertainty quantification carried out on the hourly pathway model and only using the most impacting parameters. Given the similar rankings of the parameters between these two, this comparison shows that the monthly model can be a computationally efficient proxy to quantify the uncertainties of the actual hourly model and point out the key parameters on optimisation-driving objective, the total transition cost.

Besides the top-4 parameters, rankings are slightly different. However, this does not jeopardize the comparative analysis given the similar Sobol' indices. Given their wide range of uncertainty [-64.3%; 179.8%] and their significant role to meet the CO<sub>2</sub>-budget, the cost of purchasing electrofuels is the first, by far, impacting parameter. Next, comes, naturally, the industrial EUD, representing, at the nominal value, 60% of the total demands by 2050. The top-3 is completed by the variation of the interest rate, directly impacting the annualisation and the salvage values of the assets. Finally, since the current Belgian whole-energy system deeply relies on fossil resources, and would still do in the near future, the cost of purchasing fossil fuels is part of the impacting parameters. On the contrary, due to the very low annualised, cost, long lifetime leading

to a significant salvage value and a low-emitting fuel, the parameters related to SMR barely impact the total transition cost.

**Table C.1.** Total Sobol' indices of the uncertain parameters over the total transition cost in the monthly and hourly pathway models. The similar rankings (and indices) show the validity of using the faster (even though less accurate) monthly model to assess uncertainties over the hourly model.

<b>Parameter</b>	<b>Ranking (Sobol' index)</b>	
	Monthly model	Hourly model
<b>Purchase electrofuels</b>	1 (47.4%)	1 (44.4%)
Industry EUD	2 (23.5%)	2 (26.4%)
Interest rate	3 (11.0%)	3 (13.2%)
Purchase fossil fuels	4 (6.9%)	4 (6.9%)
Variable OPEX of technologies	5 (2.9%)	6 (3.0%)
Purchase biofuels	6 (2.6%)	5 (3.0%)
Hourly load factor PV	7 (1.9%)	9 (1.3%)
CAPEX electric motor	8 (1.9%)	7 (2.5%)
Hourly load factor wind turbines	9 (1.3%)	8 (1.4%)
Max capacity PV	10 (1.1%)	14 (0.5%)
<b>Potential capacity SMR</b>	11 (0.9%)	11 (1.0%)
Available local biomass	12 (0.8%)	12 (0.7%)
CAPEX car	13 (0.7%)	10 (1.2%)
Passenger mobility EUD	14 (0.7%)	13 (0.7%)
Modal share change LT-heat	15 (0.5%)	-
Households EUD	16 (0.5%)	-
Services EUD	17 (0.4%)	-
Max capacity onshore wind	18 (0.3%)	-
Max share of public transport	19 (0.3%)	-
CAPEX PV	20 (0.2%)	-
Max capacity offshore wind	21 (0.2%)	-
Efficiency electric motor	22 (0.1%)	-
CAPEX fuel cell engine	23 (0.1%)	-
CAPEX ICE	24 (0.1%)	-
Efficiency fuel cell engine	25 (<0.1%)	-
Modal share change freight mobility	26 (<0.1%)	-
Modal share change passenger mobility	27 (<0.1%)	-
CAPEX efficiency measures	28 (<0.1%)	-
CAPEX bus	29 (<0.1%)	-
CAPEX grid reinforcement	30 (<0.1%)	-
CAPEX power grid	31 (<0.1%)	-
<b>CAPEX SMR</b>	32 (<0.1%)	-
Available electricity import	33 (<0.1%)	-
Purchase electricity	34 (<0.1%)	-

## C.2 Imported renewable electrofuels

Figure C.1 gives the distribution of the different routes of supply and consumption of gas like methane, hydrogen, ammonia and methanol, resulting from the 1260 samples of the GSA.

Given its lower cost of purchasing than its renewable equivalent (Figure 2.2) and lower GWP than other fossil fuels (i.e.  $gwp_{op,NG} = 0.27 \text{ kt}_{CO_2,eq}/\text{GWh}$  versus  $gwp_{op,LFO} = 0.31 \text{ kt}_{CO_2,eq}/\text{GWh}$  or  $gwp_{op,coal} = 0.40 \text{ kt}_{CO_2,eq}/\text{GWh}$ ), fossil NG remains the main source of gas in the system until 2040. Besides bio-hydrolysis as the main consumer of wet biomass to consistently produce gas, e-methane eventually substitutes fossil natural gas by 2045-2050 in order to respect the CO<sub>2</sub>-budget for the transition. Its versatility makes gas used by a wide variety of technologies in the different sectors. Initially, in 2020, decentralised gas boilers, CCGT and industrial gas boilers represent the biggest consumers of gas with 39%, 21% and 16% of the total consumption, respectively. Progressively, in line with the rest of the system shifting towards more efficiency in the mid-term, industrial CHP represent the lion's share, next to other usages in the transport or LT-heating sectors.

On the contrary, import of fossil-based hydrogen, largely produced from steam-methane-reforming [162], is rarely part of the solution due to the emissions related to the consumption of natural gas. E-hydrogen is the consistent source of hydrogen in the system, next to local production (i.e. steam-methane-reforming, electrolysis or ammonia-cracking) in some rare cases where low industrial EUD coincides with more abundant electricity from SMR or PV. In terms of consumption, FC-trucks are the more consistent player. FC-cars are also at stake but in specific cases where their CAPEX and the CAPEX of electric vehicles are in the bottom and the top of their respective uncertainty range.

Becoming cheaper than its fossil equivalent at early stages of the transition (i.e. from 2030 onward), e-ammonia is the exclusive stream of ammonia in the system, except rare cases. Then, on top of its consistent NED, the largest consumption of ammonia is CCGT as flexible power generation units, to substitute their e-methane equivalents that have a higher LCOE (Figure 2.3).

Similarly to ammonia, on top of local production in rare cases, e-methanol is the key source for methanol. Besides its own NED, methanol is mostly consumed to produce HVC via the MTO process instead of naphtha-cracking, in order to respect to CO<sub>2</sub>-budget for the transition.

**Table C.2.** Comparison of the quantities of imported renewable electrofuels, in TWh, between the REF case, the SMR case and the statistical features from the GSA (i.e. Q1, median and Q3). 2020 is not in the table as, per assumption, no renewable electrofuel is imported for this year. For the sake of clarity, zeroes are replaced by “-”.

Year	Case	e-methane	e-hydrogen	e-ammonia	e-methanol
2025	REF	-	-	10	52
	SMR	-	-	10	29
	Q1	-	-	9	2
	Median	-	-	10	46
	Q3	-	-	11	55
2030	REF	-	1	10	52
	SMR	-	1	10	52
	Q1	-	-	9	43
	Median	-	-	10	51
	Q3	-	1	12	57
2035	REF	-	17	10	53
	SMR	-	17	10	53
	Q1	-	-	9	44
	Median	-	4	11	52
	Q3	-	16	32	58
2040	REF	-	16	23	54
	SMR	-	16	10	54
	Q1	-	-	12	43
	Median	-	12	36	53
	Q3	10	16	68	60
2045	REF	40	16	42	54
	SMR	-	16	11	54
	Q1	-	-	24	43
	Median	-	13	49	52
	Q3	44	17	77	60
2050	REF	39	16	44	55
	SMR	7	16	11	55
	Q1	-	-	20	44
	Median	19	14	44	53
	Q3	51	17	72	61

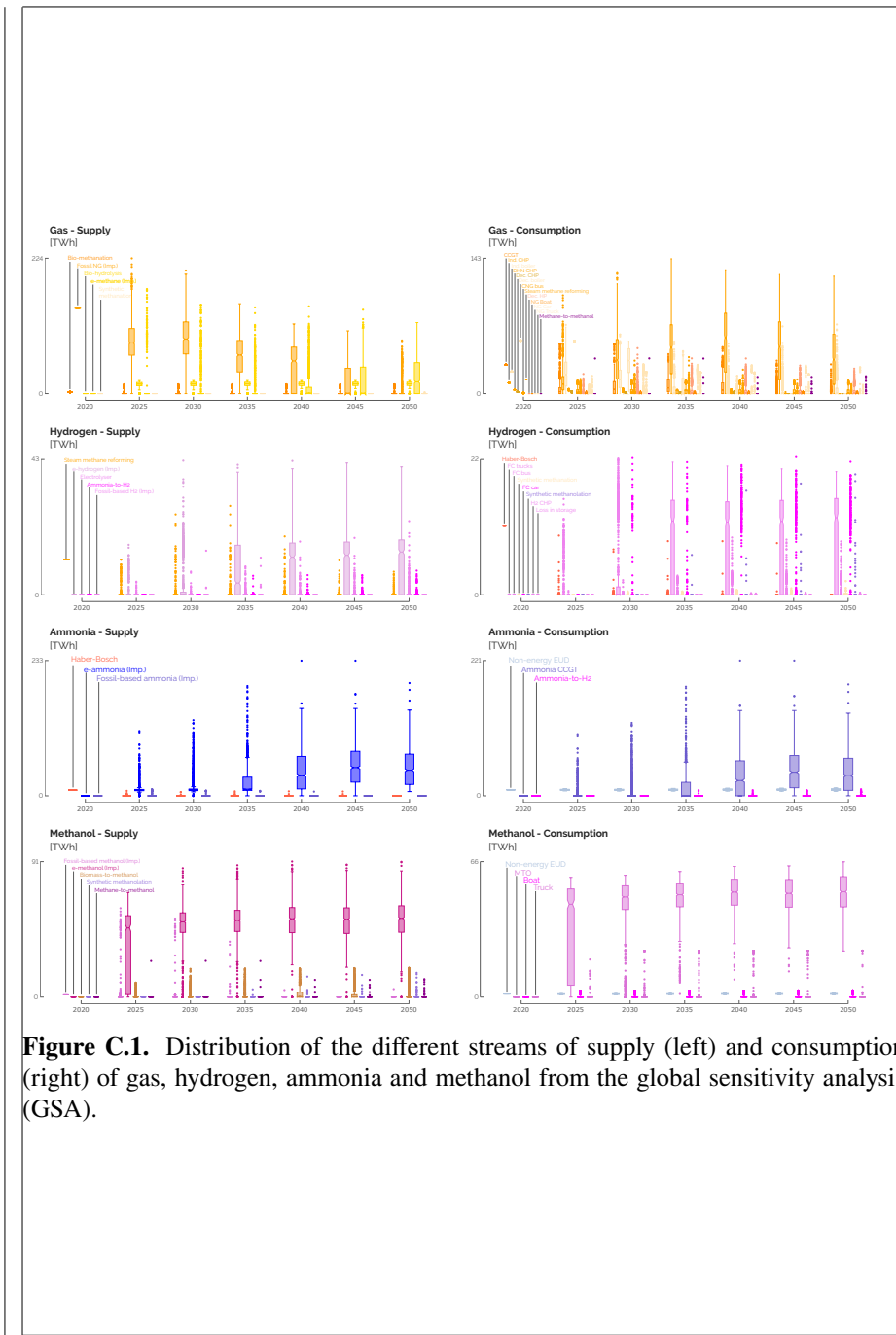


**Figure C.1.** Distribution of the different streams of supply (left) and consumption (right) of gas, hydrogen, ammonia and methanol from the global sensitivity analysis (GSA).